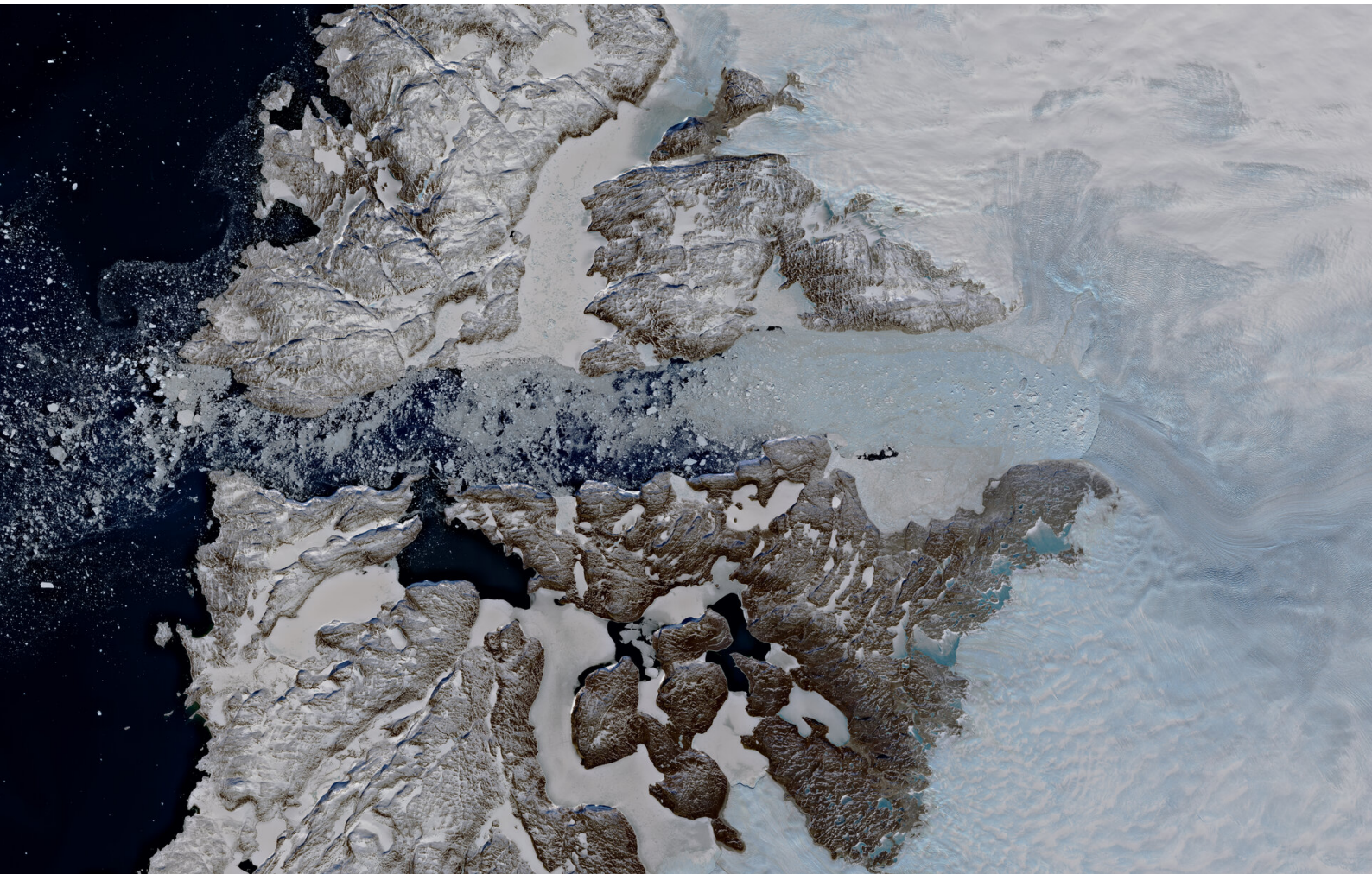


Modelling The Greenland Ice Sheet Following The Mid-Eemian

A study of the impact of including lateral variations in the sub-Greenland Earth rheology on the GrIS' evolution since the mid-Eemian in a coupled 3D ice sheet and 3D GIA model



Modelling The Greenland Ice Sheet Following The Mid-Eemian

A study of the impact of including lateral variations in the sub-Greenland Earth rheology on the GrIS' evolution since the mid-Eemian in a coupled 3D ice sheet and 3D GIA model

By

G. Kempenaar

Thesis submitted in partial fulfilment of the requirements of

*Master of Science
in Aerospace Engineering
Space Flight Track*

at the Delft University of Technology
to be defended on Friday December 9, 2022 at 13:00.

Student Number :	4238338	
Supervisor :	Dr. ir. W. van der Wal	TU Delft
Thesis Committee:	Prof. dr. L. L. A. Vermeersen	TU Delft
	Dr. M. Vizcaino	TU Delft
	Ir. C. J. van Calcar	TU Delft

An electronic version of this thesis is available at: <https://repository.tudelft.nl/>

Preface

The cover image visualises Jakobshavn Glacier terminating within the UNESCO World Heritage Site Ilulissat Icefjord in eastern Greenland. The Jakobshavn glacier is a massive fast-moving outlet glacier which, in my opinion, embodies Greenland's grandeur. The cover image is a courtesy of ESA/Copernicus Sentinel-2.

Greenland's ice sheet is subject to increased rates of ice loss caused by future (anthropogenic) climate change. This will progressively get worse as global temperatures rise which is underpinned by research regarding projected changes to Greenland's ice sheet. Key in preparing for, living with, and potentially mitigating some of the consequences of both ongoing and future changes to climate and sea level is understanding how these changes have historically affected Greenland's ice sheet. Such understanding is both extremely relevant and interesting. My intrinsic motivation to understand how the world around me is changing made it so that I wanted to pick up a topic related to the cryosphere.

In this endeavour, Caroline van Calcar and Wouter van der Wal provided me with an excellent opportunity by enabling me to study how Greenland's ice sheet has evolved in a changing climate over the past 120,000 years. Ice sheet evolution affects, and is affected by, deflection of the Earth's surface caused by changes to the ice sheet's mass. The significance of this interaction depends inherently on the Earth's viscosity which varies in three dimensions. To study how this 3D variability has affected the Greenland ice sheet's past evolution requires coupling of an ice sheet model with a solid Earth model. To this end, I've been able to use such a coupled model developed by Caroline. We find that inclusion of 3D variations in the Earth's viscosity leads to a reduction in simulated historic ice loss at the ice sheet's surface. Hence, inclusion of 3D variations in the solid Earth's viscosity may have a stabilizing effect on the ice sheet's past deglaciation.

This result is both exciting, encouraging, and worrying at the same time. I cannot wait to see what the future has in store for us. However, for me personally in the here and now, above all I consider overcoming the complexity of the topic and the unexpectedness of the result as a wonderful outcome of more than a year of arduous work. Having completed this phase of my life I feel that I can ward off any future difficulties, be it professionally or privately. However, it is not something that I have done by myself. It is very much a testament to the character of the people that have helped me throughout. It is no exaggeration that without Caroline's support, knowledge, and innumerable compliment sandwiches I would have not completed this thesis. As such, I'd like to explicitly thank you for so much of your time and effort. You have been, truly, very inspiring. I'd also like to thank Wouter for the opportunity to work on this topic and for the feedback on both the process and the content of this thesis. There are also my friends and family to whom I owe very much. Thank you for never doubting that I was soon going to wrap things up! J

Most importantly though, and instrumental in this success, has been my mother. Whom, with her unwavering support of my desire to move forward and to be ultimately successful, also in the most difficult of times, deserves my heartfelt gratitude.

Gydo Kempenaar, November 2022

Abstract

The Greenland Ice Sheet (GrIS) is one of two major remaining ice sheets. Historic and projected mean sea level variations are partially dependent on the variation in ice volume contained by the GrIS. Centennial scale projected estimates of the GrIS' contribution to rising sea levels vary upwards of $90 \pm 50\text{mm}$ (Goelzer et al., 2020). This variability in projected sea level rise contribution by the GrIS illustrates that a better understanding of the GrIS' evolution is required.

The GrIS' evolution may be simulated with a 3D ice sheet model. The model used for this study is ANICE as developed by De Boer et al. (2013). ANICE computes the GrIS' ice mass balance and ice flow. The ice mass balance is computed by determining the rate of ice ablation at the surface, ice accumulation via precipitation, and retention of ice via refreezing of meltwater and rain. Ice flow is computed by estimating horizontal flow velocities using a combination of simulated slow moving ice in central Greenland and fast moving ice-streams at Greenland's periphery. The implementation of ANICE does not allow ice shelves, floating masses of ice fed by ice flow towards the periphery, to form. Thereby negating the effect of sub-ice-shelf melt on the mass balance and the application of resistive stresses to the ice flow.

The GrIS' evolution causes temporal variations in the load applied to the Earth's surface. The change in surface load causes the solid-Earth to deform. The extent of this deformation is described by Glacial Isostatic Adjustment (GIA). The rate at which GIA occurs and the magnitude of the deflection depends on the Earth's lithosphere thickness and mantle viscosity. Lithosphere thickness and mantle viscosity determine the GIA response to changes in surface loading.

Research has found that the interaction between GIA and ice dynamics has a profound effect on the ice sheet's evolution via two feedback mechanisms. First, GIA causes a vertical displacement of the ice sheet's surface which affects the surface temperature dependent mass balance. Second, GIA causes a change in local water depth. This affects the rate of ice discharge and seawater induced ablation. These GIA-mass balance and GIA-grounding line interactions establish two negative feedback loops between GIA and the ice dynamics.

The significance of these feedback mechanisms can be studied by simulating the GrIS' evolution with an ice sheet model coupled with a solid-Earth model. Research has hitherto studied the GrIS' evolution by assuming that the sub-Greenland solid-Earth structure can be approximated by a laterally homogeneous 1D parameterisation of mantle viscoelasticity. However, seismic measurements suggest that the mantle viscosity underlying Greenland is not laterally homogeneous. Thus, a laterally homogeneous 1D parameterisation of the sub-Greenland mantle viscoelasticity negates the dependence of the GrIS' evolution on 3D variations in the solid-Earth's structure which introduces an uncertainty in the simulated GrIS' past and projected state. The results presented in this thesis include lateral variability in the sub-Greenland Earth's structure by introducing a composite solid-Earth structure that describes the stress-strain relationships in the mantle via a linear and a non-linear component. Results are obtained a 3D GIA model (Blank et al., 2021) coupled to ANICE using the routine developed by (Van Calcar, 2020).

The GrIS' evolution is simulated for three solid-Earth structures. A commonly adopted 1D laterally homogeneous solid-Earth structure and two 3D solid-Earth structures differing in the definition of their composite rheology. Comparison of the simulated ice thickness and bedrock elevation at the Last Glacial Maximum (LGM), the epoch associated with the GrIS' maximum volume, and at Present Day (PD) provide the first concrete insight into the significance of lateral variations in the sub-Greenland Earth's structure

on the GrIS' evolution. In so doing the following research question is addressed: *How do lateral variations in sub-Greenland rheology affect the GrIS' evolution since the mid-Eemian?*

The inclusion of lateral variations in sub-Greenland rheology results in a viscosity that varies several orders of magnitude and a lithosphere thickness that varies ten of kilometers underneath Greenland. The 3D viscosity is higher in northwestern Greenland and lower in southeastern Greenland when compared with a commonly adopted 1D solid-Earth structure.

The effect of a lower viscosity and thinner lithosphere underlying southeastern Greenland on the GrIS' evolution is marginal. The difference in simulated ice thickness between coupled simulations does not exceed two meters at both LGM and at PD. The interaction between GIA and ice dynamics via the GIA-mass balance and GIA-grounding line feedback mechanisms is negligible for southeastern Greenland causing this negligible difference in ice thickness.

Conversely, the increased viscosity and increased lithosphere thickness underlying northwestern Greenland have a significant effect on the GrIS' simulated evolution. In a cooling climate, GIA-mass balance feedback cause the GrIS' growth to be diminished, causing decreased subsidence and therefore also causing the ice sheet's surface to be in a cooler atmosphere. This difference in the GrIS' growth leading up to LGM has a profound effect on its subsequent evolution. The increased surface elevation leads to a large reduction in ice ablation and the decreased ice thickness leads to a reduction in initial ice discharge. The inclusion of lateral variations in sub-Greenland rheology cause the simulated ice thickness to be up to 900 meters larger than the ice thickness obtained for a commonly adopted 1D sub-Greenland rheology. Thus, lateral variations in sub-Greenland rheology can have a stabilizing effect on the GrIS' simulated evolution at the start of a warming climate, thereby delaying the onset of rapid ablation. Illustrating that the exclusion of lateral variations in sub-Greenland rheology may lead to an overestimation of the estimated ice melt in northwestern Greenland.

The significance of including lateral variations in the sub-Greenland rheology depends on the definition of the Earth's composite rheology. The composite rheology is based on assumed values for sub-Greenland mantle water content and mantle material grain size. The water content and grain size are poorly constrained which introduces an uncertainty in the simulated results. The results presented in this study are obtained for two composite rheologies that covers a limited range of feasible values of grain size and water content. Future research should consider a wider range of possible mantle definitions to improve understanding of the effect of lateral variations in sub-Greenland rheology on the GrIS' evolution.

Contents

Preface	iv
Abstract	vii
Nomenclature	x
List of Figures	xiv
List of Tables	xvi
1 Introduction	1
1.1 Ice Dynamics	2
1.2 Glacial Isostatic Adjustment	4
1.3 Research and Report Outlook	7
2 Method	10
2.1 Coupled 3D Ice Sheet and 3D GIA Modelling	10
2.2 Coupled model input	16
2.3 1D and 3D Earth Structure Definitions	20
3 Results and Discussion	28
3.1 Applicability of the simulated results	28
3.2 3D GIA feedback on mass-balance	32
3.3 3D GIA feedback on grounding line migration	43
3.4 Uncertainty in 3D GIA	47
4 Conclusion	51
5 Recommendations	54
References	63

Nomenclature

BMB	Basal Mass Balance
BP	Before Present
ELRA	Elastic Lithosphere Relaxing Asthenosphere
FEM	Finite Element Method
GIA	Glacial Isostatic Adjustment
GrIS	Greenland Ice Sheet
LGM	Last Glacial Maximum
LIG	Last Inter-Glacial
LMV	Lower Mantle Viscosity
LT	Lithosphere Thickness
MIEQ	Meter Ice Equivalent
NWG	Northwestern Greenland
PD	Present Day
PREM	Preliminary Reference Earth Model
RSL	Relative Sea Level
SIA	Shallow Ice Approximation
SLE	Sea Level Equivalent
SMB	Surface Mass Balance
SSA	Shallow Shelf Approximation
UMV	Upper Mantle Viscosity

List of Figures

2.1	Visualisation of the implementation of different flow regimes in ANICE as introduced by De Boer et al. (2013). The simulated ice flow is described by the SSA in regions characterised by slow moving ice, the SIA in regions characterised by ice shelves, and a combination of SIA and SSA in the transition zone between slow moving ice and ice shelves.	11
2.2	A comparison of the difference in ice growth when including ice shelves (left) and excluding ice shelves (right) using ELRA to determine vertical bedrock deformation. Inclusion of the ice shelves leads to rampant ice growth leading to ice shelf formation beyond Iceland and grounding into Baffin Bay.	12
2.3	The application of a high mesh at an arbitrary location is defined by the longitudinal (ϕ) and latitudinal (λ) position relative to the local (x,y,z) with the high resolution mesh characterised by the basic geometry of the required shape (e.g. circular defined by radius R relative to the defined coordinate). Image: gettyimages.	13
2.4	Application of a cutout at an arbitrary location leads to irregular mesh warping due to a mismatch in the alignment of the high resolution mesh and the adjacent low resolution mesh. The irregular warping may affect the interpretation of results and prevents the method from being employed.	13
2.5	The application of a high resolution mesh at the spherical FEM model's north pole using a method of cutting the layers and replacing the cutout with an equivalent sized high resolution mesh shape. The cutout leads to warping of the mesh with depth and a smooth mesh at the surface.	14
2.6	The application of the load, interpolated from ANICE to FEM, is correctly applied at the high resolution cutout by defining the position of the applied load relative to a secondary coordinate system rotated relative to the original coordinate system by: $\hat{\mathbf{x}} = R_x(14)R_z(14.4)\mathbf{x}$	14
2.7	A block diagram describing the forward modelling procedure by which the ANICE and FEM are coupled and iterated (Van Calcar, 2020).	16
2.8	A comparison of the performance of a 120,000 year converged coupled 3D ice sheet and 3D GIA model run by considering the convergence of the first iteration ANICE-FEM output with the final iteration ANICE-FEM output and by considering the maximum difference in vertical bedrock displacement between the first and final iteration.	17
2.9	Model input ice thickness (left), bedrock elevation (middle) and surface elevation (right) adapted from observed present day values described by Bamber et al. (2013) using Oblimap2.0 by Reerink et al. (2016).	18
2.10	Input variation in global temperature changes and sea level changes relative to present day used for model forcing (Uppala et al., 2005)	18
2.11	First iteration-first timestep estimated surface load for model initialisation obtained using ANICE with ELRA for a given initial topography and ice thickness	21

2.12	Visualisation of the effect of mantle water content, mantle material grain size, and mantle stresses on the range of feasible combinations of deep and shallow upper mantle viscosity on top of the performance in replicating uplift on southeastern Greenland's coast by V. R. Barletta. The 3DE5 and 3DE6 profiles including lateral variability in viscosity underneath Greenland are taken from the best performing combination of Shallow-UMV and Deep-UMV contained for the two extremes of realistic mantle stresses	24
2.13	3D Viscosity (3DE5) profile visualisation at depths of 100, 200, 300, and 400 kilometers for a mantle material water content of 75 ppm and an assumed grain size of 3 mm.	25
2.14	3D Viscosity profile (3DE6) visualisation at depths of 100, 200, 300, and 400 kilometers for a mantle material water content of 4.7 ppm and an assumed grain size of 3 mm.	26
2.15	Vertical viscosity profiles associated with northwestern Greenland, central Greenland, and southeastern Greenland. The inclusion of lateral variations in the sub-Greenland rheology causes an increase in viscosity near the surface in northwestern and central Greenland and a decrease in southeastern Greenland.	26
3.1	Visualisation of the bedrock response for 1DR1 (middle) and 1DR2 (right) to the estimated surface loading (left) obtained with ANICE using ELRA over the first iteration's first 5,000 year timestep.	29
3.2	Comparison of the simulated GIA and coupled effect on the ice thickness with ANICE results obtained using ELRA for 1DR1 and 1DR2. Differences in GIA and ice thickness obtained are exclusively dependent on the differences in the Earth model and reflect the effect on grounding line migration feedback and GIA-elevation mass balance feedback.	30
3.3	Assessment of the convergence of first iteration coupled ANICE:FEM simulation results towards PD observed bedrock elevation by visualising the difference for 1DR1, 1DR2, 3DE5, and 3DE6 - PD bedrock elevation	31
3.4	Assessment of the convergence of second iteration coupled ANICE:FEM simulation results towards PD observed bedrock elevation by visualising the difference for 1DR1, 1DR2, 3DE5, and 3DE6 - PD bedrock elevation	31
3.5	Assessment of the convergence of third iteration coupled simulation results towards PD observed bedrock elevation by visualising the difference for 1DR2 - PD bedrock elevation	32
3.6	Simulated difference in bedrock elevation and ice thickness at LGM for 3DE5-1DR1 and 3DE6-1DR1 respectively.	33
3.7	Difference in simulated surface elevation between 3DE5 and 1DR1 at LGM.	34
3.8	Cumulative difference in simulated precipitation between 3DE5 and 1DR1 over the period -60ka BP to LGM	36
3.9	Simulated difference in ice thickness at PD for 3DE5-1DR1 and 3DE6-1DR1 respectively. Ice thickness variation in NWG is in excess of 900 meters at the coastline and decreases to 0 when migrating inland.	37
3.10	Contour plot defined by 100 meter increments illustrating regional variations in PD simulated ice thickness for second iteration 3DE5 - second iteration 1DR1 results	38
3.11	Contour plot defined by 10 meter increments illustrating regional variations in PD simulated surface elevation for second iteration 3DE5 - second iteration 1DR1 results	38
3.12	Cumulative difference in simulated precipitation between 3DE5 and 1DR1 over the period -60ka BP to LGM	39
3.13	Temporal variation in accumulation and ablation for simulated 3D-1D results since the LGM up to PD. A negative difference in accumulation implies reduced ice volume aggregation by the GrIS and a negative difference in ablation implies increased ice retention through reduced ice melt.	39

3.14	Comparison of the variation in grounding line position (left) at LGM correlated with the difference in bedrock elevation (middle) and ice thickness (right) at LGM for 3DE5 - 1DR1 second iteration simulation results.	44
3.15	Visualisation of the temporal variation in GrIS ice discharge for 3DE5-1DR1 and 3DE6-1DR1 second iteration simulation results at LGM. A negative difference in ice discharge implies a decreased discharge of 3D results relative to 1D results	45
3.16	Difference in vertically averaged flow velocity distributed over Greenland for 3DE5-1DR1 second iteration simulation results at LGM	45
3.17	Comparison of the variation in grounding line position (left) at PD correlated with the difference in bedrock elevation (middle) and ice thickness (right) at PD for 3DE5 - 1DR1 second iteration simulation results.	47
3.18	Visualisation of the temporal variation in GrIS ice discharge for 3DE5-1DR1 and 3DE6-1DR1 second iteration simulation results at PD.	47
3.19	Difference in vertically averaged flow velocity distributed over Greenland for 3DE5-1DR1 second iteration simulation results at PD	47
3.20	Difference in simulated bedrock elevation, ice thickness, and surface elevation at LGM for 3DE5-3DE6 second iteration simulation results	48
3.21	Difference in simulated bedrock elevation, ice thickness, and surface elevation at PD for 3DE5-3DE6 second iteration simulation results	49

List of Tables

2.1	ELRA parameterisation	20
2.2	One dimensional radially stratified solid Earth model (1DR1) definition based on work by Dziewonski (1981); Lecavalier et al. (2014); Milne et al. (2018); Adhikari et al. (2021).	22
2.3	One dimensional radially stratified solid Earth model (1DR2) definition using the low UMW estimate postulated by Adhikari et al. (2021) and a low-end lithosphere thickness derived from Zhong et al. (2003); Milne et al. (2018)	23

Chapter 1

Introduction

The GrIS' waxing and waning in response to climate change contributes to changes in global sea level (Alley et al., 2010). The extent of this sea level contribution has both local and global societal and ecological implications (Pörtner et al., 2022). Accurate modelling of the GrIS' evolution is necessary to determine the magnitude of the GrIS' past and future contribution to sea level change. The ice sheet's evolution depends partly on a complex interaction between the GrIS, the solid Earth, and climate (Whitehouse, 2018). Such interaction is accounted for in studies of the GrIS' evolution by coupling an ice sheet model forced by climate change with a solid Earth model as discussed in subsection 1.2.2. The purpose of the results presented in this report is to improve understanding of the GrIS' evolution by studying the effects of varying the solid Earth's structure in three dimensions in a coupled ice sheet and solid Earth model.

Locally, the ramifications of GrIS waxing and waning is illustrated by Greenland's settlement history. First settled in 2,500 B.C. by Paleo-Inuits, Greenland has seen various cultures colonize and retreat from its (ice-free) shores Sørensen and Gulløv (2012). Recent Greenland's history is characterised by first Norse settlement in 985 A.D. at Igaliku and then its subsequent collapse in the 1400s (Buckland et al., 2008). The collapse of these different societies has been, in part, the consequence of the adverse effects associated with climate change (Dughmore et al., 2007; Sørensen and Gulløv, 2012). Conversely, PD ice retreat provides contemporary Greenlanders with novel economic opportunities (Bjork et al., 2021; Bendixen et al., 2022). This illustrates that climate change and subsequent GrIS waxing and waning has a significant societal and ecological impact locally.

Globally, the IPCC foresees that ecosystems, biodiversity, and societies will be adversely affected by ongoing and accelerated GrIS ice volume reduction in the near- and long-term (Pörtner et al., 2022). This adverse effect is evident when considering coastal-settlements, -infrastructure, and -ecosystems which are subject to complete destruction in response to rising sea levels. Severe flooding, increased precipitation, and other climate hazards are further consequences of the GrIS' waning induced sea level rise (Pörtner et al., 2022). These adverse effects underpin the global societal and ecological relevance of changes to the GrIS' ice volume.

The severity of the aforementioned consequences depends on the extent of future ice lost by the GrIS. A total of 7.42 meters Sea Level Equivalent (SLE) of ice is contained within the GrIS (Morlighem et al., 2017). In the short term, projected sea-level contributions over the Twenty-first century can amount up to 90 ± 50 mm depending on the greenhouse gas concentration scenario (Goelzer et al., 2020). Furthermore, the rate at which the GrIS loses ice mass continues to accelerate (Mouginot et al., 2019; Boers and Rypdal, 2021). In the long term, temperature change of several degrees above industrial-era temperatures could lead to the reduction of the PD GrIS' ice volume by 39% and may even cause the complete collapse of the GrIS (Alley et al., 2010; Zeitz et al., 2022). Thus, the historic precedent of significant deglaciation, ongoing accelerated and widespread ice loss, the future potential complete deglaciation of Greenland, and the severity of the associated consequences are a strong indication of the societal, ecological, and scientific importance of understanding the GrIS' behaviour completely.

Research that studies the GrIS' evolution with a coupled ice sheet and solid Earth models has hitherto assumed that the solid Earth's structure can be sufficiently described by a laterally homogeneous 1D structure (Bradley et al., 2018; Zeitz et al., 2022). The implementation of a 1D solid Earth structure negates the lateral variation in the solid Earth's structure underlying the GrIS, which is known to exist (Mordret, 2018; Milne et al., 2018), and which is known to affect an ice sheet's evolution (Milne et al., 2018; Gomez et al., 2018; Whitehouse et al., 2019; Van Calcar, 2020). Therefore, a complete understanding of the GrIS' behaviour requires an understanding of the significance of lateral variations in the solid Earth's structure on the GrIS' evolution. The results presented in this research includes, for the first time, the effect of such lateral variations in the Earth's structure on the GrIS' evolution simulated with a coupled ice sheet and solid Earth model.

First, the ice dynamics that describe the GrIS' evolution are introduced in [section 1.1](#). Second, modelling of the response of the solid Earth to changes in the GrIS' state are discussed in [section 1.2](#). Also discussed in [section 1.2](#) is the feedback that exists between the solid Earth's deformation and the simulated ice dynamics. Finally, a research question is postulated in [section 1.3](#).

1.1 Ice Dynamics

Modelling ice sheet evolution on longer than millennial timescales depends on the ability to numerically determine an ice sheet's ice mass changes and ice flow when the ice sheet is subject to climate and sea level forcing. A numerical solution of temporal variations in the GrIS' extent and ice thickness on these timescales can be obtained with an ice sheet model (Huybrechts, 2007; Goelzer et al., 2017). Ice sheet modelling approximates an ice sheet's evolution relative to an initial state by computing the rate at which ice is accumulated, the rate at which ice is lost, and the rate at which ice is displaced via horizontal ice flow velocities when forced by climate and sea level change. Ice sheet modelling is introduced in this section.

1.1.1 Ice sheet mass balance

Modelling the rate at which the GrIS loses and accumulates ice depends on several processes at the ice sheet's base, the ice sheet's surface, and at the ice sheet-ocean interface. Ice loss is driven by ice melt at the surface and subsequent meltwater runoff in lower elevation regions, ocean-induced ablation of ice in segments of the ice sheet extending into the ocean, and calving of icebergs at sections of the ice sheets characterised by floating ice (Goelzer et al., 2017). Ice gain is dominated by the rate at which ice accumulates at higher elevations via precipitation and is affected to a lesser extent by the rate at which ice is retained through refreezing of meltwater (De Boer et al., 2013; Goelzer et al., 2017). Ice sheet models describe the net change in simulated ice mass by computing the sum of the net change in ice mass at the ice sheet's surface (the Surface Mass Balance: SMB), at the ice sheet's base (the Basal Mass Balance: BMB), and at the ice sheet's ocean interface.

Simulated rates of ice loss and ice gain depends on a multitude of factors. Simulated ice loss via ice melt at the surface depends on the surface albedo and on the temperature at the ice sheet's surface and by extension of the ice sheet's surface elevation (Reeh, 1991; De Boer et al., 2013). GrIS ice mass loss via ice ablation at the ocean-ice sheet interface is driven by ocean-induced melting which depends primarily on the ocean's depth adjacent to marine grounded portions of the GrIS, the Relative Sea Level (RSL), and on both the water temperature and ice temperature at this interface (Malyarenko et al., 2020). Ice shelf formation at an ice sheet's periphery leads to an increase in ice ablation via basal melt, the ablation of the ice sheet underneath ice shelves and at the grounded ice's bed (Van den Broeke et al., 2016; Pattyn and Morlighem, 2020). A second consequence of ice shelf formation is ice discharge via the calving of icebergs which affects the rate of ice loss of marine-terminating sections of an ice sheet (Goelzer et al., 2017; King et al., 2020). Rates of iceberg calving depends partly on the rate of flow towards an ice sheet's ice shelf and

on local ice thickness but the process affecting calving are poorly resolved leading many ice sheet models to implement calving at a fixed ice shelf thickness (Rignot et al., 2013a; Depoorter et al., 2013; Mankoff et al., 2019). The loss of ice at Greenland’s surface and at the ocean-ice sheet interface via ice melt is offset by refreezing of parts of the lost ice mass. Refreezing rates of ice depend on simulated vertical profiles in temperature, ice density, and liquid water content within the ice sheet (Reijmer et al., 2012).

Rates of ice mass gain and ice mass loss depends on a complex interaction between climate forcing, sea level forcing, ice thickness variations, and ice flow. Physics based ice sheet models take large scale ice mass change processes over the modelled period of interest into account by defining or computing the parameters that drive ice mass changes and by subsequently estimating the SMB, BMB, and ice discharge at the ocean-ice sheet interface.

1.1.2 Ice flow dynamics

When a sufficiently large amount of ice is accumulated in a region the ice begins to flow through deformation under its own weight and through sliding over the local bedrock (Goelzer et al., 2017). Ice sheet models typically estimate gravity induced ice flow as a combination of slow moving ice in central ice sheet regions and fast moving ice near outlet streams and ice shelves whilst also accounting for sliding of the ice sheet where the ice is grounded to bedrock (Huybrechts, 2007).

Ice flow in central ice sheet regions can be estimated under the assumption that the horizontal scale of the ice sheet is much larger than the ice thickness which allows for the simplification that longitudinal variations in internal stresses, ice velocity, and ice temperature have no significant effect on the simulated flow (Huybrechts, 2007). This approximation of ice flow is the Shallow-Ice Approximation (SIA) Hutter (1983). Ice sheet models typically approximate the flow in central parts of the ice sheet by computing the displacement resulting from the application of shear stresses to the ice by using the Glen’s flow law under the SIA assumption(Huybrechts, 2007). The Glen’s flow law allows ice sheet models to determine horizontal flow velocities by providing an empirical relation between the ice sheet’s strain in response to applied stresses (Huybrechts, 2007). Slow moving ice flow velocities approximated with the Glen’s flow law depend on the magnitude of the self-induced stresses by the weight of the ice sheet, bedrock slope, and on the ice sheet’s rheological properties that govern the internal stress-strain relationships and are dependent on temperature gradients in the ice sheet (Van der Veen and Whilliams, 1990).

Ice flow velocities in regions of fast moving ice near outlet ice streams and ice shelves depend on longitudinal stresses in the ice sheet. The ice flow becomes dependent on the stress imparted on the ice by adjacent regions of ice and can therefore no longer be computed under the assumed SIA (Huybrechts, 2007). The flow in regions of fast moving ice where the effect of the ice sheet’s friction with the bedrock, basal friction, is minimal or nonexistent can be approximated with the Shallow Shelf Approximation (SSA) (Morland, 1987). The SSA is applicable under the assumption that horizontal flow velocities and strain rates are vertically constant such that ice flow is computed under the assumption that shear stresses are negligible (Huth et al., 2021). Ice flow modelled by ice sheet models under the SSA depend primarily on vertical temperature gradients and vertical stress gradients (Weis et al., 1999).

A tertiary component describing ice flow is the rate at which the ice sheet slides over local bedrock, the basal sliding. Basal sliding is an important component of describing the ice flow near fast moving ice streams. The presence of basal sliding depends on the formation of a lubricating layer of water at the ice sheet’s base where pressure melting criteria are met and on the characteristics of the local bedrock (Huybrechts, 2007). Ice sheet models frequently describe basal sliding by using the SSA and a variety of sliding laws such as (regularised) Coulomb type and Weertman type sliding laws (Weertman, 1979; Bueler and Brown, 2009; Schoof, 2010; Winkelmann et al., 2011).

The flow in the transition zone between regions characterised by slow moving and fast moving ice is typically coupled via a continuity equation (De Boer et al., 2013). Ice sheet models then describe the deformation of ice, and therefore ice flow velocities, by computing internal stresses in the ice based on the different flow velocity regimes and ice thickness and by coupling these regions via the continuity equation.

Ice sheet evolution described with ice sheet models typically include the possibility of simulating ice shelf formation when the SMB is sufficiently positive and the increased ice mass forces the ice sheet to grow towards the continent’s coastline. If the advance of the ice sheet is sufficiently far into the ocean then the ice begins to float as described by the flotation criterion (Schoof and Hewitt, 2013). The location where the ice sheet transitions from grounded ice in contact with the bedrock to floating ice is defined as the grounding line. Ice shelf formation simulated with ice sheet models thus depends on the ice sheet’s mass balance and on the rate at which ice flows towards the coastline. The formation of ice shelves is significant for the simulated ice sheet’s evolution because it leads to buttressing of the ice sheet, the formation of resistive stresses, which impede on the ice flow towards the ocean thereby affecting the rate of ice discharge (Rignot et al., 2013b).

Ice sheet evolution modelling is possible with ice sheet models which estimate ice mass variations and ice flow velocities. Simulated rates of ice mass accumulation and ice mass loss strongly depend on the temperature conditions at the ice sheet’s surface and ocean-ice sheet interface and on the rate of ice discharge via ice flow towards the ocean and the ice sheet’s rheological properties and temperature gradients. Ice flow modelled with ice sheet models depends primarily on stresses introduced in the ice sheet by the ice sheet’s weight, on the conditions at the ice sheet’s base, and on rheological properties and temperature gradients in the ice. This strong dependence of ice dynamics on gradients of temperature in the ice and the ice sheet’s properties imply that the ice sheet may be coupled with a climate model when simulating long-term, longer than millennial, ice sheet evolution. However, here, as with many models, climate forcing is used to determine the ice sheet’s waxing and waning.

1.2 Glacial Isostatic Adjustment

Changes in the global mass distribution lead the solid Earth to deform, the Earth’s gravity field to become perturbed, and sea levels to adjust regionally. The deformation, gravity field perturbations, and sea level adjustment, associated with this change in global ice mass and melt-water redistribution is Glacial Isostatic Adjustment (GIA) (Whitehouse, 2018). This section will introduce key concepts of GIA, how GIA may be determined, how GIA depends on the Earth’s assumed structure, how GIA affects ice dynamics in a coupled ice dynamics and GIA model, and how lateral variations in the Earth’s rheology may affect the simulated GrIS’ evolution.

1.2.1 Glacial isostatic adjustment modelling

Temporal variations in ice sheet extent and volume, resulting from ice sheet waxing and waning in a changing climate, leads to variations in the surface load on the Earth by both ice mass changes and a redistribution of meltwater. The change in applied surface load results in a deviation away from isostatic equilibrium which causes the viscoelastic Earth to deform through a redistribution of mantle material (Van der Wal et al., 2015). This deformation translates into a vertical and horizontal displacement of the Earth’s surface. GIA, dependent on the Earth’s structure and changes in surface loading, is prevalent on a (multi-)millennial timescale and affects an ice sheet’s evolution (Whitehouse, 2018). As such, GIA is a crucial component in studies of the GrIS’ evolution (Stuhne and Peltier, 2015; Kappelsberger et al., 2021; Goto-Azuma et al., 2021; Zeitz et al., 2022), studies of the viscosity underlying Greenland (Van der Wal et al., 2015; Mordret, 2018; Milne et al., 2018; Adhikari et al., 2021; Bagherbandi et al., 2022), and vice-versa (Khan et al., 2015; Whitehouse, 2018).

There are two principal methods for determining GIA. GIA may be derived with a geophysical model tied to an ice loading history or coupled with an ice sheet model (Whitehouse, 2018). Alternatively, GIA may be inferred from contemporary observations of vertical bedrock displacement using GPS or satellite altimetry (Van der Wal et al., 2015). When using a geophysical model, simulated GIA differs between mod-

els due to differences in the physics which are implemented in the model, the computational approach to resolving the GIA, and the defined Earth rheology (iMBIE, 2020). Various solid Earth models are available to determine the Earth’s deformation in response to ongoing and historic changes in local ice mass. The deformation in response to changes in the applied surface load is typically determined with a bi-layered solid Earth structure, a (semi-)spherical radially stratified laterally homogeneous solid Earth structure, or with a laterally heterogeneous solid Earth structure (Whitehouse, 2018).

Bi-layered solid Earth models include Elastic Lithosphere Relaxing Asthenosphere (ELRA) and Lingle-Clarke models which simulate GIA using an elastic lithosphere applied over a relaxing viscous mantle layer (Lingle and Clark, 1985; Le Meur and Huybrechts, 1996). Alternatively, solid Earth deformation is commonly simulated with a laterally homogeneous radially varying solid Earth structure such as a linear Maxwell viscoelastic (and more recently elasto-brittle) body (Christmann et al., 2021; Adhikari et al., 2021; Olason et al., 2022), where the deformation is determined in response to the application of a number of applied point loads, or by using a less common bi-viscous Burgers rheology (Caron et al., 2017; Ivins et al., 2021), which determines deformation by differentiating between a short-term and long-term viscosity component. These 1D solid Earth structures yield a better estimate of the GIA signal than ELRA models whilst being computationally efficient but negate the effects of a possible laterally varying 3D solid Earth structure which can have a profound influence on the simulated GIA signal (Blank et al., 2021). As a third method, deformation which includes the effect of lateral variations in rheology can be determined with a power-law approach where the deformation is computed as a function of a time-varying mantle-stress described by a stress-strain relationship that includes a linear (diffusion creep) and non-linear (dislocation creep) component (Van der Wal et al., 2013; Blank et al., 2021; Van Zelst et al., 2022).

The simulated GIA depends, for all models, on the Lithosphere Thickness (LT) and on the effective mantle viscosity. The lithosphere is modelled as a (visco-)elastic layer that responds (largely) elastically to variations in the applied surface loading. Conversely, the mantle is allowed to respond to changes in the applied surface loading. Variations in LT define the wavelength of the simulated GIA signal and thereby determine the spatial extent to which changes in the applied surface loading cause vertical and horizontal deformation of the solid Earth’s surface (Spada et al., 2006; Nield et al., 2018). The rate at which the Earth deforms is determined by the magnitude of the viscosity of the mantle. Where a lower viscosity leads to increased rates of modelled GIA. However, this dependency of the GIA signal on mantle viscosity decreases with depth (Mitrovica and Forte, 2004). Thus, viscosity variations near the solid Earth’s surface in either the lithosphere or the upper mantle have a stronger influence on an ice sheet’s evolution meaning that high variability in the Earth’s structure near the surface can have a strong influence on modelled GIA.

A bi-layered model such as ELRA may lead to a gross underestimation of ice volume variations and does not incorporate effects of local sea level change via a gravitationally self consistent meltwater redistribution (Konrad et al., 2014). 1D Maxwell rheologies typically do account for such a meltwater redistribution leading to better simulation results but negate the effect of lateral variations in rheology on GIA which, for Antarctica, were found to have a significant effect on the ice sheet’s evolution (Gomez et al., 2018). Lateral variations in rheology are also present in the sub-Greenland’s Earth structure and lead to a 3D variation in lithosphere thickness (Zhong et al., 2003; Nield et al., 2018) and mantle viscosity (Khan et al., 2016; Milne et al., 2018; Mordret, 2018; Weerdesteijn et al., 2022). Thus, to accurately resolve spatial variations in GIA and to study its effect on the GrIS’ evolution it is necessary to include lateral variations in the sub-Greenland rheology.

1.2.2 Glacial isostatic adjustment and ice dynamics feedback for the Greenland Ice Sheet

Using a 3D solid Earth structure when modelling the GrIS is only meaningful if the effect of a spatially variable GIA response has a demonstrable effect on the GrIS’ evolution. The interaction between the GrIS and GIA is reflected in the interaction between negative elevation-precipitation feedback, negative elevation-melt feedback, and negative grounding line feedback on the GrIS’ evolution.

In [section 1.1](#) the dependence of the ice mass balance on precipitation via the SMB is introduced. The SMB depends on the rate of ice accumulation which is affected by variations in simulated precipitation and retention of snowfall and rainfall at the surface. Rates of precipitation vary spatially and temporally over the GrIS with increased precipitation at lower elevations and lower latitudes ([Bales et al., 2001](#); [Roe, 2002](#); [Wong et al., 2015](#)). In addition, precipitation over the GrIS is found to be dependent on the ice sheet’s surface elevation which affects temperature at the surface and which affects large scale atmospheric circulation ([Edwards et al., 2014](#)). Reduced temperature at the ice sheet’s surface leads to a reduction in atmospheric water content which adversely affects rates of precipitation ([Roe, 2002](#)). This elevation-accumulation effect may be non-negligible in simulating the GrIS’ evolution ([Malyarenko et al., 2020](#)). Furthermore, rates of precipitation depend on the interaction between atmospheric circulation and the ice sheet’s surface topography ([Pettersen et al., 2018](#)). Precipitation also depends on the interaction between the GrIS’ surface topography and wind direction, however. this effect is found to be limited for the GrIS ([Reeh, 1991](#)). The rate of precipitation is also subject to climate change. When global temperatures increase the effect of GIA on precipitation will increase because of the increased water content in the atmosphere. However, this precipitation does not lead directly to an increase in GrIS wide ice accumulation because of a decrease in snowfall relative to rainfall in low elevation regions ([Fettweis et al., 2013](#)).

The apparent dependence of precipitation over the GrIS on the ice sheet’s surface elevation and surface topography implies that there may be a feedback mechanism between the simulated GrIS’ state and the simulated ice mass balance via the amount of precipitation received at the ice sheet’s surface. This feedback is then affected by GIA which leads to a vertical displacement of the ice sheet’s surface and which affects the ice sheet’s topography, thereby influencing such elevation-accumulation feedback. The inclusion of lateral variations in sub-Greenland rheology may affect the simulated GIA by introducing regional differences in mantle viscosity and LT. Thus, the elevation-precipitation feedback for the GrIS which is affected by GIA may also depend on lateral variations in the sub-Greenland rheology. However, the explicit effect of GIA on elevation-precipitation feedback for the GrIS has not yet been studied.

Climate change induced increase in global mean temperatures, which does not necessarily lead to increased ice accumulation via increased precipitation ([Van den Broeke et al., 2016](#)), does lead to an increase in GrIS wide surface melt by affecting both the low-elevation and high-elevation ice loss ([Poinar et al., 2015](#); [Herman et al., 2020](#)). Ice melt at the surface and subsequent meltwater runoff increase exponentially in a warming climate ([Fettweis et al., 2013](#)). This exponential increase in surface melt causes the GrIS’ surface elevation to reduce in ablation zones (low elevation areas dominated by ice melt) leading to higher surface temperatures which causes increased ice melt via a negative elevation-melt feedback ([Edwards et al., 2014](#); [Levermann and Winkelmann, 2016](#)). The rate of GrIS meltwater runoff further depends on large scale atmospheric circulation, bringing in warm air from remote regions, on an ice-albedo feedback, where increased ice melt at the surface exposes bare ice leading to further ice melt, and on decreased retention of precipitation, which are also processes that are affected by elevation-melt feedback in low elevation regions of the GrIS ([Edwards et al., 2014](#); [Kuipers Munneke et al., 2015](#); [Zeit et al., 2021](#)). Melt-elevation feedback, which has a significant influence on the ice sheet’s mass balance, is affected by GIA ([Zeit et al., 2022](#)). However, the effect of GIA on melt-elevation feedback does not take into account the effect of lateral variations in sub-Greenland rheology which, as with precipitation, may affect the regional significance of elevation-melt feedback.

Simulated GIA, which affects the GrIS’ evolution via the ice sheet’s mass balance, also affects the ice sheet’s ice flow dynamics. Elevation-melt and elevation-precipitation feedback, which are influenced by GIA, change the GrIS’ surface geometry leading to a change in ice sheet surface slopes towards peripheral regions which has implications for the ice flow velocity towards the GrIS’ coastal regions ([Le Clec’h et al., 2019](#)). In addition, GIA affects the bedrock slope which further influences the rate of ice flow towards coastal regions ([Rémy et al., 1999](#); [ADikhari et al., 2014](#); [Gao et al., 2020](#)). A secondary consequence of these GIA induced changes in ice flow dynamics is a variable ice thickness at the grounding line ([Malyarenko et al., 2020](#)) which drives the rate of solid ice discharge ([Schoof, 2007](#)). The ice thickness at the grounding line is also affected by grounding line migration which is dependent on the RSL and is directly

affected by GIA induced vertical displacement of bedrock underlying marine-grounded ice sheets. When the RSL increases as a result of a global rise in eustatic sea level or because of GIA the grounding line will retreat inland leading to increased ice shelf (Winkelmann et al., 2011; Pattyn and Morlighem, 2020) and a subsequent increase of solid ice discharge and ice sheet melting at the ice sheet-ocean interface (Slater et al., 2013). Thus, GIA is an important factor in accurately describing ice flow dynamics in peripheral regions of the ice sheet by affecting the mass balance, bedrock slope, and the grounding line’s position. Observational evidence indicates that the GrIS must have grown onto the continental plate and towards the shelf break and that significant ice shelf formation must have been present at the GrIS’ maximum extent (Vasskog et al., 2015; Van Dam et al., 2017; Bradley et al., 2018; Gowan et al., 2021; Couette et al., 2022). As such, the GrIS’ ice flow dynamics must also be affected by GIA and is therefore possibly susceptible to lateral variations in the sub-Greenland rheology.

The potential importance of lateral variations in GIA on GrIS modelling may become evident when considering the current state of GrIS modelling. Currently, The GrIS covers eighty percent of Greenland’s landmass and contains 2.9 km^3 or 7.42m SLE of water-ice (Alley et al., 2010; Vasskog et al., 2015; Morlighem et al., 2017). Modelling of the GrIS shows that the ice volume contained by the GrIS oscillates between lows and highs on glacial timescales (Miller et al., 2011; Bradley et al., 2018). At present, the GrIS is more extensive than during the LIG but is much reduced in size compared to the Last Glacial Maximum (LGM) (Alley et al., 2010; Bradley et al., 2018). The ice retreated inland during the LIG exposing vast areas of Western- and Northern-Greenland as substantiated by simulated ice histories and through observational evidence (Goelzer et al., 2016; Bradley et al., 2018; Plach et al., 2019). Subsequent climate cooling lead to the GrIS’ advancement towards Greenland’s coastline and to the formation of ice shelves and grounded ice along much of the GrIS’ periphery (Vasskog et al., 2015; Bradley et al., 2018; Gowan et al., 2021). Although trends in ice sheet waxing and waning in response to climate change are generally well understood, the magnitude and timing of the GrIS’ contribution to a global mean sea level budget at both LIG and LGM are poorly constrained (Stone et al., 2013; De Boer et al., 2013; Plach et al., 2019). Additionally, projected centennial and multi-millennial scale contributions to the global mean sea level budget are also subject to large uncertainties (Goelzer et al., 2020; Zeitz et al., 2022). The increasing prevalence of melt-elevation feedback in a warming climate, the possible significance of regional differences in ice accumulation in a cooling climate, substantial ice loss via solid ice discharge near the grounding line, a historic precedence for large ice volume fluctuations, and the possible ramifications of lateral variations in sub-Greenland rheology on simulated GIA which influences these processes, demonstrates that a study of the GrIS’ evolution using a coupled 3D ice dynamics and 3D GIA model that integrates lateral variations in sub-Greenland rheology may lead to improved understanding of the GrIS’ evolution as a whole.

1.3 Research and Report Outlook

Contemporary climate change causes the GrIS to rapidly lose ice volume. Estimates on its minimum extent during the LIG are a strong indication that much ice may yet be lost. Existing uncertainty in projected estimates of the GrIS’ sea level contribution on centennial and multi-millennial timescales imply the need for improved understanding of the GrIS’ evolution. A factor that is not included in GrIS evolution modelling using coupled ice dynamics and solid Earth models is the effect of lateral variations in the sub-Greenland rheology. This negates the potential effect of such a 3D structure on the GrIS’ evolution through feedback via the rate of ice accumulation, ice melt, and grounding line migration.

The results presented in this research provide, for the first time, a study of the significance of lateral variations in the sub-Greenland rheology on the GrIS’ evolution through a comparison with simulated results obtained for a commonly adopted laterally homogeneous Earth rheology. The period considered is between the mid-Eemian (120,000 years before present) to PD. Leveraging understanding of past climate change, developments in coupled 3D GIA and 3D ice sheet modeling, and understanding of PD Greenland topography and the GrIS’ current state. This facilitates improved understanding of the effect of GIA on the

GrIS' past evolution and by extension on its future evolution. The following research question is postulated:

- How do lateral variations in sub-Greenland rheology affect the GrIS' evolution since the mid-Eemian?

Three characteristics of the GrIS' evolution which may depend on lateral variations in sub-Greenland rheology are of interest. First, the potential effect of lateral variations in sub-Greenland rheology on the ice sheet's simulated surface mass balance via induced changes in rates of precipitation and ablation is of interest. Second, the effect on GIA-grounding line feedback which may affect local ice growth and rates of ice discharge is of interest. Finally, the uncertainty in the modelled lateral variations in sub-Greenland rheology may affect the outcome of this study. The significance of which can be evaluated by comparing the GrIS' evolution obtained for two differently defined 3D solid Earth structures. Thus, insights derived from the following three sub-questions are to provide a template for answering the research question:

- How is the GrIS' elevation-mass balance feedback affected by the inclusion of lateral variations in sub-Greenland rheology?
- How is the GrIS' grounding line evolution affected by the inclusion of lateral variations in sub-Greenland rheology?
- What are the ramifications of uncertainty in mantle water content on the GrIS' evolution?

The model used for simulating a coupled 3D Earth model and 3D ice sheet model is developed by [Van Calcar \(2020\)](#). The coupled model, adaptations to the coupled model in order to simulate the GrIS, and the modelled sub-Greenland rheology are discussed in [chapter 2](#). The obtained simulation results are analysed and discussed in [chapter 3](#). First, the applicability of the simulated results in describing the effect of 3D GIA on the GrIS' evolution is discussed in [section 3.1](#). Then, the effect of including lateral variations in sub-Greenland rheology on the ice sheet's mass balance will be discussed in [section 3.2](#). Subsequently, the ramifications of lateral variations in sub-Greenland rheology on the grounding line's migration and feedback on the GrIS' evolution are discussed in [section 3.3](#). Finally, a discussion of the significance of uncertainty in the modelled sub-Greenland's rheology on the simulated GrIS' evolution is introduced in [section 3.4](#). Results are aggregated in a concluding chapter and recommendations for future work are provided in [chapter 4](#) and [chapter 5](#) respectively.

Chapter 2

Method

Studying ice sheet behaviour when coupled with a 3D solid-Earth model on glacial timescales necessitates the implementation of a fully coupled 3D ice sheet and GIA model. Nuance in modelled physics, ice dynamics parameterisation, model input, Earth’s modelled approximation, and coupling approach affect simulation results. As such, clarification on the implemented model is required for understanding of the significance of the simulated ice sheet and topographic evolution. The models used to simulate the ice sheet’s evolution and the Earth’s deformation, as well as the coupling method of these models, are described in [section 2.1](#). Simulation input, required to initialise the simulation, is discussed in [section 2.2](#). One dimensional and three dimensional Earth structure approximations are introduced in [section 2.3](#).

2.1 Coupled 3D Ice Sheet and 3D GIA Modelling

The method for coupling 3D ice sheet with 3D GIA is taken from [Van Calcar \(2020\)](#) and adapted to apply to the GrIS. The Finite Element Method (FEM) approach to determine the 3D GIA response to lateral variations in Earth rheology is also adapted from [Van Calcar \(2020\)](#). The FEM’s initial implementation modified by [Van Calcar \(2020\)](#) is described by [Blank et al. \(2021\)](#). The simulated ice dynamics are modelled with an adapted version of ANICE as developed by [De Boer et al. \(2013\)](#) and coupled to the GIA model by [Van Calcar \(2020\)](#). The modelled results are interpolated between the ice sheet grid and FEM grid using OBLIMAP as discussed by [Reerink et al. \(2016\)](#). The coupled model and adaptations to the model (components) are introduced in this section.

2.1.1 ANICE

The GrIS’ ice dynamics are simulated using the 3D ice sheet model ANICE developed by ([De Boer et al., 2013](#)). The model determines both ice flow and the ice sheet’s mass balance. The GrIS can be described by regions of fast moving ice flow near glacier outlet and at marine terminating grounded ice and slow moving grounded ice in central Greenland regions ([Aschwanden et al., 2016](#)). Thus, to realistically describe the ice dynamics, ANICE needs to implement difference methods for simulating these flow regimes. The implementation determines flow by using the Weertman sliding law and differentiates between types of flow through a combination of SSA and SIA. This implementation for ANICE is visualised in [Fig. 2.1 \(De Boer et al., 2013\)](#). Modelling of the GrIS’ mass balance depends on the rate of precipitation and ablation at the ice sheet’s surface. We adopt the method used by [De Boer et al. \(2013\)](#) where accumulation is modelled as a fraction of the precipitation ([Equation 2.1](#)) which depends exponentially on the temperature at the inversion layer and is directly affected by the temperature at the surface ([Equation 2.2](#)). Combined with ablation ([Equation 2.3](#) and refreezing this described the ice sheet’s $SMB = Accumulation - Ablation + Refreezing$.

$$P = P_{PD} 1.04^{T_I - T_{I.PD}} \quad (2.1)$$

$$T_I = 88.9 + 0.67T_s \quad (2.2)$$

$$A = \frac{\Delta t (\epsilon_{atm} (1 - \alpha) Q + 10T_s + C_{abl})}{\rho_{fw} L} \quad (2.3)$$

Here, P [m/yr] is the precipitation, T [K] is the temperature above the atmospheric inversion layer, and subscript PD describes present day reference values. A is ablation [Water equivalent/yr], Δt [yr] is the timestep, ϵ_{atm} is the atmosphere's average transmissivity, α [-] is the surface albedo, Q_{sw} [W/m^2] is the incident radiation at the TOA, T_s [K] is the surface temperature, C_{abl} is the Greenland specific ablation coefficient (40), ρ_{fw} [kg/m^3] is the fresh water density, and L [J/kg] is the latent heat of fusion. These equations as defined and implemented in ANICE are taken directly from (De Boer et al., 2013).

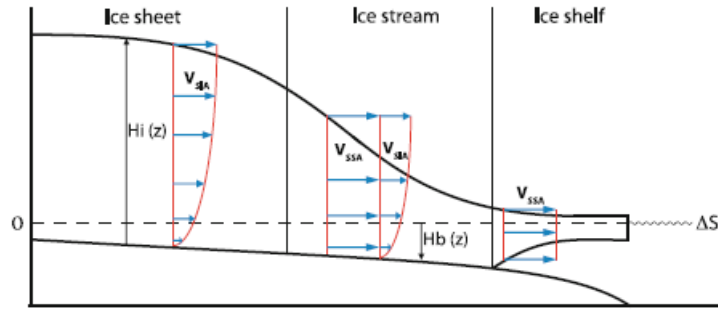


Figure 2.1: Visualisation of the implementation of different flow regimes in ANICE as introduced by De Boer et al. (2013). The simulated ice flow is described by the SSA in regions characterised by slow moving ice, the SIA in regions characterised by ice shelves, and a combination of SIA and SSA in the transition zone between slow moving ice and ice shelves.

Accurate ice dynamics simulations require the simulation of ice shelves which are significant in buttressing the ice sheet and affect ice motion, ice loss through calving, ice loss through basal melting, and ice discharge at the grounding line. Furthermore, the ice dynamics are affected by the potential onset of marine ice sheet instability and are significant in increasing stability of the GrIS through re-advancement of the grounding line.

Inaccuracies in ANICE's Greenland specific implementation results in simulated ice growth onto the continental plate as reflected in Fig. 2.2. The visualised results are obtained at $t = -115$ ka BP and differ in the inclusion of ice shelves. The results with shelves grow beyond the maximum extent observed at LGM and ground into Baffin Bay resulting in the formation of a continuous ice mass between Greenland and Ellesmere Island. Varying flow enhancement parameters to reduce growth towards the periphery or increased calving (up to 200 meters) does not affect the results. This effect is caused by a combination of erroneous flow description in response to the complex local geography and because of an improper description of the SMB. The result is rampant ice sheet growth visualised in Fig. 2.2.

Resolving this is non-trivial and requires a dedicated parameter study and a revision of the implemented flow description and mass balance definitions. This is outside of the scope of the current research. As such, ice shelves are not simulated and the growth of ice shelves is truncated by the immediate calving of any ice shelf formation. The resultant growth in the absence of ice shelf formation is also visualised in Fig. 2.2 over the initial 5,000 year period and shows the much reduced and, for the purpose of this study, acceptable ice growth. The exclusion of ice shelf formation from this study has important ramifications for the effect of grounding line feedback on the GrIS' evolution because it leads to the exclusion of ice shelf buttressing

which affects ice flow towards Greenland’s periphery.

The inability to accurately simulate ice shelf formation has consequences for the GrIS’ mass balance. The mass balance implemented in ANICE is described by $MB = SMB + BMB - \text{Ice Discharge}$ (De Boer et al., 2013). The exclusion of ice shelves in ANICE results in the exclusion of basal melt. Consequently, the relevance of marine-grounded ice growth onto the continental shelf and variations in relative sea level do not affect the rate of basal melt. It does, however, still affect the rate of ice discharge.

In addition, the SMB is affected by the exclusion of ice shelves through the increased growth of ice on the periphery. The increased surface load causes a stronger GIA signal which theoretically leads to increased subsidence of coastal bedrock. A change in ice thickness and change in bedrock elevation combine to change the surface elevation which leads to differences in elevation dependent accumulation and ablation. Furthermore, Increased subsidence leads to an increased RSL and therefore increased ice discharge. In addition, the increased ice thickness at the periphery leads to increased ice thickness at the grounding line which further affects the ice discharge. Thus, the effect of excluding ice shelves is significant by affect the MB through the changes to the SMB, the basal mass balance, ice discharge, and has ramifications for the ice dynamics.

Nevertheless, the effect of GIA on grounding line migration feedback and GIA-elevation-mass balance feedback is diminished but not absent. As such, the choice to exclude ice shelf formation from ANICE will affect the accuracy of the ice growth and will affect the extent of the aforementioned feedback mechanisms but will not completely eliminate these effects from the coupled simulation results. Therefore, allowing a study of the research question via the subquestions postulated in section 1.3.

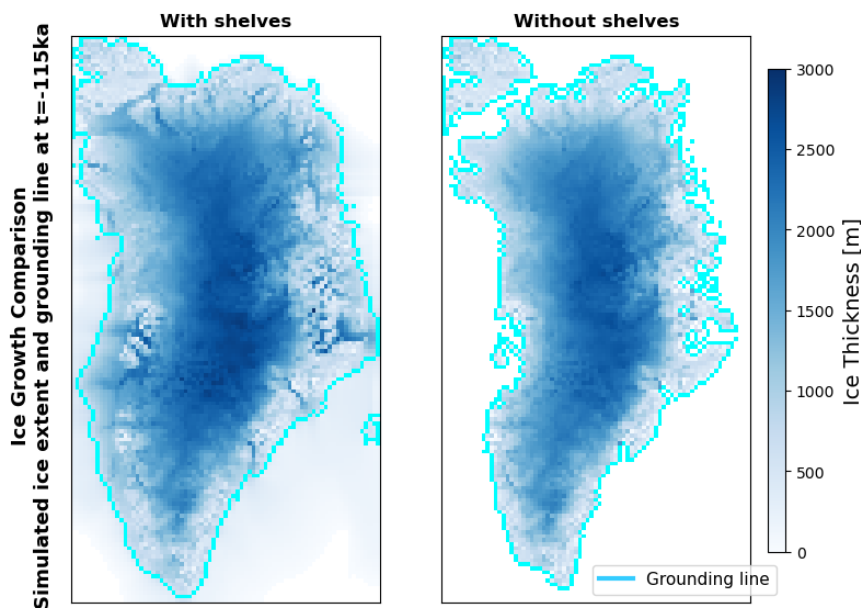


Figure 2.2: A comparison of the difference in ice growth when including ice shelves (left) and excluding ice shelves (right) using ELRA to determine vertical bedrock deformation. Inclusion of the ice shelves leads to rampant ice growth leading to ice shelf formation beyond Iceland and grounding into Baffin Bay.

2.1.2 3D Earth Modelling - FEM

The coupled 3D ice sheet and 3D GIA model uses a FEM approach that computes the modelled Earth’s deformation in three dimensions to determine GIA. The deformation depends on internal stresses within the Earth model that are dictated by the applied loading history. The loading history is obtained with

ANICE.

The FEM approach used by [Van Calcar \(2020\)](#) simulates deformation globally at a low resolution and underneath the AIS at a high resolution. The high resolution mesh is applied to all model layers above the core-mantle interface as defined by a half-angle relative to the $-Z$ axis (south). This method is efficient because the AIS is largely centered on the south pole. This is not true for the GrIS which exists south of the North Pole and which is present in a single quadrant of the northern hemisphere. Consequently, application of high resolution meshing by seeding a section of the spherical Earth approximation characterised by a half angle about the $+Z$ axis (north) would be inefficient. This reduces the computational performance of the coupled 3D GIA and 3D ice sheet simulation by needing to compute the GIA at a high resolution for an area ~ 160 times larger than the 2.166 km^2 covered by Greenland.

To improve efficiency of the FEM by reducing the area meshed at a high resolution two novel approaches are implemented. The first approach takes an arbitrary shape and uses ABAQUS to create N-3D components of the shape with a thickness corresponding to each of the N-layers above the core-mantle interface included with the Earth model. These shapes are defined by their basic geometry (e.g. cylindrical to create a spherical-section cutout and rectangular to create a slab cutout) and the depth of the N^{th} layers. The shapes are used to create similar sized cutouts in ABAQUS' assembled Earth model at a location specified by ϕ and λ relative to the local coordinate system (see [Fig. 2.3](#)). This allows for increased flexibility and control over the application of a high mesh resolution with a radially and laterally homogeneous seeding as defined by the user. However, the consequence of creating cutouts using such shapes at arbitrary locations is the warping of the mesh adjacent to the applied cutout (see [Fig. 2.4](#)). Simulated GIA signals in response to the application of a slab load to the warped mesh diverged from results obtained for a smooth mesh by upwards of 6.5 meters. The difference can have significant repercussions for ice growth on long timescales which necessitated the development of a second approach.

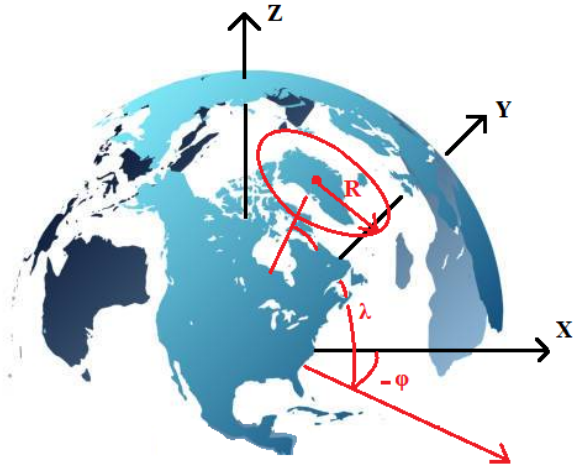


Figure 2.3: The application of a high mesh at an arbitrary location is defined by the longitudinal (ϕ) and latitudinal (λ) position relative to the local (x,y,z) with the high resolution mesh characterised by the basic geometry of the required shape (e.g. circular defined by radius R relative to the defined coordinate). Image: gettyimages.

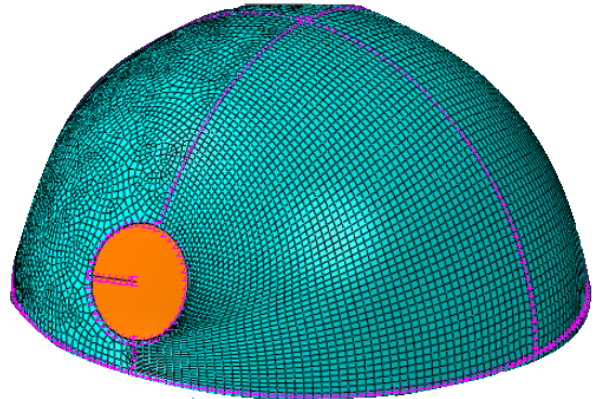


Figure 2.4: Application of a cutout at an arbitrary location leads to irregular mesh warping due to a mismatch in the alignment of the high resolution mesh and the adjacent low resolution mesh. The irregular warping may affect the interpretation of results and prevents the method from being employed.

The second approach that was developed uses the same cutout principle to create a high resolution mesh at any of the intersections between the local axis system and the solid-Earth model. Subsequently, a second local coordinate system (\hat{x}) is made by rotating the original coordinate system (x) about the positive X

(north locally) and positive Z (Greenwich locally) axis by 14 and 14.4 degrees respectively. The new coordinate system is then defined as $\hat{\mathbf{x}} = R_x(14)R_z(14.4)\mathbf{x}$ using basic rotations described by Equation 2.4.

Application of the load relative to this novel coordinate system, consistent with the interpolation from the computed surface load using ANICE as defined by the latitude and longitude taken from the ANICE grid, leads to the application of the load over the high resolution grid defined in the original coordinate system. Therefore, rather than bringing the high resolution area to Greenland, Greenland is taken to the high resolution area. The consequence is a homogeneous mesh at the surface with slight irregularity in meshing with depth resulting from the incompatibility of the seeding in radial direction with the defined layer thickness. A cutout of the high resolution mesh is visualised in Fig. 2.5. The difference in simulated GIA following the application of a slab load reduces to less than 3 meters. The result of the application of the load associated with the simulation's first timestep is visualised in Fig. 2.6 and demonstrates the proper implementation of the method for simulating the GrIS at a high resolution cutout characterised by a small area (half angle of 15° relative to the positive Z axis).

Finally, the method for determining the GIA disables part of the spherical harmonics. Consequently, the application of the surface load at the north pole creates a misalignment with the Earth's spherical harmonics. Thus, the entire system is rotated a second time such that the applied load is aligned with the spherical harmonics. Furthermore, the method by Blank et al. (2021) for determining the effect of a stress dependent viscosity through a composite rheology characterised by creep and dislocation parameters also needs to be aligned with the novel coordinate system. Thus, when determining the dislocation and diffusion parameters using the method by Van der Wal et al. (2010) and subsequently assigning them to the FEM mesh, a third rotation is required. This concludes the changes to the FEM approach necessary to efficiently simulate the GIA for Greenland.

$$R_x(\alpha) = \begin{bmatrix} 1 & 0 & 0 \\ 0 & \cos(\alpha) & -\sin(\alpha) \\ 0 & \sin(\alpha) & \cos(\alpha) \end{bmatrix} R_y(\beta) = \begin{bmatrix} \cos(\beta) & 0 & \sin(\beta) \\ 0 & 1 & 0 \\ -\sin(\beta) & 0 & \cos(\beta) \end{bmatrix} R_z(\gamma) = \begin{bmatrix} \cos(\gamma) & -\sin(\gamma) & 0 \\ \sin(\gamma) & \cos(\gamma) & 0 \\ 0 & 0 & 1 \end{bmatrix} \quad (2.4)$$

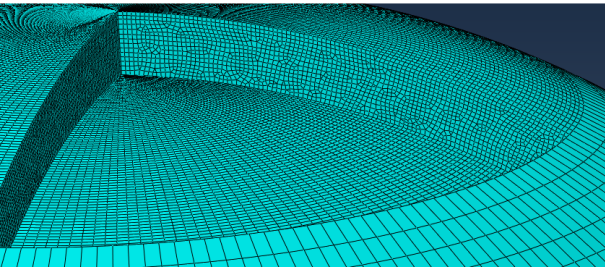


Figure 2.5: The application of a high resolution mesh at the spherical FEM model's north pole using a method of cutting the layers and replacing the cutout with an equivalent sized high resolution mesh shape. The cutout leads to warping of the mesh with depth and a smooth mesh at the surface.

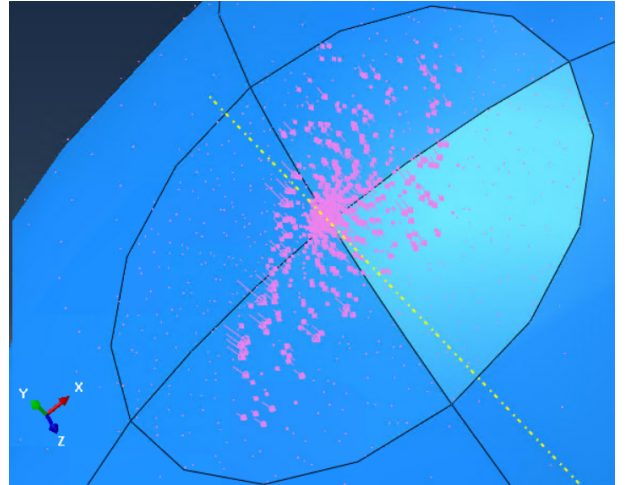


Figure 2.6: The application of the load, interpolated from ANICE to FEM, is correctly applied at the high resolution cutout by defining the position of the applied load relative to a secondary coordinate system rotated relative to the original coordinate system by: $\hat{\mathbf{x}} = R_x(14)R_z(14.4)\mathbf{x}$.

2.1.3 Model Interpolation - Oblimap

Oblimap’s implementation is taken from (Reerink et al., 2016). It provides a method for the rapid interpolation of data between two grids. The original implementation accounts for the input of data onto an ANICE grid of 141 by 91 grid cells with cell sizes of 20x20 kilometers. However, adaptations to ANICE have changed the scale of the simulation to a 141 by 77 grid of the same 20x20km cell size. This necessitated an update of the input fields for bedrock topography, ice thickness, and surface elevation. However, back and forth interpolation between the ANICE and GIA grid causes a shift in the applied surface loading and the computed deflection. This occurs because the center of the input fields has become misaligned with the assumed center of the interpolation. Thus, the applied load is displaced relative to the original load and the computed GIA will reflect on this translation in load by under- and over-estimating the simulated GIA in relation to the misalignment.

To remedy this, a series of tests were run that allowed for the unperturbed input of the ice thickness. The twice interpolated (ANICE to FEM, FEM to ANICE) ice thickness was subtracted from the original ice thickness and the resulting difference can be used as a gauge for the necessary shift in the assumed center of the interpolation. Visual observation of the first run demonstrated that the input was estimated to be further south-west than the actual input. As such, the latitude and longitude of the interpolation was incrementally increased to replicate the necessary shift in the assumed center of the interpolation. In addition, the standard parallel of the projection (α) was iterated for each combination of λ and ϕ . Using this iterative procedure the best performing combination of λ , ϕ , and α were found to be $\lambda_M = 319^\circ$, $\phi_M = 72^\circ$, $\alpha = 7.1^\circ C$. For future reference: this describes the center of the projected input bedrock, ice thickness, surface elevation, surface velocity, ice temperature, and mass balance fields for Greenland.

2.1.4 Model Interpolation - Coupling

The ANICE and FEM models, adapted for Greenland, are coupled using the approach developed by Van Calcar (2020). The method is visualised in Fig. 2.7. The timesteps used to iterate on are 5,000 year steps for the initial simulated 100,000 years since the mid-Eemian and steps of 1,000 years over the last 20,000 years.

The coupled model’s implementation iterates between ANICE and FEM until the convergence criteria is satisfied. Initial simulation results for a coupled 3D ice sheet and a laterally homogeneous 3D Earth model demonstrate that the simulated bedrock deflection approaches the converged solution’s mean bedrock elevation within 98.5% following on the first iteration of ANICE. The variation in convergence with every simulated timestep is visualised in Fig. 2.8. The notable improvement in performance following timestep 19 is a consequence of the reduction in timestep size from 5,000 to 1,000 years.

Also visualised in Fig. 2.8 is the maximum difference in vertical bedrock displacement on the simulated 77x141 ANICE grid. Comparison of the difference in maximum vertical displacement demonstrates that the difference does not exceed 2.5 meters for every timestep, anywhere on the simulated field. Thus, there are no significant regional differences in the simulated deflection that are not reflected in the percent convergence towards the converged solution of the iteration ANICE-FEM run. The single iteration approximates the converged solution very well.

The convergence performance of a single iteration coupled run demonstrates that multiple iteration simulations (up to 9) which force the model towards convergence is not required. Consequently, a ~threefold improvement in coupled simulation performance may be obtained by assuming that the single iteration simulation results are descriptive of the studied behaviour. Thus, similar to Van Calcar (2020), convergence is assumed at the end of the first iteration for every timestep for both literal homogeneous and laterally heterogeneous Earth approximations.

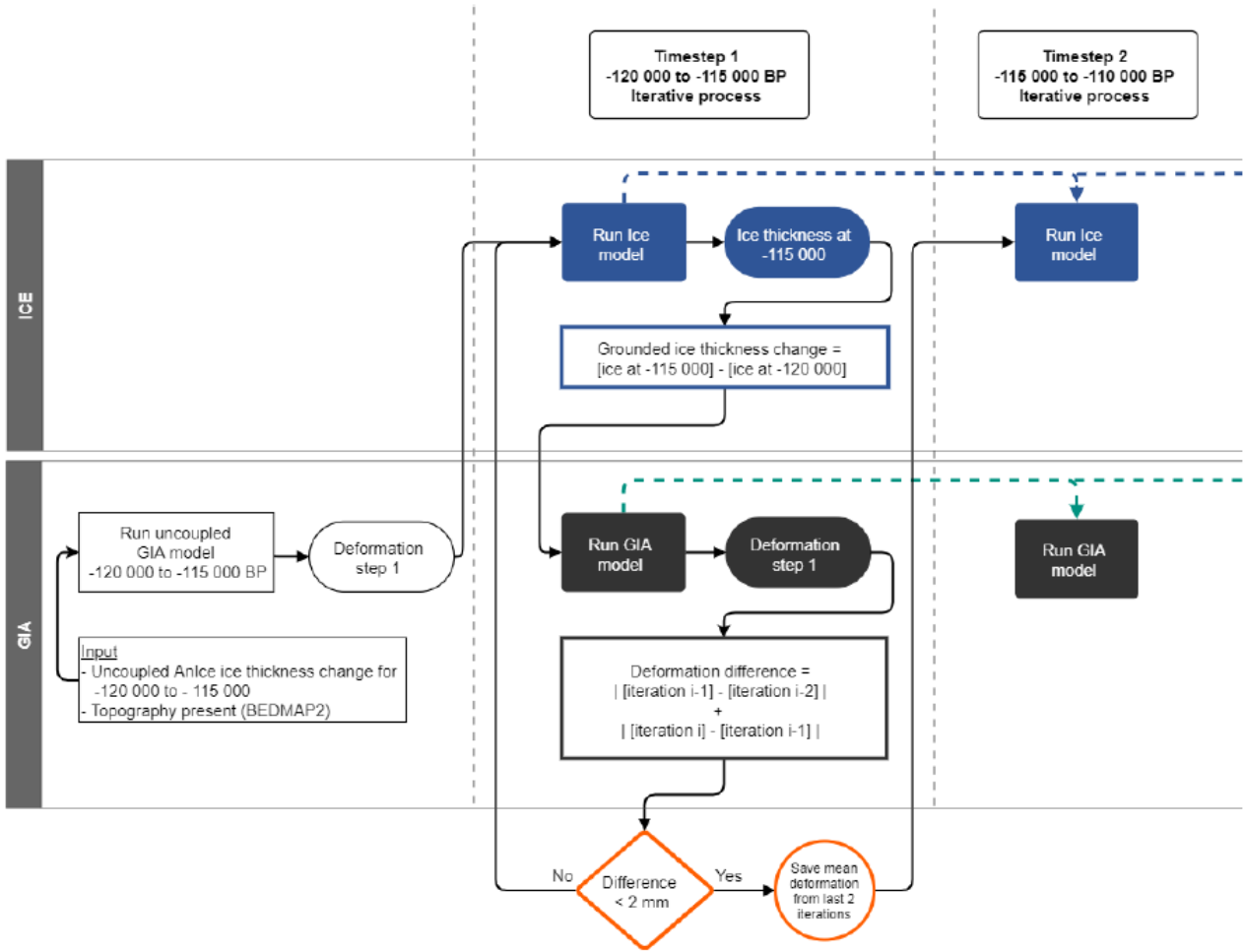


Figure 2.7: A block diagram describing the forward modelling procedure by which the ANICE and FEM are coupled and iterated (Van Calcar, 2020).

2.2 Coupled model input

Coupled ANICE-FEM simulations require model input to replicate the environment in which the GrIS evolves. Necessary model input is taken from a variety of sources and crucial input is reiterated here. This does not include an extensive discussion on model parameterisation which is largely defined in cited papers or as used in previous version of ANICE and FEM iterations unless stated otherwise.

2.2.1 Ice sheet model input

Present day ice thickness (H_i [m]), bedrock elevation (H_b [m]), and surface elevation (H_s [m]) are adapted from Bamber et al. (2013) and are visualised in Fig. 2.9. These fields are taken as model input at the mid-Eemian simulation start (-120ka BP) for first iteration coupled runs and a reference ANICE run using ELRA as mechanism for computing bedrock deflection. Second and third iteration coupled model runs append the input fields for bedrock elevation and surface elevation using the difference in output from the preceding run with the bedrock visualised in Fig. 2.9. Bedrock input is updated with Equation 2.5 and elevation input with Equation 2.6. Where H_{b_i} and H_{s_i} are the i^{th} iteration's input bedrock elevation and surface elevation respectively, where $H_{b_{PD\ Observed}}$ and $H_{i_{PD\ Observed}}$ are the observed present day bedrock elevation and ice thickness respectively, and where SL, ρ_{ice} , and ρ_{sea} are the sea level, ice density, and sea water density respectively. Finally, note that the ice sheet is assumed to be in isostatic equilibrium at

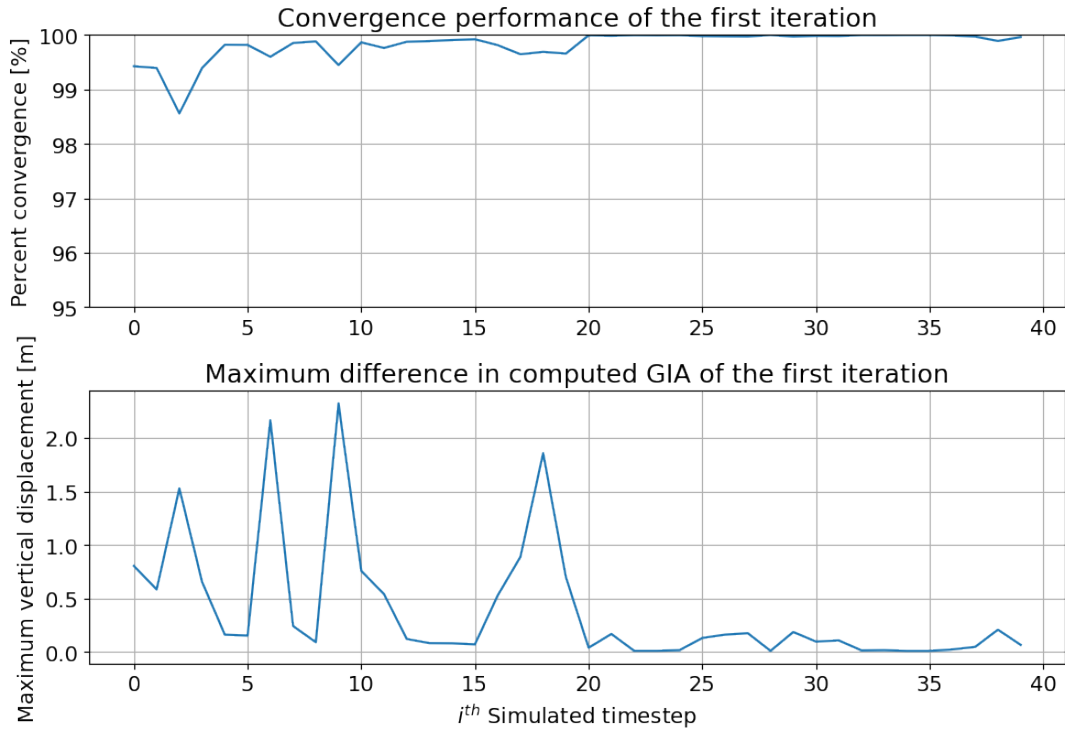


Figure 2.8: A comparison of the performance of a 120,000 year converged coupled 3D ice sheet and 3D GIA model run by considering the convergence of the first iteration ANICE-FEM output with the final iteration ANICE-FEM output and by considering the maximum difference in vertical bedrock displacement between the first and final iteration.

simulation start and the horizontal surface velocity and rate of melt at the ice sheet’s bedrock are set to zero at simulation start.

$$H_{b_i} = H_{b_{PD\ observed}} - (H_{b_{PD\ i-1}}) - H_{b_{PD\ observed}} \quad (2.5)$$

$$H_{s_i} = H_{i_{PD\ observed}} + MAX \left(SL - \frac{\rho_{ice}}{\rho_{sea}} * H_{i_{PD\ observed}}, H_{b_i} \right) \quad (2.6)$$

The model is forced by a time varying global temperature and eustatic sea level estimate taken relative to PD. These values are obtained from the ERA-40 monthly averaged dataset by Uppala et al. (2005) and are visualised in Fig. 2.10. Temperature and sea-level forcing is invariant between different model runs and iterations. The applied insolation forcing is taken from Laskar et al. (2004). Regional variations in precipitation, surface temperature, and heat flux are also adapted from the ERA-40 re-analysis (Uppala et al., 2005). Other model input includes the deflection computed with FEM and interpolated using Oblimap which is applied as a linear bedrock elevation change over the timestep at the start of the ANICE run. Other ANICE model input and model parameterisation is defined in De Boer et al. (2013, 2014) This includes the parameterisation of e.g. water salinity, water density, ice density, sliding coefficients, atmospheric lapse rates, Earth geometry, frictional heating coefficients, Greenland specific ablation, Greenland specific flow laws, etc.

2.2.2 FEM input

Relevant FEM input includes information on the to-be-applied initial load and the definition of the 3D Earth’s structure, viscosity, and elastic parameters. The first iteration coupled model runs are provided

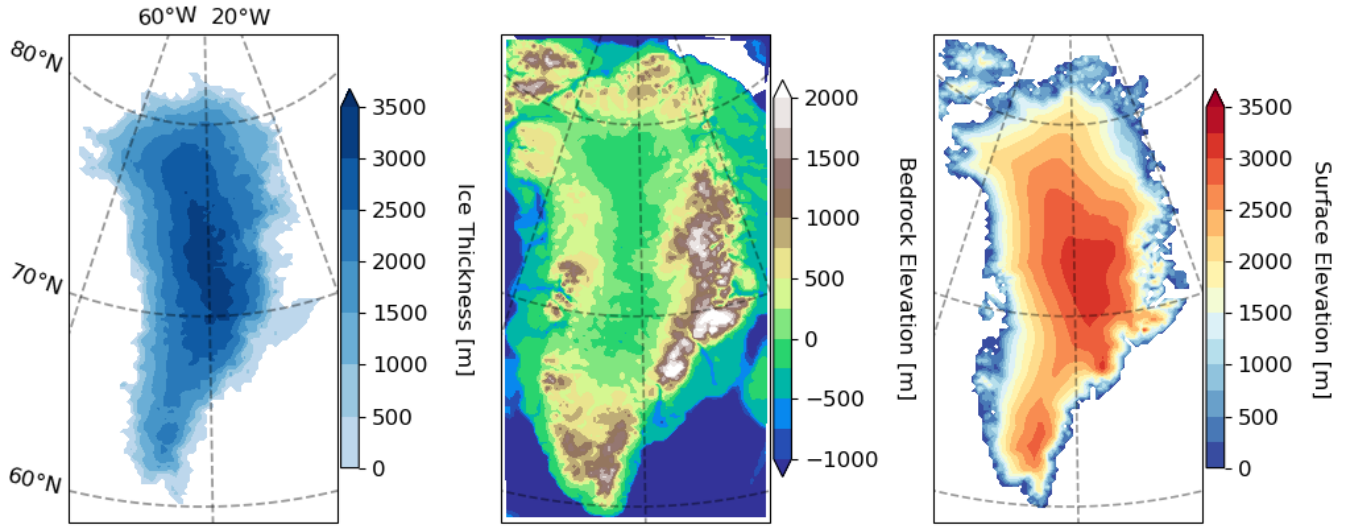


Figure 2.9: Model input ice thickness (left), bedrock elevation (middle) and surface elevation (right) adapted from observed present day values described by [Bamber et al. \(2013\)](#) using Oblimap2.0 by [Reerink et al. \(2016\)](#).

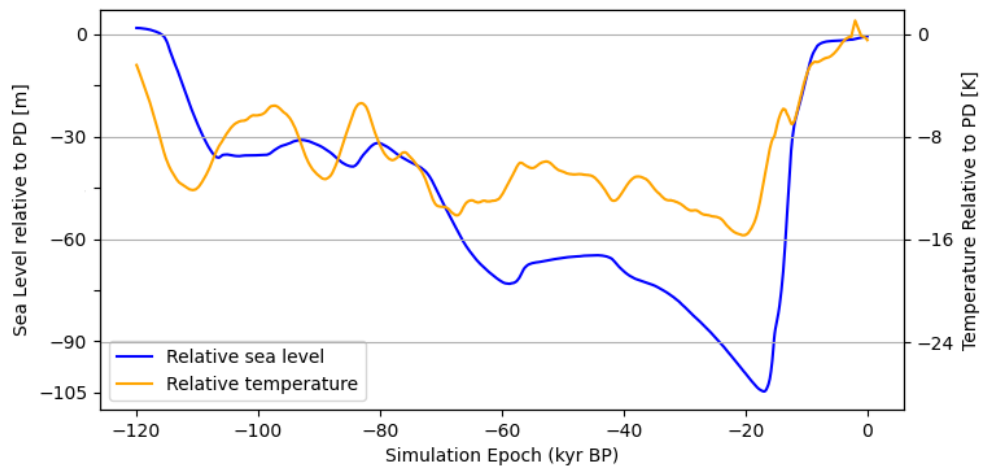


Figure 2.10: Input variation in global temperature changes and sea level changes relative to present day used for model forcing ([Uppala et al., 2005](#))

an estimate of the applied surface load over the first timestep in accordance with the coupling method described in [Fig. 2.7](#). The estimated load is obtained using ANICE which uses ELRA as mechanism for computing the bedrock deflection. Each subsequent timestep is then forwarded a new surface load which is computed with ANICE over the $i+1^{th}$ timestep. The estimated load is applied to the FEM as a linearly increasing load over the simulated timestep. Similarly, the computed deflection is applied to the ice sheet model as a linearly changing deformation. This processes of successively computing deformation and load changes and applying them to ANICE and the FEM model respectively is repeated until the simulation ends at PD. One consequence of the chosen routine is an overestimation of the changes in applied surface loading. Ice sheet waxing and waning in marine-grounded sections of the ice sheet causes ice to occupy space previously occupied by water. The model does not consider the previous application of load by the replaced ice or water. Thereby overestimating the applied variation in surface loading leading to larger simulated GIA. However, this effect is small and can be neglected.

Large parts of central Greenland's ice mass redistributes to the periphery and where significant growth at the periphery up to the coastline establishes an alternating pattern of positive and negative applied loads. The simulated load in meter-ice equivalence (MIEQ) is then applied to the FEM which computes an estimated pattern of uplift and depression in response to the visualised change in surface loading. The estimated deflection is applied to ANICE to obtain an improved loading scenario which is used as starting point for the coupled ANICE and FEM simulation. All first iteration simulation results employ the visualised divergence from equilibrium as initial loading scenario. Each subsequent iteration, where the first timestep's model input at the mid-Eemian is iterated using the previous iteration's output at PD, are provided a novel loading estimate obtained with ANICE using ELRA. Thus, the first iteration coupled runs have equivalent loading of the first timestep and the applied loading diverges for each subsequent timestep and iteration in response to the defined sub-Greenland viscosity. The first iteration-first timestep's surface load estimated with ANICE using ELRA is visualised in [Fig. 2.11](#).

FEM input also requires the definition of the 3D Earth's structure. Two laterally homogeneous and two laterally heterogeneous Earth structures are used for the purpose of this study. These are introduced in [section 2.3](#).

2.3 1D and 3D Earth Structure Definitions

Essential in understanding the effect of lateral heterogeneity on the GrIS' evolution is a representative 3D Earth model. Three models are used to construct a framework for discussion. First, a bi-layered Elastic Lithosphere Relaxing Asthenosphere (ELRA) is used with ANICE to generate initial load estimates for simulation initialisation. Second, two stratified radially varying one dimensional Earth structures are defined through layer viscosity and elastic parameters. Finally, a number of three dimensional (3D) Earth structures are defined by the definition of element-wise dislocation and diffusion creep parameters dependent on mantle water content and grain size estimates. The models are defined and elaborated on in this section.

2.3.1 ELRA Earth structure approximation

Initial reference GrIS evolution results are obtained using ANICE which approximates bedrock deformation with Elastic Lithosphere Relaxing Asthenosphere. This reference simulation does not couple the 3D ice sheet model ANICE with a Finite Element Model. Instead, bedrock evolution is obtained by "internally" computing bedrock deformation in response to a changing ice load at 10 year intervals.

ELRA approximates the Earth's response to changes in surface loading by computing elastic deformation of a linearly elastic lithosphere top layer and the deformation rate of a viscous asthenosphere bottom layer [Le Meur and Huybrechts \(1996\)](#); [De Boer et al. \(2013\)](#).

The magnitude and wavelength of the computed deformation, W (m), depends on the lithosphere's definition as described by [Equation 2.7](#). Here, q is the applied load, L_r the relative stiffness, D_e is the lithosphere's flexural rigidity, and χ the zero order Kelvin function. The computed response rate, $\frac{\partial W}{\partial t}$ ($m\ yr^{-1}$), to changes in applied load is dictated by the asthenosphere, detailed by [Equation 2.8](#). Where the rate of uplift depends on the divergence from the simulation's equilibrium state $W - W_0$ and the inverse of the relaxation time τ^{-1} ([De Boer et al., 2013](#)).

The bedrock adjustment computed with ELRA at step $i + 1$ is then a product of the combined elastic and viscous response [Le Meur and Huybrechts \(1996\)](#); [De Boer et al. \(2013\)](#). The implemented ELRA is then defined by [Table 2.1](#) and a lithosphere thickness of 100 kilometers.

$$W(z) = \frac{qL_r^2}{2\pi D_e} \chi(z) \quad ; \quad L_r = \left(\frac{D_e}{\rho_a g} \right)^{1/4} \quad (2.7)$$

$$\frac{\partial W}{\partial t} = \frac{-(W - W_0)}{\tau} \quad (2.8)$$

Lithosphere			Asthenosphere		
Constant - definition	Value	unit	Constant - definition	Value	unit
D_e - flexural rigidity	$1 \cdot 10^{25}$	$kg\ m^{-2}\ s^{-2}$	τ - relaxation time	3000	yr
ρ_a - mantle density	3300	$kg\ m^{-3}$			
g - gravitational accel.	9.81	$m\ s^{-2}$			

Table 2.1: ELRA parameterisation

ANICE with ELRA as specified by [Table 2.1](#) is used to approximate the first timestep's initial divergence from an assumed isostatic equilibrium at simulation start. Using input as specified in [section 2.2](#) and computing bedrock elevation change at 10 year intervals over a period of 5,000 years results in the changing surface loads visualised in [Fig. 2.11](#).

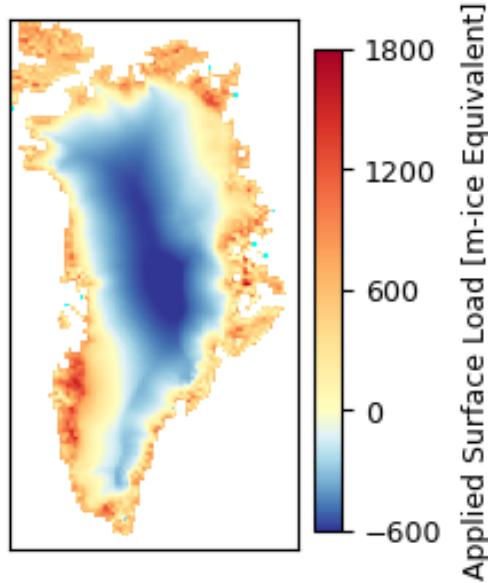


Figure 2.11: First iteration-first timestep estimated surface load for model initialisation obtained using ANICE with ELRA for a given initial topography and ice thickness

2.3.2 One dimensional Earth approximation

Computing surface deflection in response to changes in applied surface loading is possible using ELRA. In addition, ELRA allows for the simulation of lateral variation in sub-Greenland rheology through laterally varying relaxation times. ELRA thus provides a means for computing the response to a bi-layered 1D and a bi-layered 3D varying Earth rheology. However, ELRA computes a linear response to changes in surface loading. Furthermore, ELRA is an inherently simplified flat-Earth approximation that negates the effects of mantle variability with depth.

Conversely, computing the Earth's deformation using a Finite Element Methods (FEM) permits the analysis of the effects of including full spherical 3D visco-elastic Earth models characterised by both radially and laterally varying (non-)linear rheologies. In addition, computing deflection for such Earth models allows for the inclusion of self-gravitation and in extension of a perturbed gravity field. This results in temporal- and spatial-variability in the computed deformation in response to changes in applied surface loading which cannot be resolved, to this extent, with ANICE when using ELRA.

Therefore, studying the ramifications of variability in Earth rheology on the GrIS' evolution benefits from a higher fidelity FEM approach in the context of coupled ice sheet and solid Earth modelling. Two 1D Earth models are defined for analysis. Uncertainty in sub-Greenland Earth rheology and mantle composition has resulted in the definition of a relatively strong and a relatively weak 1D sub-Greenland Earth rheology. A relatively strong rheology is specified to simulate the response to a commonly accepted "realistic" sub-Greenland 1D viscosity profile and will be used as benchmark. The weak 1D rheology is defined to study the response of the GrIS in extreme scenarios where (rates of) depression and uplift are large and feedback between the GrIS and the GIA may be assumed strongest. The strong 1D rheology will henceforth be labeled as *1DR1* and the weak 1D rheology as *1DR2*.

The 1DR1 model is defined as a 5-layered radially varying Earth structure. The layers are characterised by their depth, viscosity, shear modulus, and density. [Table 2.2](#) describes the 1DR1 Earth structure. Studying the effects of radially varying and laterally varying Earth rheology on the GrIS' evolution requires the definition of a realistic sub-Greenland rheology. Such a rheology must result in simulated Earth deformation and sea-level changes that show good agreement with recorded sea level histories and observed

PD GIA signals when using a global ice loading chronology. Various authors have defined different ice histories for which various sub-Greenland 1D rheology definitions have been postulated. 1DR1 is then defined by considering these rheologies and isolating a "most common" sub-Greenland rheology as benchmark for initialising the coupled ANICE-FEM study. This method is required because the coupled model is not constrained by ice histories, where both the GIA and ice sheet are to evolve, meaning a reference must be used.

Lecavalier et al. (2014) introduces a spherically symmetric Maxwell viscoelastic rheology to compute the Earth's deflection underneath the GrIS. The approach combines insights from the Preliminary Reference Earth Model (PREM) on elastic and density parameters with layer-differentiated viscosity to generate simulation results differentiated by their fit of available RSL estimates. An optimal fit of available RSL data is obtained when defining a 1D Maxwell rheology characterised by a 120 kilometer Lithosphere Thickness (LT) with a viscosity of $\nu_{LV} = 1E44 Pa \cdot s$, a 550 kilometer upper mantle with an Upper Mantle Viscosity (UMV) of $\nu_{UMV} = 5E20 Pa \cdot s$, and a lower mantle extending to the outer core's interface with the lower mantle (at 2891 kilometers below the surface) with a Lower Mantle Viscosity (LMV) of $\nu_{LMV} = 1E21$ for the Huy2 ice history. The optimal fit for the improved ice history Huy3 is obtained by varying the LMV to $Pa \cdot s$ or $\nu_{LMV} = 2E21 Pa \cdot s$ (Lecavalier et al., 2014). A similar 1D viscosity was obtained for PREM which defines the optimal rheology as $\nu_{UMV} = 5E20 Pa \cdot s$ and $\nu_{LMV} = 2E21 Pa \cdot s$ (Dziewonski, 1981). Further research on Greenland specific GIA demonstrates that the same 120km LT, 5E20 UMV, and 2E21 LMV structure yields good results for simulating GIA in Greenland (Milne et al., 2018; Adhikari et al., 2021).

Thus, the little variability in optimal viscosity for ice histories Huy2, GrB, and Huy3 demonstrated by Lecavalier et al. (2014) and the precedent of using rheologies similar to that found by Lecavalier's in Greenland specific GIA studies by Milne et al. (2018); Adhikari et al. (2021) underpins the definition of a 1D Earth rheology benchmark as defined by Table 2.2. Where two sections of upper mantle are defined as "Upper Mantle-1" and "Upper Mantle-2" to reflect on a discontinuous shear modulus and density variation with depth. The elastic parameters and density parameters are defined by using PREM and the model is made incompressible.

Earth Layer	Layer Depth <i>km</i>	Viscosity <i>Pa · s</i>	Shear Modulus <i>Pa</i>	Density <i>kg · m⁻³</i>
Core	[0-3480]	0	1E-20	10750
Lower Mantle	[3480-5701]	2E21	2.28340E11	4978
Upper Mantle - 2	[5701-5951]	5E20	1.05490E11	3871
Upper Mantle - 1	[5951-6311]	5E20	0.70363E11	3438
Lithosphere	[6311-6371]	1E44	0.50605e11	3037

Table 2.2: One dimensional radially stratified solid Earth model (1DR1) definition based on work by Dziewonski (1981); Lecavalier et al. (2014); Milne et al. (2018); Adhikari et al. (2021).

The results obtained by Lecavalier et al. (2014) are skewed towards western Greenland by the large number of GPS stations in this region. The optimal 1D Maxwell rheology is therefore skewed towards matching the signal on the western coast. The spread of feasible combinations of LT, UMV, and LMV underpins the uncertainty in defining a 1D sub-Greenland rheology. Adhikari et al. (2021) finds that an optimal fit for eastern Greenland may be obtained for a 1D rheology defined by a LT of 120km, an UMV of $3E20 Pa \cdot s$, and a LMV of $5E22 Pa \cdot s$. Adhikari et al. (2021) also indicates that a viscosity as low as $6E19 Pa \cdot s$ may be required to accurately reflect recent changes in GIA following the Little Ice Age.

The possibility of a far reduced UMV is supported by results presented by Milne et al. (2018); Mordret (2018) which are indicative of such low UMV in (south)eastern Greenland due to the presence of a supposed "hot-spot track". Consequently, to gauge the difference in GrIS evolution when the upper mantle is described by a low viscosity a second 1D profile is defined to reflect on the possibility of this low $6E19 Pa \cdot s$ UMV. The possibility of a significant reduction in lithosphere thickness underlying southeastern Greenland,

evident in work by [Zhong et al. \(2003\)](#); [Milne et al. \(2018\)](#), is translated into a reduced LT for the 1DR2 model. As such, the 1DR2 will be described by [Table 2.3](#). The elastic parameters and density parameters are invariable relative to 1DR1.

Earth Layer	Layer Depth <i>km</i>	Viscosity <i>Pa · s</i>	Shear Modulus <i>Pa</i>	Density <i>kg · m⁻³</i>
Core	[0-3480]	0	1E-20	10750
Lower Mantle	[3480-5701]	2E21	2.28340E11	4978
Upper Mantle - 2	[5701-5951]	6E19	1.05490E11	3871
Upper Mantle - 1	[5951-6311]	6E19	0.70363E11	3438
Lithosphere	[6311-6371]	1E44	0.50605e11	3037

Table 2.3: One dimensional radially stratified solid Earth model (1DR2) definition using the low UMV estimate postulated by [Adhikari et al. \(2021\)](#) and a low-end lithosphere thickness derived from [Zhong et al. \(2003\)](#); [Milne et al. \(2018\)](#)

2.3.3 Three dimensional Earth approximation

A study of the effects of lateral variability in sub-Greenland rheology on the GrIS' evolution necessitates the definition of a global 3D Earth rheology. The model developed by [Van der Wal et al. \(2010\)](#) and expanded on in [Van der Wal et al. \(2013, 2015\)](#) is used for defining a 3D composite Rheology through the assignment of dislocation and diffusion creep to every element in the FEM model developed by [Van Calcar \(2020\)](#) based on work by [Blank et al. \(2021\)](#).

The 3D viscosity profiles are defined by their lithosphere thickness and dislocation and diffusion creeps. The dislocation and diffusion creep are dependent on the mantle material grain size and mantle water content. As such, a realistic bound on mantle material water content and mantle material grain size need to be established.

Both the mantle material grain size and mantle water content underlying Greenland are spatially variable and poorly constrained. A mantle material water content ranging from 0 to 100 ppm is considered realistic, however, studies of mid ocean ridge basalt and ocean island basalt have found that a water content in excess of 100 ppm may be feasible ([Ohtani, 2019](#)). The presence of ocean island basalt near Greenland may indicate the local presence of a (semi-)wet mantle ([Ohtani, 2019](#)). This observation is supported by [Karato \(2003\)](#) who finds that the potential hotspots underlying Greenland may be referenced as "wet-spots" which can have a water content varying from 600-1000 ppm ([Behn et al., 2019](#)).

Mantle material grain size is depth dependent and can vary up to centimeters in size ([Behn et al., 2019](#)). A plausible sub-Greenland grain size can be obtained by considering work by [Mordret \(2018\)](#) who finds that the grain size underlying Greenland at 180 kilometers depth can vary from 1 to 20 millimeters. Thus, mantle material grain size can vary from a sub-millimeter scale to tens of millimeters and is depth dependent. Additionally, water content is found to vary from dry (0 ppm) to wet (1000 ppm).

This wide range in feasible mantle material grain size and water content combinations leads to differences of several orders of magnitude in sub-Greenland stress dependent rheology. Consequently, additional input is required to constrain the feasible range of values further. The external input is provided by a study of GIA and GPS uplift rates in East-Greenland by V. R. Barletta. By studying a wide range of shallow and deep upper mantle viscosity values Barletta creates an overview of model performance when looking to replicate the recorded uplift in southeastern Greenland GPS measurement stations. The results for a lithosphere thickness of 90 kilometers are visualised in [Fig. 2.12](#). Darker colours reflect on improved fit for the Deep-UMV and Shallow-UMV indicated on the y and x axis respectively. The best fit for a 90km lithosphere thickness is obtained for a shallow upper mantle viscosity of 6E18 *Pa · s* and deep upper mantle viscosity of 4E19 *Pa · s*.

This provides the additional constraint required. The purpose of this study is to inquire into the effects of lateral variability on the GrIS' evolution. Of particular interest is the consequence of the locally decreased sub-Greenland viscosity underlying southeastern Greenland. Therefore, by creating a 3D profile that emulates the viscosity in the deep and shallow upper mantle at the KUAQ location a realistic description of the GIA and therefore the lateral variability in rheology for this region should be acquired. Visualised on Fig. 2.12 is the outline of possible combinations of shallow and deep upper mantle viscosity obtained when simulating the range of feasible mantle material water content and grain size. Since the viscosity is affected by stress contained within the mantle, two realistic stresses are used to make the outlines (1E5 Pa at model initialisation and 1.905E6 Pa at LGM). The best performing combination of Shallow-UMV and Deep-UMV contained by the respective outlines defines realistic 3D models that describe the effect of interest and is bound by a realistic grain size, a realistic water content, observed PD rates of uplift in southeastern Greenland, and realistic stresses contained within the mantle.

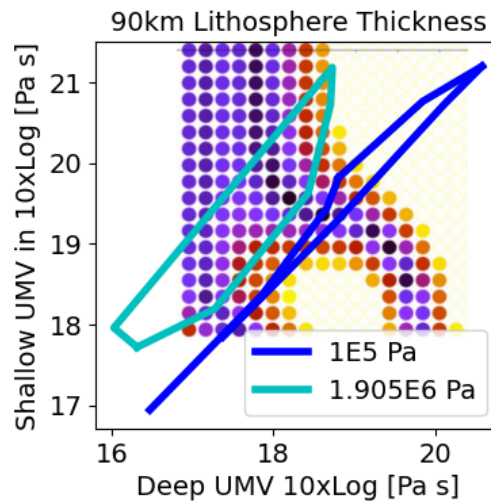


Figure 2.12: Visualisation of the effect of mantle water content, mantle material grain size, and mantle stresses on the range of feasible combinations of deep and shallow upper mantle viscosity on top of the performance in replicating uplift on southeastern Greenland's coast by V. R. Barletta. The 3DE5 and 3DE6 profiles including lateral variability in viscosity underneath Greenland are taken from the best performing combination of Shallow-UMV and Deep-UMV contained for the two extremes of realistic mantle stresses

The best performing combination of grain size and mantle water content for a mantle stress of 1E5 Pa is described by a 3 mm mantle material grain size and a water content of 75 ppm, henceforth labeled as 3DE5. The best performing combination for a stress of 1.905E6 Pa is described by a 3mm mantle material grain size and water content of 4.7ppm. The resulting viscosity profile underlying Greenland is visualised for an assumed mantle stress of 1E5 Pa in Fig. 2.13 for 3DE5 and in Fig. 2.14 for 3DE6.

2.3.4 3D and 1D solid Earth comparison

The reduced water content leads to a significant increase in viscosity for 3DE6 relative to 3DE5. The inclusion of lateral variation in sub-Greenland rheology leads to increased lithosphere thickness underlying western, northern, and central Greenland and reduced viscosity underlying southeastern coastal regions.

Two regions that are particularly important for the GrIS' ice loss are northwestern Greenland (Chen et al., 2011; Khan et al., 2016; Mouginit et al., 2019) and southeastern Greenland (Khan et al., 2016; Bunce et al., 2018; Weerdesteijn et al., 2022). To study the effect of including lateral variations in the sub-Greenland rheology a vertical viscosity profile is made for northwestern Greenland, southeastern Greenland, and central Greenland as a reference. These profiles are included in Fig. 2.15. The profile demonstrates that the viscosity in northwestern and in central Greenland is higher than the commonly adopted laterally homogeneous sub-Greenland rheology (indicated by a vertical blue line) near the surface and decreases below the 1D viscosity at increasing depths. In southeastern Greenland the viscosity profile is an order of magnitude smaller than 1DR1 for 3DE5 and similar to 1DR1 for 3DE5.

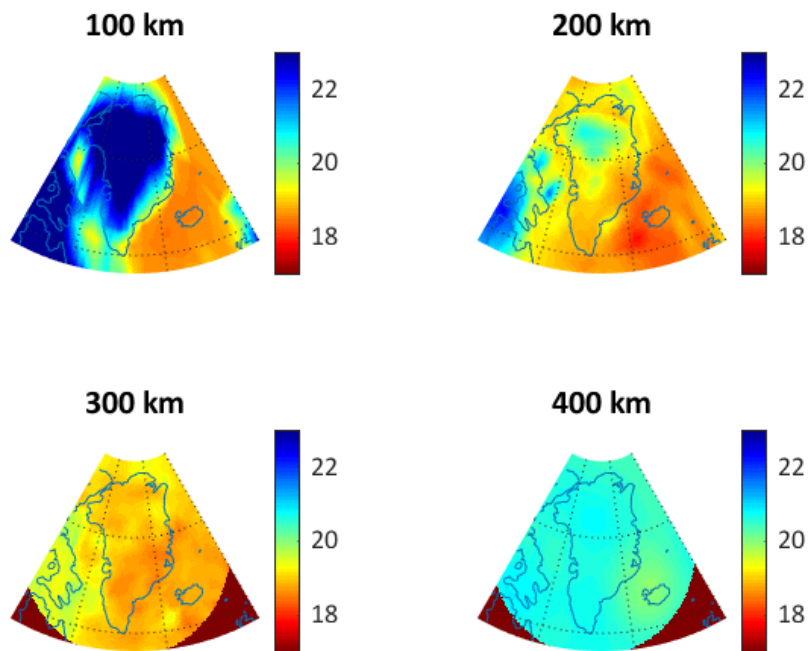


Figure 2.13: 3D Viscosity (3DE5) profile visualisation at depths of 100, 200, 300, and 400 kilometers for a mantle material water content of 75 ppm and an assumed grain size of 3 mm.

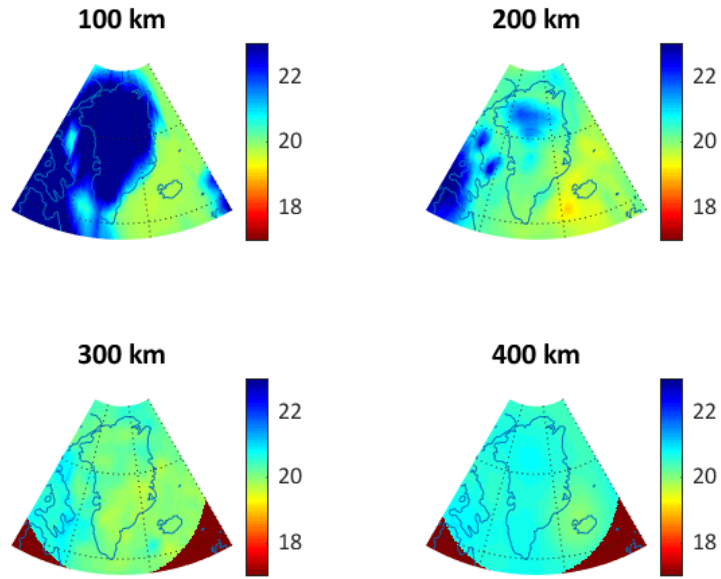


Figure 2.14: 3D Viscosity profile (3DE6) visualisation at depths of 100, 200, 300, and 400 kilometers for a mantle material water content of 4.7 ppm and an assumed grain size of 3 mm.

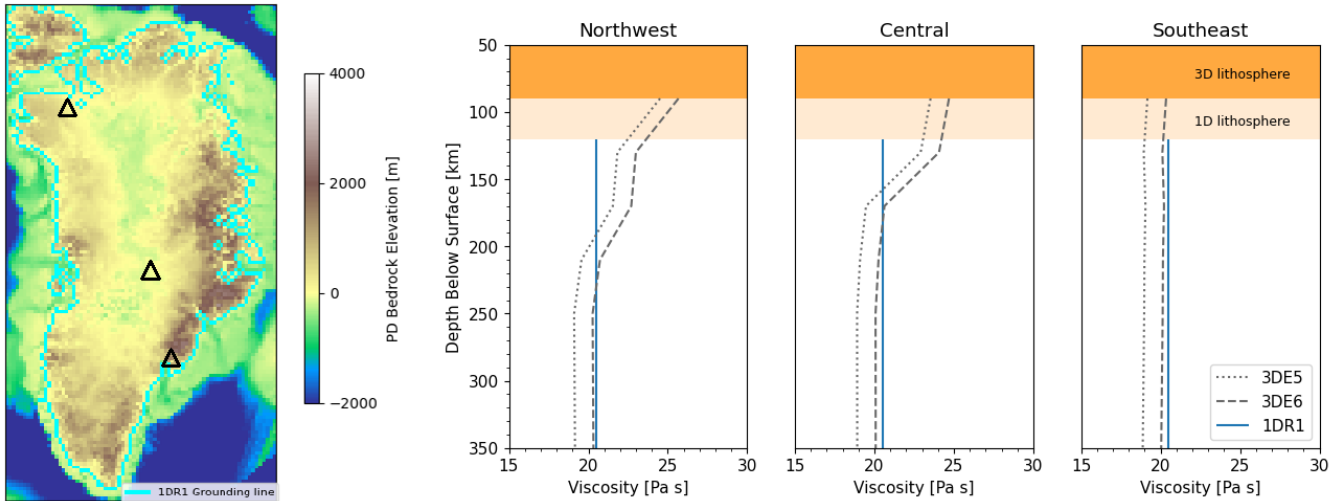


Figure 2.15: Vertical viscosity profiles associated with northwestern Greenland, central Greenland, and southeastern Greenland. The inclusion of lateral variations in the sub-Greenland rheology causes an increase in viscosity near the surface in northwestern and central Greenland and a decrease in southeastern Greenland.

Chapter 3

Results and Discussion

Four 3D Earth models have been defined to study the effect of lateral variations in sub-Greenland rheology on the GrIS' evolution in a coupled 3D ice sheet and 3D GIA model. The results will be discussed in this chapter.

First, the applicability of the simulated results will be asserted by evaluating the results obtained for the radially stratified laterally homogeneous viscosity profiles following the first iteration's first timestep in [section 3.1](#). The same section will present a discussion on the need for, and process of, iterating the model input to obtain realistic ice histories for a given viscosity profile. Subsequently, the effect of lateral variations in sub-Greenland rheology on GIA-elevation-mass balance feedback will be considered in [section 3.2](#). Thereafter, the effect of a 3D rheology on the grounding line migration and feedback on the ice sheet's growth and decline will be discussed in [section 3.3](#). Finally, the ramifications of varying the mantle water content on the GrIS' evolution will be elucidated in [section 3.4](#).

3.1 Applicability of the simulated results

The applicability of the simulated results depends on their ability to meaningfully describe the GrIS' evolution within the context of a coupled 3D GIA and 3D ice sheet model. Here, the first iteration first-timestep results will be analysed for the 1DR1 and 1DR2 laterally homogeneous Earth models to ascertain the relevance of the simulated results. Subsequently, the iterated model input and convergence to PD observed bedrock elevation is discussed.

3.1.1 One dimensional first iteration-first timestep simulation results

The simulated GIA response to the assumed ice loading obtained with ANICE using ELRA, see [subsection 2.3.1](#), is visualised in [Fig. 3.1](#). Consideration of the first timestep-first iteration's output is meaningful because input is equivalent and therefore any difference in the simulated GIA and subsequent ANICE is exclusively dependent on the difference in the 3D solid-Earth model's definition.

Comparison of the simulated GIA for 1DR1 and 1DR2 with the applied surface loading over the first timestep shows that the pattern of bedrock uplift and subsidence correlates with the magnitude of the applied surface loading. GIA in central Greenland characterised by a negative surface load leads to a positive vertical bedrock displacement and GIA on Greenland's periphery characterised by a positive load leads to negative vertical bedrock displacement. Furthermore, the magnitude in GIA for 1DR1 and 1DR2 aligns with the magnitude of the applied surface loading. Where regions characterised by increased loads applied over a large region result in increased bedrock displacement. The increased magnitude of the GIA simulated for 1DR2 reflects on the lower UMV and the reduced LT. The reduced wavelength of the response, reflected in the displacement of bedrock closer to the applied loads, is reflected in the difference in simulated GIA between 1DR1 and 1DR2. Thus, the difference in sub-Greenland rheology is accurately reflected in the

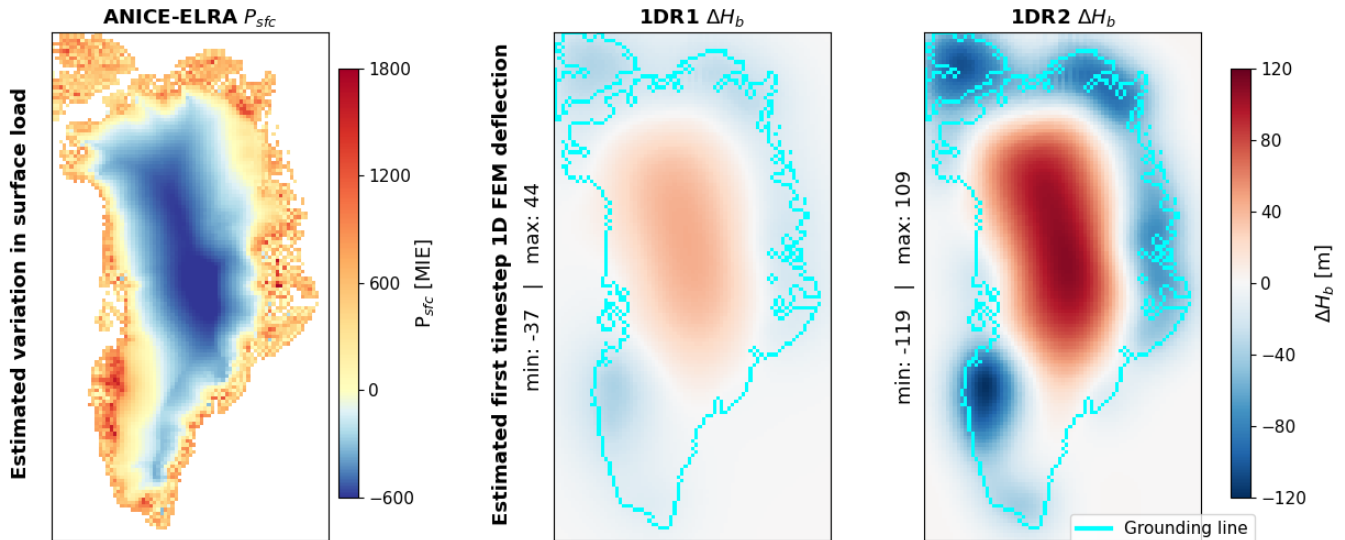


Figure 3.1: Visualisation of the bedrock response for 1DR1 (middle) and 1DR2 (right) to the estimated surface loading (left) obtained with ANICE using ELRA over the first iteration's first 5,000 year timestep.

computed GIA.

Coupling of GIA with ANICE through the inclusion of the simulated difference in GIA as a linear deformation applied to the bedrock in ANICE results in the difference with bedrock elevation and ice thickness results obtained for ANICE when using ELRA (ANICE:ELRA) as visualised in Fig. 3.2. Comparison of 1DR1 with ANICE:ELRA demonstrates that the increased lithosphere thickness and UMV leads to relative subsidence in central Greenland and relative uplift on Greenland's coastline. This is a consequence of the reduced effect of GIA caused by the stronger rheology. The results obtained for the first 5,000 years demonstrate that the difference in GIA leads to advancement of the grounding line through relative bedrock uplift (i.e. decreased 1DR1 subsidence) and increased ice thickness inland of the advanced grounding line. Also visible is the effect of GIA-elevation-accumulation feedback in a cooling climate which leads to increased ice accumulation at lower surface elevations (central Greenland) and reduced ice accumulation at increased surface elevations (coastal Greenland). Also represented must be the difference in ice ablation due to relative changes in surface elevation at lower altitudes. Thus leading to the inclusion of GIA-elevation-melt feedback. The significance of the effect is proportional to the difference in computed GIA which becomes apparent when comparing the difference in ice thickness in relation to the difference in GIA for 1DR1 and 1DR2 results. Thus, the simulation incorporates the effects of GIA-elevation-mass balance feedback and grounding line advancement feedback on the GrIS' growth starting from the first timestep. Differences in simulated GrIS histories in the coupled 3D ice sheet and 3D GIA model therefore reflect on the effects of variation in sub-Greenland rheology on the feedback mechanisms of interest. Thereby validating the simulated results.

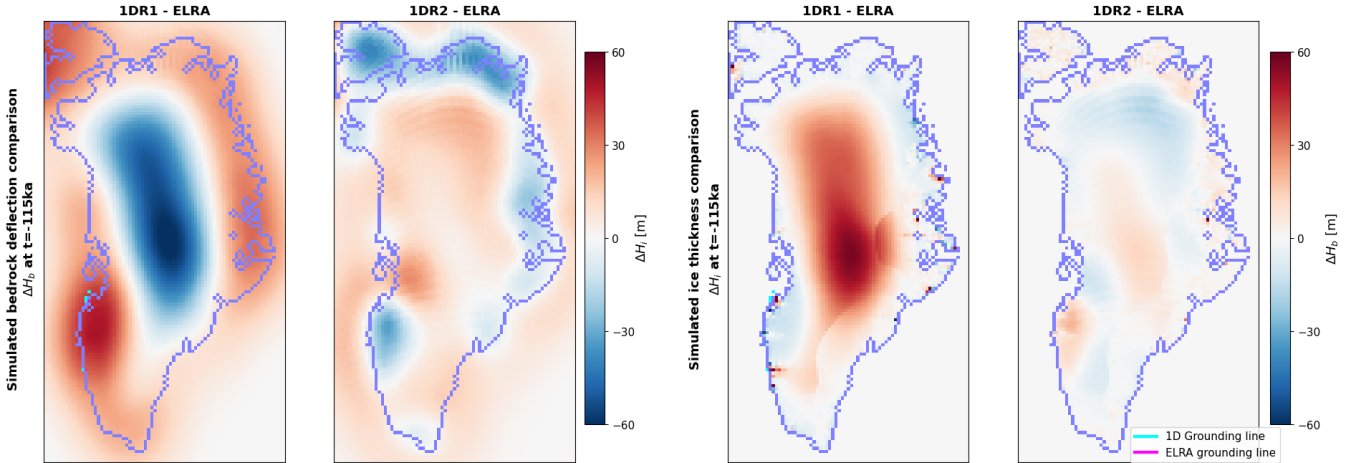


Figure 3.2: Comparison of the simulated GIA and coupled effect on the ice thickness with ANICE results obtained using ELRA for 1DR1 and 1DR2. Differences in GIA and ice thickness obtained are exclusively dependent on the differences in the Earth model and reflect the effect on grounding line migration feedback and GIA-elevation mass balance feedback.

3.1.2 Simulation convergence to present day observed bedrock elevation

The evaluation of the first iteration-first timestep coupled simulation results validates the correct implementation of the model’s intended functionality. The results demonstrate that variability in sub-Greenland viscosity is accurately reflected in the simulated GIA and that the simulated GIA affects the ice thickness via melt-elevation-mass balance and grounding line advancement following model initialisation. Thus, the effect of both feedback mechanisms, which is the topic of this study, must also be included. However, a large divergence in simulated bedrock elevation relative to the PD observed bedrock elevation is obtained when simulating the GrIS to PD. The difference with PD observed bedrock elevation for the first iteration simulated output is visualised in Fig. 3.3. This demonstrates, for a given viscosity, that the ice history is unrealistic which leads to an over- or under-estimation of the simulated GIA. Thus, the simulated results cannot be directly compared for the first iteration coupled 3D ice sheet and 3D GIA model runs.

The ice history can be improved by iterating the model input using the method discussed in section 2.2. The iterated model input employs the difference observed at PD for the previous iteration coupled model output to modify the initial surface elevation and bedrock topography. This differences in initial topography leads to an improved ice history for a given viscosity which leads to improved convergence to the PD observed bedrock topography for the second iteration coupled model run, visualised in Fig. 3.4. Then, simulation results at any recorded timestep may be compared under the premise that the GrIS’ state and sub-Greenland’s topography as recorded depends entirely on the used Earth model by eliminating the propagation of errors introduced by uncertainties in the definition of the initial topography. Thus allowing for a direct comparison of simulation results at the LGM and at PD.

Divergence from PD observed topography visualised in Fig. 3.4 demonstrates the inability of the coupled model characterised by the 1DR2 Earth representation to converge to PD observed bedrock topography. A third iteration of model input does not improve the convergence at PD as visualised in Fig. 3.5. Upon closer inspection of the difference in bedrock elevation at PD it becomes obvious that the formation of inland lakes through extreme subsidence under the positive applied surface loading leads to lake formation in northwestern Greenland (NWG) which causes an unrealistic negative applied surface load. Thus, further depression of the input bedrock elevation will result in increased lake formation which will reduce the applied surface load further and lead to yet increased relative uplift. Consequently, the 1DR2 model’s current definition cannot lead to convergence to PD observed bedrock elevation and is eliminated from the

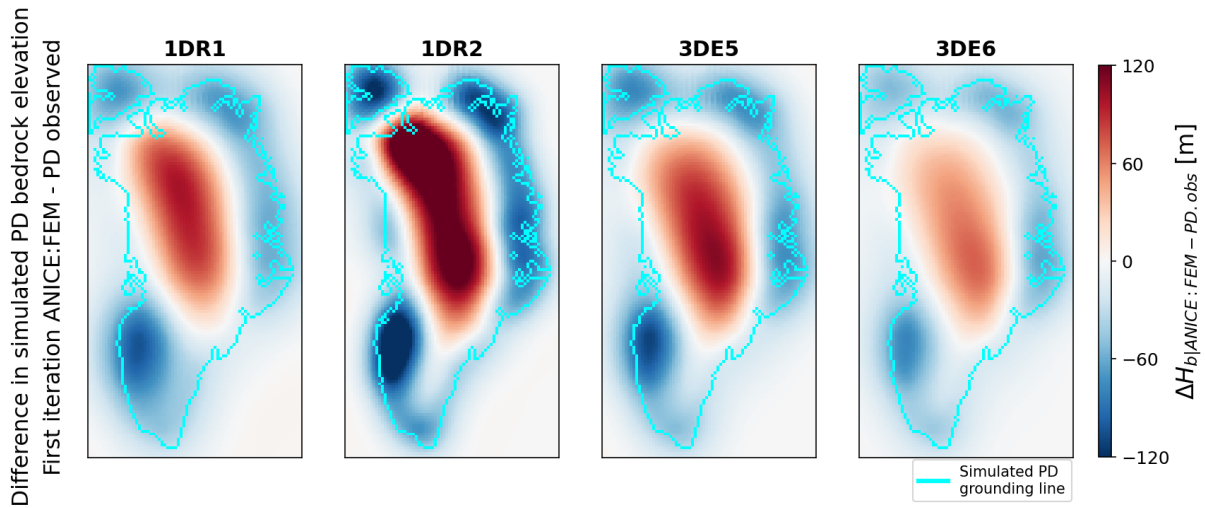


Figure 3.3: Assessment of the convergence of first iteration coupled ANICE:FEM simulation results towards PD observed bedrock elevation by visualising the difference for 1DR1, 1DR2, 3DE5, and 3DE6 - PD bedrock elevation

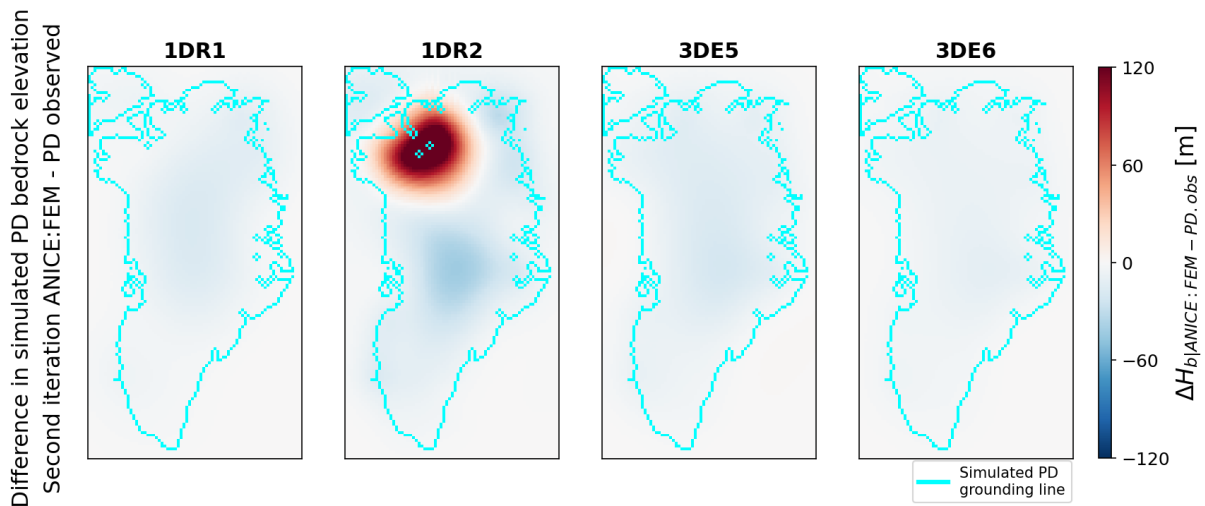


Figure 3.4: Assessment of the convergence of second iteration coupled ANICE:FEM simulation results towards PD observed bedrock elevation by visualising the difference for 1DR1, 1DR2, 3DE5, and 3DE6 - PD bedrock elevation

discussion. Therefore, the research question will be investigated by considering the simulated results for 3DE5 and 3DE6 relative to the simulated results obtained for 1DR1.

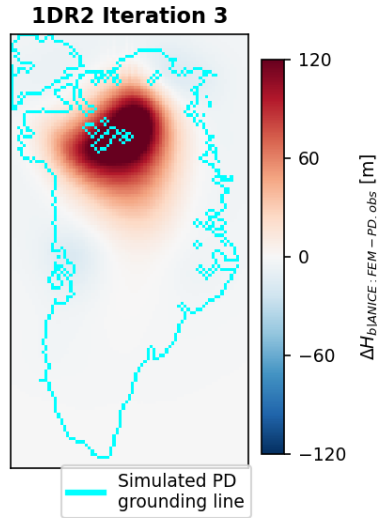


Figure 3.5: Assessment of the convergence of third iteration coupled simulation results towards PD observed bedrock elevation by visualising the difference for 1DR2 - PD bedrock elevation

3.2 3D GIA feedback on mass-balance

GIA leads to a vertical displacement of the bedrock which leads to a similar vertical displacement of the GrIS' surface elevation. Vertically displacing the ice sheet's surface leads to a change in surface temperature determined by a constant atmospheric lapse rate. Precipitation over the GrIS, introduced in [section 1.1](#) and [section 1.2](#) and modelled as discussed in [section 2.1](#), depends on the temperature at the inversion layer which is directly affected by temperature at the ice sheet's surface as described by [Equation 2.1](#) and [Equation 2.2](#) respectively. Ice melt at the ice sheet's surface, described by [Equation 2.3](#), is similarly dependent on the surface temperature and thus the surface elevation. Therefore, an increased surface elevation caused by GIA induced uplift leads to reduced precipitation and reduced melting of surface ice. The converse is also true when the bedrock subsides. Thus, one consequence of GIA is to affect the ice sheet's SMB by establishing a negative feedback loop between ice mass changes and both precipitation and surface melt. This section will discuss the effect of including lateral variations in the sub-Greenland rheology on the GrIS' evolution via the mass balance. To this end, coupled simulation results obtained for a laterally varying sub-Greenland rheology will be compared with results obtained for a commonly adopted laterally homogeneous sub-Greenland rheology at both LGM and at PD.

3.2.1 Mass Balance: Mid-Eemian to Last Glacial Maximum

Global mean temperature decreased by 15°C between the mid-Eemian and the LGM. As a result, this period is characterised by a waxing ice sheet resulting from a net positive SMB. Simulated results demonstrate that ice melt at the ice sheet's surface becomes negligible as global temperatures decreased by approximately 4°C in the initial 5,000 years following on the mid-Eemian. Thus, any difference in simulated GrIS waxing up to LGM can be primarily attributed to differences in ice flow dynamics and ice mass accumulation. Here, the effect of a difference in simulated GIA on the difference in ice accumulation is considered.

The applied surface loading is negative in central Greenland and positive at Greenland's periphery, see [Fig. 2.11](#). Therefore, vertical bedrock displacement in central Greenland is characterised by uplift and bedrock displacement in coastal regions is characterised by depression. The weaker GIA response to changes in applied surface loading resulting from a relatively strong 3DE5 and 3DE6 upper mantle rheology leads to a weaker uplift in central Greenland and a weaker depression in coastal regions relative to simulated 1DR1

results. The decreased bedrock uplift in central Greenland will place the 3DE5 and 3DE6 bedrock below the simulated 1DR1 bedrock. Conversely, the decreased 3DE5 and 3DE6 bedrock depression relative to the 1DR1 depression will place the 3DE5 and 3DE6 bedrock above the 1DR1 bedrock in coastal regions. The simulated difference in bedrock elevation and ice thickness at LGM is visualised in Fig. 3.6. The difference in bedrock elevation between 3DE5 and 1DR1 (1DR1 results subtracted from 3DE5) is visualised in Fig. 3.6A and the difference in ice thickness in Fig. 3.6C. The difference in bedrock elevation between 3DE6 and 1DR1 (1DR1 subtracted from 3DE6) is visualised in Fig. 3.6B and the difference in ice thickness in Fig. 3.6D.

Results simulated for both 3DE5 and 3DE6 show a comparable pattern of variation with 1DR1 in terms of both bedrock elevation difference and ice thickness difference at LGM. As such, processes that cause 3DE5 results to diverge from 1DR1 results at LGM also apply to 3DE6. Therefore, only 3DE5 results will be compared with 1DR1 results and any insights can be extended to the 3DE6 results. Differences between 3DE5 and 3DE6 will be discussed in section 3.4. The difference between 3DE5 and 1DR1 will be discussed by considering three regions of interest for which the vertical viscosity profiles were introduced in subsection 2.3.3: Southeastern Greenland, central Greenland, and northwestern Greenland.

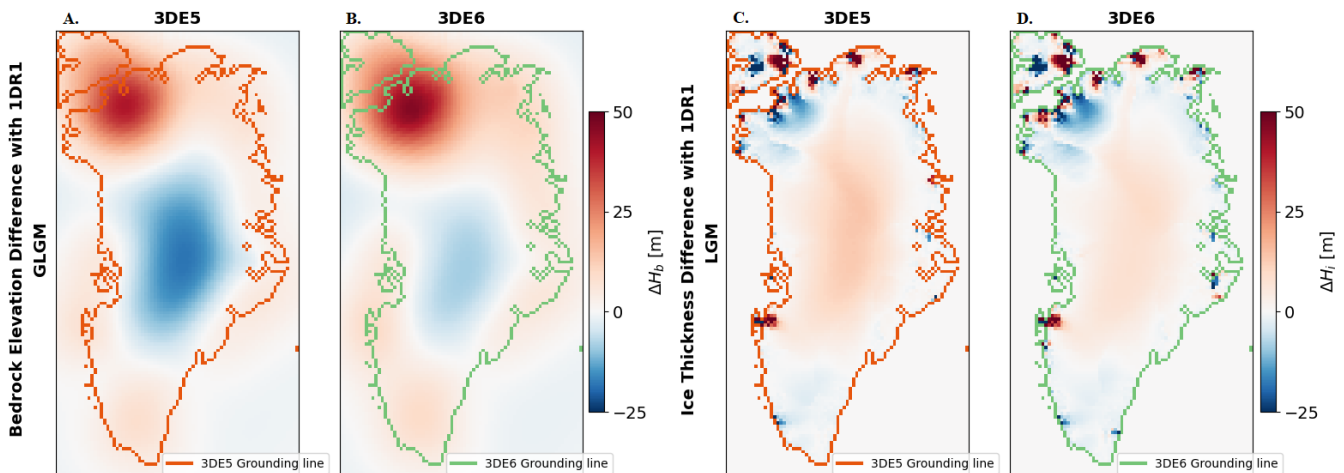


Figure 3.6: Simulated difference in bedrock elevation and ice thickness at LGM for 3DE5-1DR1 and 3DE6-1DR1 respectively.

Central Greenland is characterised by a negative difference in bedrock elevation (Fig. 3.6A.). This is a consequence of the inclusion of lateral variations in sub-Greenland rheology which leads to an increased mantle viscosity up to depths of 220 kilometers. This increased viscosity near the surface causes a weaker GIA signal which results in reduced uplift in central Greenland when compared with 1DR1 causing a negative difference in bedrock elevation at LGM. The region characterised by a negative difference in bedrock elevation corresponds to a region of positive difference in ice thickness (Fig. 3.6C.). As such, simulated ice thickness at LGM is larger for 3DE5 in central Greenland than for 1DR1 whilst bedrock elevation for 3DE5 is lower in central Greenland than for 1DR1. The difference in simulated ice thickness in central Greenland is a consequence of either differences in the simulated ice sheet’s SMB (SMB = accumulation - ablation + refreezing) or in the simulated ice flow. The waxing GrIS simulated for both 3DE5 and 1DR1 is not affected by ice melt at the surface after the initial simulated 5,000 years. Limited precipitation as

rainwater and insignificant meltwater runoff cause refreezing to have a marginal effect on the GrIS' waxing in central Greenland.

The GIA induced vertical displacement of bedrock underlying the GrIS leads to an approximately proportional vertical displacement of the ice sheet's surface elevation. Therefore, the difference in bedrock elevation between 3DE5 and 1DR1 translates into a comparable difference in surface elevation between 3DE5 and 1DR1. This difference in surface elevation is visualised at LGM in Fig. 3.7. The increased viscosity underlying central Greenland which causes a decreased GIA signal translates into a lower surface elevation of 3DE5 relative to 1DR1 in the southern portion of central Greenland. In the northern part of central Greenland the increased viscosity results in reduced uplift but this does not translate into a decreased surface elevation.

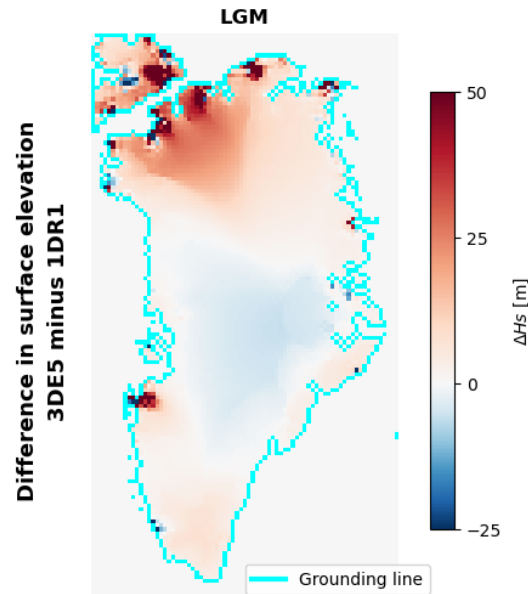


Figure 3.7: Difference in simulated surface elevation between 3DE5 and 1DR1 at LGM.

The reduced surface elevation in the southern section of central Greenland leads to increased precipitation and subsequent ice accumulation for simulation 3DE5 relative to simulation 1DR1. This is visible in the cumulative difference in simulated Accumulation (Gigatonne) between 3DE5 and 1DR1 in the 40ka leading up to LGM, visualised in Fig. 3.8A. Also visualised is the difference in simulated vertically averaged ice flow velocity between 3DE5 and 1DR1 40,000 years before LGM (Fig. 3.8B.) and at LGM (Fig. 3.8C.). Combined, these two dynamics describe the difference in simulated GrIS evolution up LGM and illustrate the significance of a difference in precipitation on the GrIS' growth. Cumulative differences in accumulation prior to 60ka BP are not included because the accumulation is affected by a melt component for the initial 5,000 years, a component attributed to the difference in the initial bedrock elevation state, and because the accumulation is subject to significant temporal variations due to the simulated ice flow resulting from an initial GrIS state that is not in equilibrium.

The difference in the simulated ice accumulation leading up to LGM Fig. 3.8A demonstrates that the positive difference in ice thickness between 3DE5 and 1DR1 in the southern section in central Greenland (Fig. 3.6 C.) is the consequence of a positive difference in accumulation between 3DE5 and 1DR1. Increased accumulation resulting from an increase in precipitation leads to a positive difference in mass accumulation up to 50 Gigatonnes over the 40,000 years leading up to LGM. Furthermore, the difference in flow velocity for this slow moving grounded ice is limited to less than 0.1 m/yr barring the formation of a number of streams towards Greenland's coast where flow velocity differences increase to approximately 1 m/yr as seen in Fig. 3.8B and Fig. 3.8C. Also visible is that this difference in simulated flow velocity between 3DE5

and 1DR1 does not vary significantly between 60ka BP and LGM. Thus, the effect of ice flow dynamics on the GrIS' evolution in the southern regions of central Greenland is limited and the majority of ice thickness variations can be attributed to a difference in accumulation which relates directly to a difference in simulated GIA caused by the inclusion of lateral variations in the sub-Greenland rheology. The simulated results for the northern sections of central Greenland show an increase in ice thickness (Fig. 3.6C.) whilst the increased surface elevation results in a decreased accumulation. The difference in ice thickness is a consequence of the difference in ice flow towards Greenland's periphery which is caused by a combination of a decrease in bedrock slope and a decrease in surface slope.

The same observations apply to other regions. A difference in bedrock elevation (Fig. 3.6A.), which is a result of the inclusion of lateral variations in the sub-Greenland rheology, largely translates into a difference in surface elevation. This difference in surface elevation is directly correlated to different rates of accumulation where an increased surface elevation leads to reduced precipitation because of a decrease in surface temperature and where a decreased surface elevation leads to an increased surface temperature and by extension increased precipitation (Fig. 3.8A). The difference in accumulation causes a difference in ice thickness (Fig. 3.6C). Alternatively, a difference in bedrock slope and in the ice sheet's surface slope result in a difference in the vertically averaged flow velocity (Fig. 3.8C) which explains the observed difference in ice thickness where differences in simulated ice thickness cannot be related to the difference in accumulation, such as in the northern parts of central Greenland. As such, the increase in mantle viscosity in the upper section of the upper mantle underlying the GrIS (Fig. 2.15), through the inclusion of lateral variations in the sub-Greenland rheology, cause the GrIS' waxing to diverge from results obtained for a commonly adopted laterally homogeneous rheology. One region where this does not apply is southeastern Greenland where the inclusion of lateral variations in rheology results in a decreased viscosity in the upper section of the upper mantle. The results presented here suggest that this decreased viscosity does not affect the GIA signal and by extension does not affect the GrIS' waxing in southeastern Greenland. A plausible explanation for this will be proposed in subsection 3.2.2.

The difference in simulated results at LGM demonstrate that both the simulated bedrock elevation (Fig. 3.6A.) and simulated ice thickness (Fig. 3.6C.) are affected by the inclusion of lateral variations in sub-Greenland rheology. Increased viscosity underlying most of Greenland (Fig. 2.13) lead to reduced uplift in regions that are unloaded and to reduced subsidence in regions that are depressed. Conversely, the decreased viscosity underlying southeastern Greenland does not result in an increased GIA signal. The difference in bedrock elevation between 3DE5 and 1DR1, as observed at LGM, is a consequence of the difference in the assumed model input at simulation start (subsection 3.1.2, the difference in the simulated GIA rates resulting from differences in the sub-Greenland viscosity (subsection 2.3.4), and a component can be attributed to the difference in GrIS waxing caused by diverging rates of ice accumulation at different altitudes (Fig. 3.8A.).

Results indicate that the simulated SMB responds to a vertical displacement of the ice sheet's surface elevation with a corresponding change in precipitation and subsequent ice accumulation. A relative decrease in surface elevation in central Greenland resulting from reduced uplift when including lateral variations in the sub-Greenland rheology results in an increased surface temperature which causes increased precipitation. Similarly, reduced subsidence in coastal regions results in reduced surface temperatures which causes decreased precipitation. Thus, the simulated difference in surface elevation at LGM (Fig. 3.7), which is partially due to different rates of GIA, correlates strongly with divergent rates of accumulation in the 40,000 years leading up to LGM (Fig. 3.8A.). This effect is self-reinforcing in regions characterised by a stronger sub-Greenland rheology because the reduced GIA signal leads to a proportional ice thickness change which leads to a yet reduced GIA signal. The result is a difference in accumulation of up to ± 50 Gigatonnes. This suggests that the inclusion of lateral variations in the sub-Greenland rheology is significant because the locally increased viscosity leads to a large difference in the ice sheet's waxing when compared with results obtained for a commonly adopted laterally homogeneous sub-Greenland rheology.

This result is inevitable because of how precipitation is implemented in ANICE. Precipitation, discussed in section 2.1, depends on the temperature at the inversion layer (Equation 2.1) which is a function of the

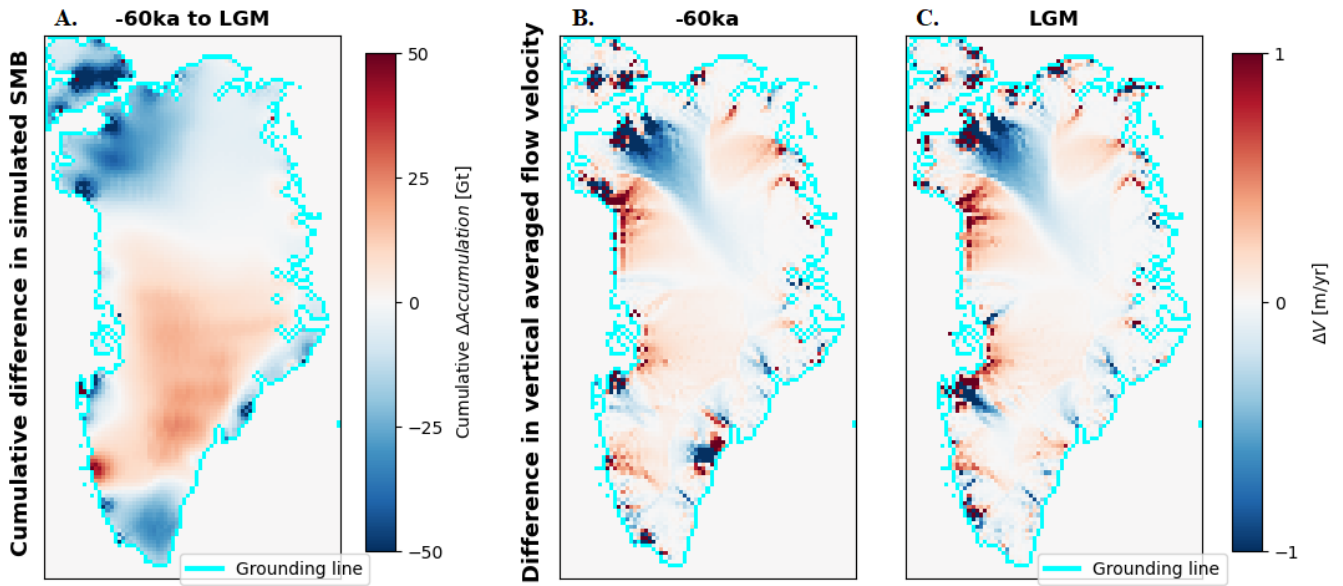


Figure 3.8: Cumulative difference in simulated precipitation between 3DE5 and 1DR1 over the period -60ka BP to LGM

temperature at the ice sheet’s surface (Equation 2.2) and responds proportionally to differences in surface elevation via the constant atmospheric lapse rate. Therefore, over a glacial period, a small difference in surface elevation will translate into a large difference in ice accumulation. This is possible, however, research has found that the SMB above the equilibrium line can either decrease or increase with an increase in surface elevation (Edwards et al., 2014). Furthermore, the differences in surface elevation are less than 50 meters. Such a small difference in surface elevation is poorly suited to resolve a difference in precipitation (Fettweis et al., 2013; Edwards et al., 2014). Additionally, the effect of a difference in altitude on precipitation is stronger in southern Greenland than in northern Greenland. A five-fold larger difference in surface elevation between northern and southern Greenland (Fig. 3.7) results in a comparable difference in simulated ice accumulation (Fig. 3.8A.) leading up to LGM. This is a consequence of the spatial variation in precipitation over the GrIS which is stronger in southeastern Greenland and which diminishes towards northwestern Greenland (Bales et al., 2001; Roe, 2002; Wong et al., 2015). An increased viscosity in lower latitude regions will have a stronger effect on the elevation-precipitation feedback which is reflected in the results. However, because the largest differences in accumulation are observed in northern Greenland, and because the differences in surface elevation are small, the significance of elevation-precipitation feedback resulting from the difference in the modelled sub-Greenland rheology is tenuous. Improved implementation of precipitation and subsequent ice accumulation by consider e.g. the effects of an ice sheet’s albedo, large scale circulation patterns over the GrIS, and wind direction in relation to the local topography, all of which affect the atmosphere’s water content (Edwards et al., 2014; Kuipers Munneke et al., 2015) which drives precipitation over the GrIS (Roe, 2002), should improve the significance of the results presented in this section.

Finally, there exist regions along the GrIS’ grounding line that are characterised by both positive and negative ΔH_i which cannot be correlated with differences in the local simulated SMB. Regions of positive ΔH_i near the grounding line, e.g. in northernmost Greenland, are a result of the difference in grounding

line position between simulations 3DE5 and 1DR1 which affects the ice thickness at the grounding line (Malyarenko et al., 2020) and therefore ice flow towards the periphery and subsequent solid ice discharge (Schoof, 2007). These results will be discussed in section 3.3. Regions of negative ΔH_i where there is no difference in simulated grounding line position between 3DE5 and 1DR1, e.g. southernmost Greenland, are the result of a difference in locally simulated ice dynamics. This difference in simulated ice dynamics is a consequence of a change in ocean facing bedrock slope. The simulated bedrock gradient increases for 3DE5 which causes increased flow towards the ocean. The relevance of such a difference in simulated glacier ice flow is limited because of the insufficient resolution on which the 3D ice sheet model is simulated leading to an inability to accurately resolve the dynamics of individual glaciers. Such regions of negative ΔH_i will not be discussed.

3.2.2 Mass Balance: Last Glacial Maximum to Present Day

The inclusion of lateral variations in the sub-Greenland rheology which causes the reduced GIA signal and subsequent effect on elevation-precipitation when the GrIS is waxing during glaciation, discussed in subsection 3.2.1, also affects the GrIS' waning when global temperatures increase following on the LGM. The difference in simulated ice thickness at PD between 3DE5 and 1DR1 is visualised in Fig. 3.9A and the difference in ice thickness between 3DE6 and 1DR1 is visualised in Fig. 3.9B. This discussion will be limited to evaluating the difference in the GrIS' evolution between 3DE5 and 1DR1 as the processes that cause 3DE5 to diverge from 1DR1 also affect 3DE6.

Comparison of the difference in ice thickness at PD demonstrates that the effect of including lateral variations in the sub-Greenland rheology is largely constrained to northwestern Greenland. Difference in simulated ice thickness in other regions is limited. Some difference exists along Greenland's grounding line which is associated with the migration of the grounding line and will be discussed in section 3.3. difference in ice thickness elsewhere is close to zero.

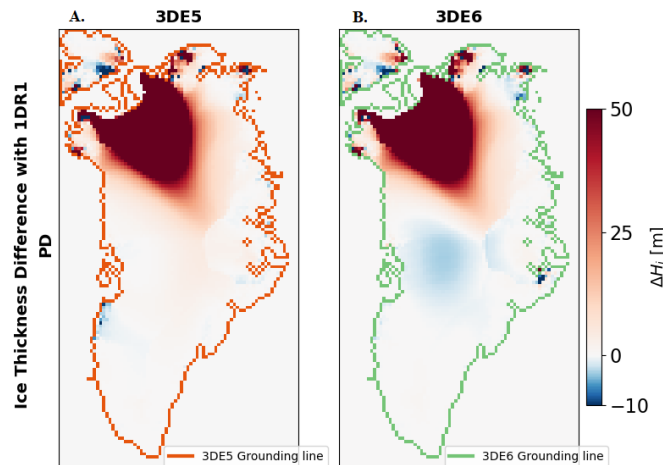


Figure 3.9: Simulated difference in ice thickness at PD for 3DE5-1DR1 and 3DE6-1DR1 respectively. Ice thickness variation in NWG is in excess of 900 meters at the coastline and decreases to 0 when migrating inland.

Upon closer inspection of the ice thickness in northwestern Greenland, visualised as a contour plot in Fig. 3.10, we find that the simulated ice thickness for 3D is 900 meters larger than that simulated for 1D near the coast. The difference decreases to zero when moving inland. This difference in ice thickness can be identified when considering the difference in surface elevation at LGM visualised in Fig. 3.11. The increased surface elevation in northwestern Greenland simulated for 3DE5 relative to 1DR1 is a consequence of the reduced subsidence during the GrIS' glaciation which is a result of the increased upper mantle viscosity

underlying northwestern Greenland when including lateral variations in the sub-Greenland rheology, as discussed in [subsection 3.2.1](#). The increased elevation at LGM results in reduced surface melt during the GrIS' deglaciation when global temperatures increase because temperatures at the surface are reduced compared to the lower elevation 1DR1's surface. This reduced surface melt is reflected in the difference in simulated mass balance visualised in [Fig. 3.12A](#). The difference is characterised by a large positive ΔSMB in northwestern Greenland. The extent of this region correlates with the positive difference in elevation at LGM visualised in [Fig. 3.11](#). Illustrating that the difference in the GrIS' state at LGM which is a consequence of the difference in sub-Greenland rheology between 3DE5 and 1DR1 causes a significant divergence in the GrIS' decline during deglaciation.

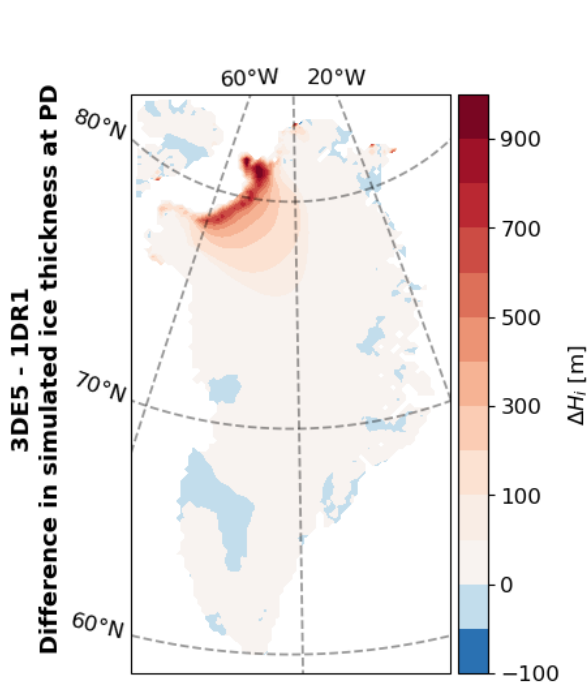


Figure 3.10: Contour plot defined by 100 meter increments illustrating regional variations in PD simulated ice thickness for second iteration 3DE5 - second iteration 1DR1 results

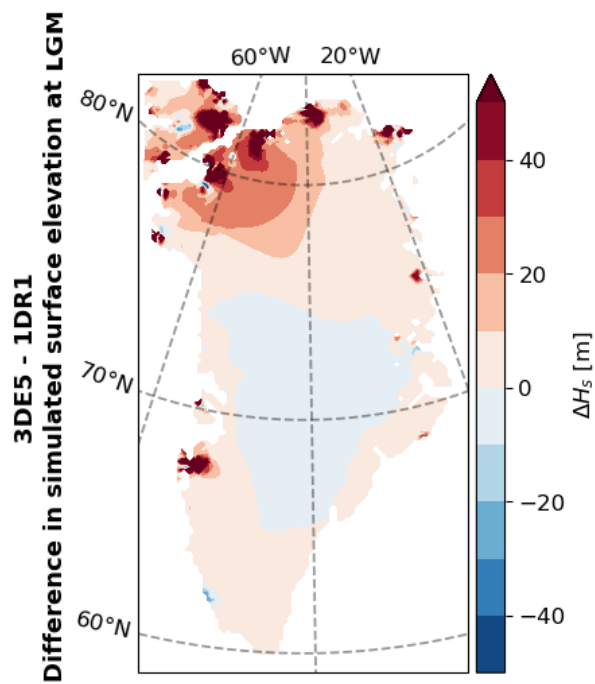


Figure 3.11: Contour plot defined by 10 meter increments illustrating regional variations in PD simulated surface elevation for second iteration 3DE5 - second iteration 1DR1 results

The difference in SMB also illustrates that the increased ice thickness further inland cannot be a consequence of the reduced ablation at the coast. The importance of ablation is constrained to the ablation zone below the ELA indicated in [Fig. 3.12A](#). Below which the self-reinforcing melt-elevation feedback causes rapid decline of ice volume present in 1DR1 that is not present in 3DE5. This is evident in the GrIS' accumulation and ablation visualised in [Fig. 3.13](#). The difference in ablation visualised in [Fig. 3.13](#) demonstrates that the difference in ice loss via ablation progressively increases with time as melt-elevation feedback causes increased ice loss in 3DE5. The relative increase in ice thickness further inland must be a consequence of the difference in ice flow towards the periphery between 3DE5 and 1DR1 resulting from the difference in the ice sheet's surface slope. This difference in ice flow is visualised in [Fig. 3.12C](#) and confirms that large volumes of ice are transported towards Greenland's periphery in 1DR1 which is not true for 3DE5.

The results presented in this section demonstrate that the inclusion of lateral variations in sub-Greenland rheology (3DE5, [subsection 2.3.3](#)) leads to a significant divergence from coupled simulation results obtained for a commonly adopted laterally homogeneous 1D rheology (1DR1, [subsection 2.3.2](#)). Conversely, the inclusion of lateral variations in the sub-Greenland rheology has a limited effect on the GrIS' evolution

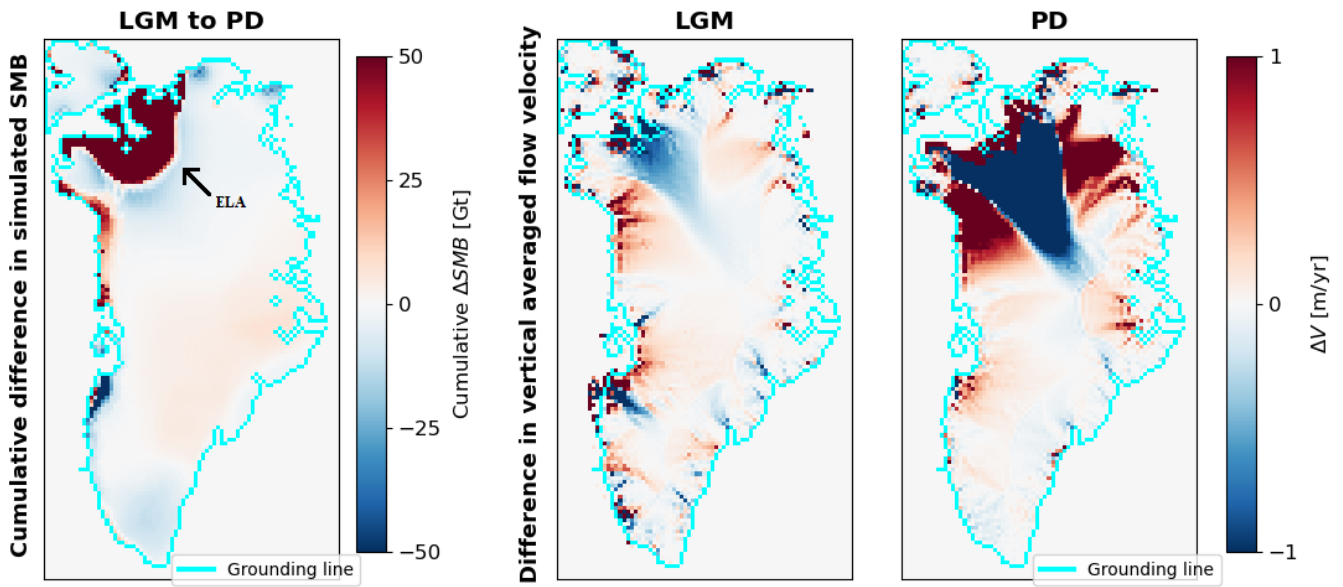


Figure 3.12: Cumulative difference in simulated precipitation between 3DE5 and 1DR1 over the period -60ka BP to LGM

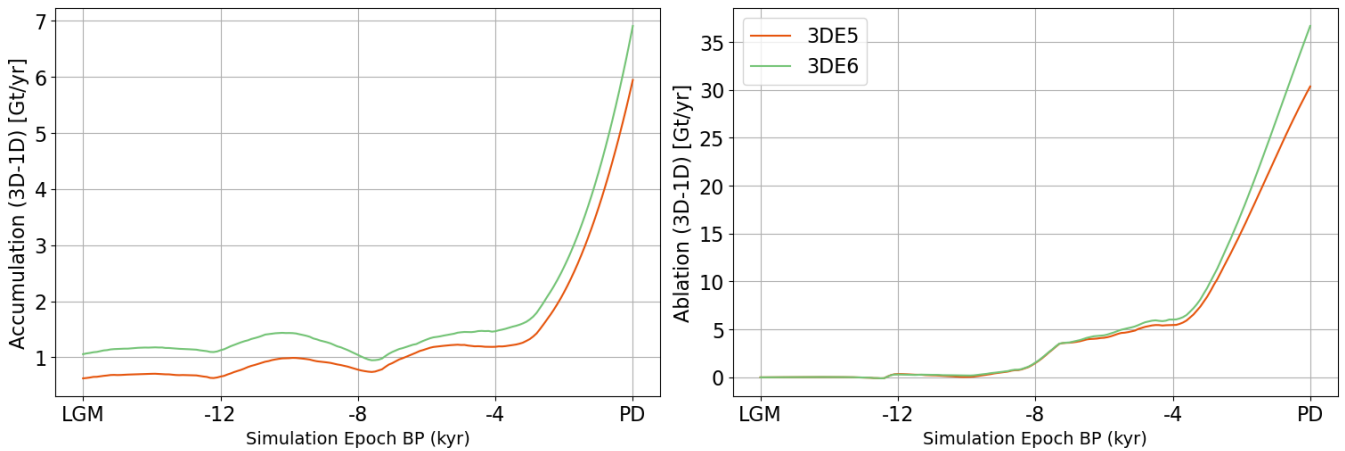


Figure 3.13: Temporal variation in accumulation and ablation for simulated 3D-1D results since the LGM up to PD. A negative difference in accumulation implies reduced ice volume aggregation by the GrIS and a negative difference in ablation implies increased ice retention through reduced ice melt.

in western, central, and northern Greenland and a marginal effect on the GrIS' evolution in southeastern Greenland.

The inclusion of lateral variations in the Sub-Greenland rheology in southeastern Greenland leads to a relatively low mantle viscosity when compared with 1DR1, as described in [subsection 2.3.4](#). The reduced viscosity underlying southeastern Greenland is associated with an observed and modelled increase in the local GIA signal resulting from recent unloading of the Earth's surface that cannot be explained with commonly adopted laterally homogeneous sub-Greenland rheologies ([Khan et al., 2016](#); [Van Dam et al., 2017](#);

Mordret, 2018; Weerdesteijn et al., 2022). This increased GIA signal is likely to affect the ice sheet’s mass balance and ice dynamics in southeastern Greenland (Wake et al., 2015; Weerdesteijn et al., 2022). This is supported by a review of possible feedback mechanisms that indicate that increased GIA locally affects the GrIS’ mass balance and ice flow dynamics via elevation-melt feedback and grounding line migration in a warming climate, as discussed in section 1.2. However, results presented in this section demonstrate that unloading of the Earth’s surface due to the GrIS’ waning in southeastern Greenland has a marginal effect on the simulated GIA and the GrIS’ evolution. Simulated differences in ice thickness along Greenland’s southeastern seaboard are less than three meters (Fig. 3.9C.) with a negligible effect on both the ice sheet’s simulated mass balance (Fig. 3.12A.) and the simulated ice flow (Fig. 3.12C.).

The apparent insignificant effect of the low viscosity region underlying southeastern Greenland on the GrIS’ waning in this region can be attributed to the geometry of the low viscosity region (Fig. 2.13) and to the local topography combined with the ice sheet’s assumed initial state at the mid-Eemian (Fig. 2.9). The simulated GIA and its effect on the ice dynamics near low viscosity regions is dependent on the low viscosity region’s horizontal extent and on the viscosity’s magnitude (Weerdesteijn et al., 2022). The low viscosity region, obtained through the inclusion of lateral variations in sub-Greenland rheology, is narrow near the surface and becomes progressively wider with increasing depth, effectively curving underneath the GrIS. Thus, the effect of the low viscosity region on the simulated GIA at Greenland’s southeastern coast is limited as GIA is more sensitive to differences in viscosity near the surface. Furthermore, the assumed ice sheet’s initial state is more extensive than common estimates for the ice sheet’s state at LIG (Plach et al., 2018). The assumed initial state combined with the local topography, which is characterised by the presence of mountain ranges along Greenland’s southeastern coast, constrains the GrIS’ potential for large scale waxing and waning. The result is an alternating pattern of loading and unloading which varies by -300 to +600 MIEQ over a 200 kilometer width along Greenland’s southeastern coast (Fig. 2.11). The constrained spatial extent and constrained magnitude of loading and unloading, a lithosphere thickness of 90 kilometers which dictates the GIA’s wavelength (Nield et al., 2018), and the narrowness of the low viscosity region near the surface, lead to marginal differences in simulated GIA between 3DE5 and 1DR1. Thus, the presence of a lower viscosity underlying southeastern Greenland has a negligible effect on the GrIS’ waning because local differences in GIA are marginal and do not cause significant differences in the simulated surface elevation or in the RSL which could cause a diverging rate in ice loss via melt-elevation feedback or increased ice discharge across the grounding line.

These results do not take into consideration the formation of ice shelves and the propagation of the ice sheet onto the continental shelf in southeastern Greenland between the mid-Eemian and PD (Van Dam et al., 2017; Bradley et al., 2018). One of the principal effects of an increased rate of GIA associated with a low viscosity region is the migration of the grounding line and the ramifications that this has on the local ice thickness at the grounding line, ice discharge, and by extension on the mass balance, as introduced in section 1.2. Thus, the insignificant effect of a reduced viscosity on the GrIS’ evolution identified in these results may be biased because of the exclusion of ice shelf formation. This possible bias is not insignificant because southeastern Greenland’s outlet glaciers are a primary contributor to Greenland’s PD observed dynamic ice mass loss and because southeastern Greenland is associated with rapid changes in the ice sheet’s ice dynamics over the past deglaciation period (Khan et al., 2016; Bunce et al., 2018; Weerdesteijn et al., 2022). As such, future work should reconsider the significance of the low viscosity region underlying Greenland’s southeast when including ice shelf formation which may lead to differing insights.

A second region that causes a significant portion of Greenland’s observed sea level rise contribution is northwestern Greenland (Chen et al., 2011; Khan et al., 2016; Mouginit et al., 2019). Northern Greenland is also where Zeitz et al. (2022) finds that ice mass loss is initiated when simulating the GrIS’ future evolution with a coupled ice sheet and solid Earth model. Comparison of the simulated ice thickness difference between 3DE5 and 1DR1 (Fig. 3.9C.) suggests that the increased viscosity in northwestern Greenland, following on the inclusion of lateral variations in the sub-Greenland rheology, causes a reduction in ice loss through a significant reduction in ice melt (Fig. 3.12A.) and a subsequent decrease in ice flow towards Greenland’s northwestern coast from central regions of the GrIS (Fig. 3.12C.). The increased viscosity

in northwestern Greenland leads to a simulated ice thickness difference at PD upwards of 900 meters at the coast which gradually decreases to zero some 700 kilometers inland (Fig. 3.10). This is contrary to what could be expected as an increased viscosity reduces the rate of GIA induced uplift when the surface is unloaded, thereby diminishing the stabilizing effect of GIA on the ice sheet’s elevation-melt feedback leading to progressively accelerating ice melt at the surface when compared with GIA obtained for a lower viscosity (Levermann and Winkelmann, 2016; Zeitz et al., 2022).

The difference in the simulated SMB since LGM can be traced back to the difference in the ice sheet’s surface elevation (Fig. 3.11), difference in bedrock elevation (Fig. 3.6A.), and difference in ice thickness (Fig. 3.6C.) at LGM. The increased viscosity underlying northwestern Greenland is found to result in decreased subsidence which causes a decreased prograde bedrock slope, a decrease in ice thickness, and an increase in surface elevation, as discussed in subsection 3.2.1. The rate of ice melt depends on the temperature at the ice sheet’s surface and melt in the ablation zone increases exponentially when global temperatures increases (Fettweis et al., 2013; Poinar et al., 2015; Herman et al., 2020). The increased surface elevation at LGM in northwestern Greenland results in a lower surface temperature as defined by the atmospheric lapse rate which results in reduced ice loss via surface melt. This reduced loss in ice at the ice sheet’s surface resulting from the increased surface elevation delays the onset of a negative elevation-melt feedback which leads to progressive accelerated ice loss via surface melt below the ELA (Edwards et al., 2014; Levermann and Winkelmann, 2016). The consequence is a difference in ice melt at the surface of 35 Gt/yr at PD (Fig. 3.13). Simulated differences in ice thickness are not constrained to low elevation regions below the ELA as illustrated in Fig. 3.9. The increased rate of ice loss via surface melt that affects 1DR1 but does not affect 3DE5 causes the surface geometry to diverge leading to a relative decrease in surface slope towards Greenland’s periphery over time for an increased viscosity. This difference results in reduced ice flow towards the margin (Fig. 3.12C.) which depends on the ice sheet’s surface slope (Le Clec’h et al., 2019). This decreased flow towards the ice sheet’s margin causes the difference in surface elevation to propagate inland thereby affecting regions above the ELA. When the ELA increases in a warming climate this difference in inland surface elevation causes the weaker viscosity to progressively lose yet more ice via ice melt at the surface. Thus, the increased viscosity leads to a significant reduction in ice loss via surface melt because of a difference in surface elevation in a warming climate. This is in line with the observation that ice loss in northwestern Greenland is accelerated because of increased glacier discharge as opposed to inland processes (King et al., 2020). The inclusion of lateral variations in sub-Greenland rheology and the subsequent increased viscosity underlying northwestern Greenland leads to a significant reduction in simulated ice loss, positively affecting the SMB. The apparent stabilizing effect of including lateral variations in the sub-Greenland rheology on its simulated deglaciation does not extend towards the (long-term) future. The increased viscosity will inevitably lead to an accelerated elevation-melt feedback that is not compensated for by rapid GIA. Zeitz et al. (2022) finds that an upper mantle viscosity of $5E21$ Pa·s combined with a sufficiently high lapse rate ($\leq 5K/km$) will lead to a complete loss or oscillation of the GrIS’ volume initiated from the north for a temperature anomaly $>1.5K$. The increased viscosity underlying northwestern Greenland when including lateral variations in the sub-Greenland rheology suggests that such a scenario is probable and that the increased viscosity will have a destabilizing effect on the GrIS’ future evolution, particularly in northern Greenland. However, the results presented here suggest that the increased viscosity in northwestern Greenland may have a stabilizing effect on the GrIS’ waning through affecting its waxing. Thus, the inclusion of lateral variations in sub-Greenland rheology has important implications for the GrIS’ future evolution as substantiated by Zeitz et al. (2022) and, based on the results presented in this section, has important implications for the GrIS’ past evolution in northwestern Greenland between the LGM and present day by reducing the rate of ice loss at the ice sheet’s surface.

The effect of lateral variations in the sub-Greenland rheology on the GrIS’ waning depends strongly on the observation that there is a sufficiently large difference in modelled surface elevation at LGM to cause a divergence in the rates of self-reinforcing elevation-melt feedback. This difference in surface elevation at LGM is identified as a consequence of differences in simulated depression and in simulated ice thickness in northwestern Greenland leading up to LGM. The latter is caused by a differences in simulated vertically av-

eraged ice flow and by an elevation-precipitation feedback that leads to reduced ice accumulation at a higher elevation. In [subsection 3.2.1](#), we deduced that the significance of this elevation-precipitation feedback is tenuous because of relatively small differences in the simulated elevation and because of the high latitude of the region of interest. However, if there were no elevation-precipitation feedback, then the difference in surface elevation would be increased because there would be no modelled decrease in ice thickness that can be attributed to elevation-precipitation feedback. Therefore, the observations in this section are applicable regardless of the existence of melt-precipitation feedback and depends, at the very least, on the difference in simulated rates of subsidence leading up to LGM which are lower for an increased viscosity when including lateral variations in the sub-Greenland rheology.

The effect of an increased mantle viscosity underlying other regions of the GrIS has a limited influence on its evolution via the SMB and via the ice flow. Elevation-accumulation feedback causes ice gain and ice loss in proportion to the difference in surface altitude in regions above the ELA for central and southern Greenland. Regions below the ELA on Greenland’s western coast and on Greenland’s northern coast where there are large differences in the SMB are a consequence of local increase in ice thickness following on the different grounding line positions at LGM which will be discussed in [section 3.3](#). The effect of a forebulge formation and subsequent collapse caused by the waxing and waning of the Laurentide Ice Sheet which affects the GrIS’ evolution are not considered ([Wake et al., 2015](#)). Also not considered are the effects of large scale circulation, ice-albedo feedback, and decreased retention of precipitation in a warming climate which affect the SMB ([Edwards et al., 2014](#); [Kuipers Munneke et al., 2015](#); [Zeitz et al., 2021](#)).

In conclusion, including lateral variations in the sub-Greenland rheology by modelling the solid Earth using a composite rheology, as described in [subsection 2.3.3](#), causes the GrIS’ evolution to diverge from the GrIS’ evolution obtained with a commonly adopted laterally homogeneous solid Earth structure, described in [subsection 2.3.2](#). Contrary to expectations, this divergence in simulated ice thickness and bedrock elevation does not extend to southeastern Greenland. Differences in simulated ice thickness and bedrock elevation in southeastern Greenland are marginal and do not exceed 3 meters at either LGM or at PD despite a tenfold local reduction in viscosity underlying Greenland’s southeastern coast. Instead, the ramifications of including lateral variations in the sub-Greenland rheology are most pronounced in regions where the local viscosity increases above that of the commonly adopted laterally homogeneous solid Earth.

During glaciation, including lateral variations in the sub-Greenland rheology leads to a simulated reduction in subsidence in northern and western Greenland and reduced uplift in central Greenland. Reduced uplift and decreased subsidence result in a corresponding decrease and increase in ice thickness respectively. This is due to varying rates of precipitation caused by differences in temperature at the ice sheet’s surface. The inclusion of lateral variations in sub-Greenland rheology has a non-negligible effect and can lead to a regional difference in simulated ice accumulation of ± 50 Gigatonnes. This difference in accumulation also has an effect on the simulated vertically averaged ice flow by changing the surface slope.

In a warming climate, deglaciation is also significantly affected by the inclusion of lateral variations in the sub-Greenland rheology. The inclusion of lateral variations in the sub-Greenland rheology and the corresponding increase in viscosity delay the ice sheet’s decline by reducing the effect of self-accelerating elevation-melt feedback leading to a large positive difference in the simulated SMB up to the ELA when compared with a laterally homogeneous sub-Greenland rheology ([Fig. 3.12 A.](#)). The retention of ice at Greenland’s northwestern coast ([Fig. 3.9 C.](#)) by the reduction in surface melt leads to a substantial reduction in ice flow towards Greenland’s periphery from central regions of the ice sheet ([Fig. 3.12 C.](#)) causing a positive difference in ice thickness above the ELA that is not directly dependent on the elevation-melt feedback ([Fig. 3.9C.](#)). The decreased surface melt and decreased flow of ice towards Greenland’s periphery causes the GrIS to retain ice relative to results obtained with a laterally homogeneous sub-Greenland rheology. As such, the inclusion of lateral variations in the sub-Greenland rheology has a significant effect on both the ice sheet’s waxing during the glaciation phase and the ice sheet’s waning during the deglaciation phase via both melt-precipitation and melt-elevation feedback processes. This affects the simulated ice sheet thickness and topography meaning that accurate simulations of the GrIS’ past and possibly future

evolution may benefit from the inclusion of lateral variations in sub-Greenland rheology. The same observations extend to a comparison of 3DE6 results with 1DR1 results. The difference between 3DE5 and 3DE6 will be discussed in [section 3.4](#).

3.3 3D GIA feedback on grounding line migration

A marine-grounded ice sheet’s grounding line is defined by the location where it transitions to a floating ice mass. The position of the grounding line and the rate of ice mass loss at the grounding line are both dependent on the RSL and local ice thickness (h). Both eustatic sea level change and GIA contribute to a changing RSL. GIA is the dominant factor in local changes in RSL through vertical bedrock displacement at the ice sheet’s periphery in response to increased or reduced surface loading ([Whitehouse, 2018](#); [Strunk et al., 2018](#)). Here, the ramifications of lateral variations in sub-Greenland rheology on the grounding line and grounding line feedback on ice thickness are discussed.

3.3.1 Last glacial maximum

The variation in grounding line position at LGM is visualised for 1DR1 (purple), 3DE5 (red), and 3DE6 (green) in [Fig. 3.14](#). Also visualised is the difference in bedrock elevation and ice thickness at LGM for 3DE5-1DR1.

The variation in grounding line position at LGM is limited. The simulated grounding lines are characterised by significant overlap. Approximately 97% of cells flagged as grounding line coincide at LGM. The rapid ice growth following the mid-Eemian forces the GrIS to grow towards the coastline in all directions over the initial simulated 5,000 year period. The out of phase global sea level response to an increase in global ice volume combined with a steep prograde coastal bedrock slope means that the initial ice growth towards the periphery is comparable for all simulated ANICE:FEM models. The simulated grounding line’s position, forced by an equivalent change in temperature and sea level, is then dependent only on local differences in bedrock elevation. Thereby explaining the significant overlap of the simulated grounding line at LGM.

The difference in bedrock elevation which affects the grounding line position is a consequence of the inclusion of lateral variations in sub-Greenland rheology. The definition of a 3D rheology leads to an increased depth-averaged viscosity which reduces the simulated GIA signal leading to the pattern of relative uplift and subsidence visualised, as discussed in [section 3.2](#). A consequence of the higher viscosity is the relative uplift of coastal bedrock at the grounding line. The relative coastal uplift causes parts of the submerged bedrock ahead of the 1DR1 grounding line to be elevated to within 20 meters of the geoid. Consequently, marine-grounded ice becomes capable of migrating onto these cells. This results in the advancement of 260 kilometers of simulated 3DE5 grounding line beyond the 1DR1 grounding line (visualised as orange) and is a result of the increased sub-Greenland viscosity. The relative coastal uplift for 3DE6- 1DR1 is stronger at LGM (see [Fig. 3.6](#)). This results in the advancement of a further 100 kilometers of 3DE6 grounding line beyond the 1DR1 and the 3DE5 grounding lines (visualised as green).

The limited relative advancement of the 3DE5 grounding line is a consequence of the local topography and the magnitude of the relative uplift. The area outside the grounding line that is less than 60 meters below sea level at LGM is $66,000 \text{ km}^2$. The steep drop-off in bedrock near coastal areas prevents significant advancement for the maximum relative uplift of 40 meters which decreases to a minimum relative uplift of 1.2 meters. The relative uplift resulting from the increased sub-Greenland viscosity and the further increase of uplift resulting from the GIA-elevation-accumulation feedback dependent decrease in coastal ice thickness has a marginal effect on the advancement of the grounding line at LGM. The effect of ablation is negligible leading up to LGM.

The effect of grounding line advancement on ice thickness becomes apparent when considering the differ-

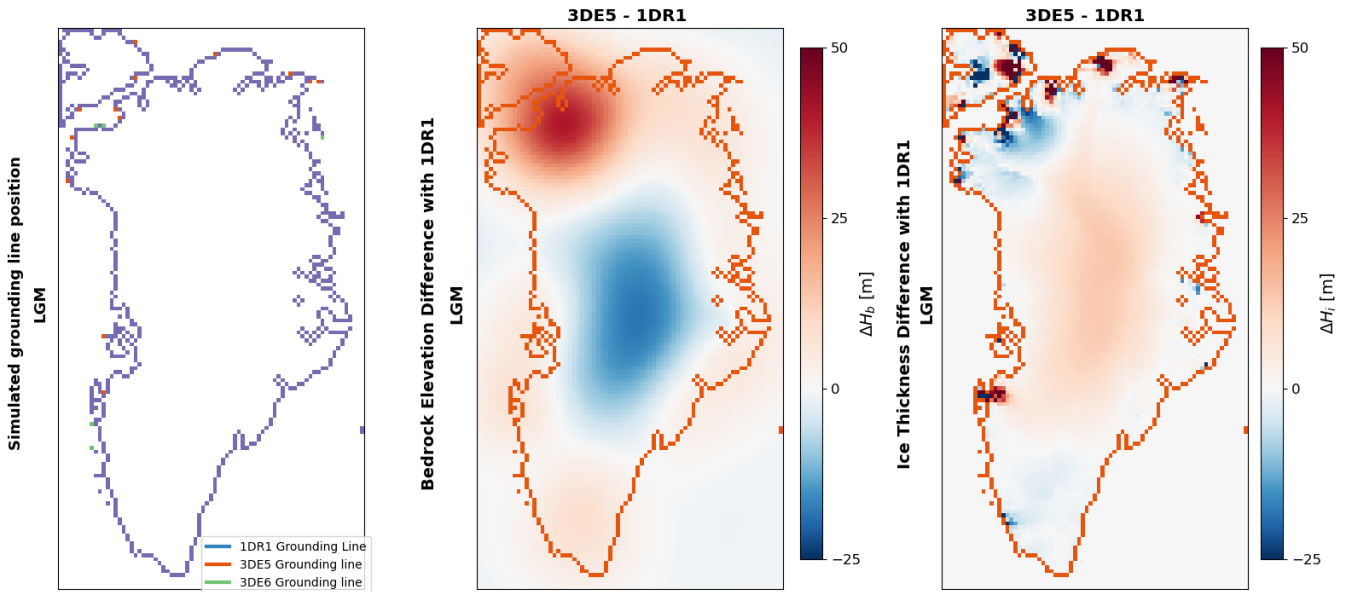


Figure 3.14: Comparison of the variation in grounding line position (left) at LGM correlated with the difference in bedrock elevation (middle) and ice thickness (right) at LGM for 3DE5 - 1DR1 second iteration simulation results.

ence in ice thickness in coastal regions visualised in Fig. 3.14. Advancement of the 3DE5 grounding line correlates with a relative increase in ice thickness locally. The advancement of the grounding line causes an ice cliff to form in the absence of shelf formation. This leads to the formation of an ice ramp which leads to a reduction in ice thickness adjacent to the migrated grounding line and an increase in ice thickness inland. The extent of relative ice thickness increase following the grounding line migration is dependent on the local topography and is contained by valleys, fjords, and other relative low-lying topography. This is evident when correlating input topography (see Fig. 2.9) with regions of increased ice thickness inland of the migrated grounding line.

The increased ice thickness results in an increased surface load locally. The increased surface load causes the relative uplift to decrease. Consequently, the relative increase in bedrock elevation resulting from the higher viscosity and reduced ice thickness via GIA-elevation-accumulation feedback which in turn leads to the advancement of the grounding line works to prevent the further advancement of the grounding line by increasing the applied surface load. The bedrock's steep coastal gradient combined with the negative grounding line advancement-GIA feedback stabilises the position of the grounding line. As a consequence, the regional variation in ice thickness remains limited and the effect on the coupled effect on GIA cannot be inferred from the pattern of relative uplift and depression in bedrock elevation when compared with 1DR1. The topography is poorly suited for the effects of grounding line-GIA feedback because of the local geography.

Grounding line advancement and subsequent local increase in ice thickness apply equally to the simulated 3DE6 results. The relatively strong 3D Earth rheology characterised by a lower estimated mantle water content (4.7 ppm) demonstrates further propagation of the grounding line due to the reduced depression in response to a relatively higher viscosity and therefore further relative uplift.

A secondary effect of the relative increase in bedrock elevation is a reduction in the RSL near marine grounded ice. The ice discharge across the grounding line is dependent on the RSL and the ice thickness at the grounding line. Therefore, a relative increase in bedrock elevation and the subsequent decrease in ice thickness via GIA-elevation-accumulation feedback leads to reduced ice discharge. Conversely, the advancement of the grounding line and the subsequent increase in ice exposure to ocean water leads to increased ice loss across the grounding line. This reflects on the simulated difference in ice discharge (3D-1D) visualised in Fig. 3.15. Where a decreasing trend in the difference reflects on increased ice loss at the grounding line for 3D relative to 1D simulations. This is a consequence of the increased exposure by advancement of the grounding line offset by a relative decrease in RSL and a relative reduction in ice thickness. Where fluctuation in the trend is a consequence of the changing climate and sea level and the sudden advancement of the grounding line. Note however, that the difference in discharge is marginal which reflects on the limited extent of marine-grounding for both 3D and 1D models and the limited variation in grounding line position.

A tertiary effect of the difference in RSL and ice thickness at the grounding line is reflected in the difference in vertically averaged ice flow velocity near the grounding line. This is also affected by variation in basal stress and flow velocity resulting in a difference in bedrock slope. A comparison of the effect at LGM, visualised in Fig. 3.16, demonstrates that the 3DE5 experiences a reduction in ocean moving ice flow velocity relative to 1DR1 in NWG and that there is an erratic change in locations where the grounding line has advanced. The erratic change follows the negative trend in ice thickness increase and decrease behind the migrated 3DE5 grounding line and reflect on the convergence to a new equilibrium ice thickness. The difference in velocity is negative in NWG due to the reduced RSL of significant portions of marine grounded ice near Humboldt and Petermann glaciers caused by a relative increase in bedrock elevation combined with a local reduction in ice thickness.

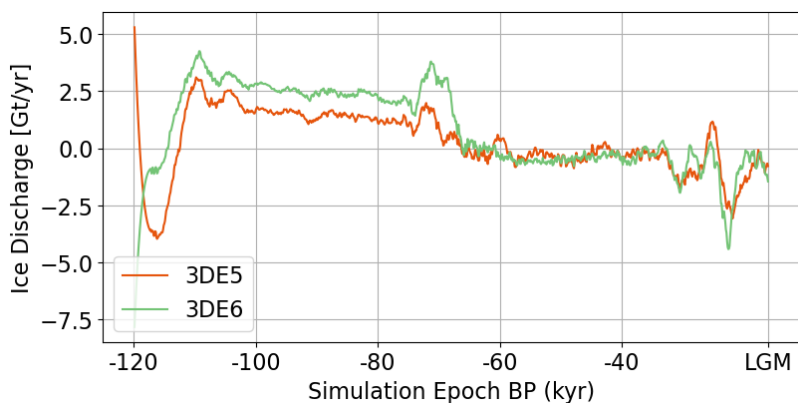


Figure 3.15: Visualisation of the temporal variation in GrIS ice discharge for 3DE5-1DR1 and 3DE6-1DR1 second iteration simulation results at LGM. A negative difference in ice discharge implies a decreased discharge of 3D results relative to 1D results

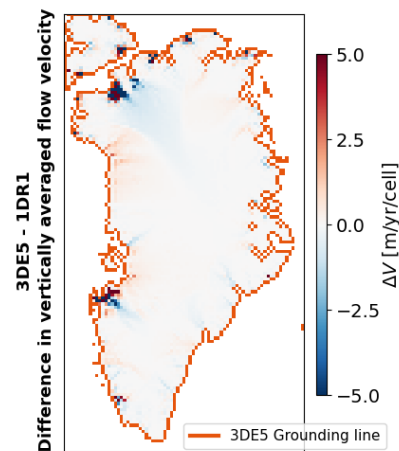


Figure 3.16: Difference in vertically averaged flow velocity distributed over Greenland for 3DE5-1DR1 second iteration simulation results at LGM

3.3.2 Present day

The difference in grounding line position at PD is visualised in Fig. 3.17. Also visualised are the difference in bedrock elevation and ice thickness for second iteration 3DE5 - 1DR1 simulation results.

Comparison of the grounding line position at LGM with the grounding line position at PD demonstrates

that the grounding line is characterised by a limited retreat in selection regions in response to an increased global mean temperature and an increased eustatic sea level. First, consider southeastern Greenland. A local increase in viscosity through the inclusion of lateral variations in sub-Greenland rheology caused the advancement of the 3DE5 grounding line ahead of the 1DR1 grounding line at LGM. The advancement of the grounding line resulted in a local increase in ice thickness inland of the grounding line. The subsequent increase in global eustatic sea level forced the retreat of the 3DE5 grounding line to the same position of the 1DR1 grounding line. The low-lying local bedrock topography caused the previously grounded ice sheet to float and subsequently calve causing the retreat. However, the increased ice thickness previously inland now results in a steep increase in ice thickness at the grounding line leading to increased ice discharge. Thus, one consequence of an increased sub-Greenland viscosity in regions characterised by a deep submerged topography is the initial advancement of the grounding line, the increase in ice thickness locally, and the subsequent increased ice discharge because of an increase in ice thickness at the grounding line when it is forced to retreat. This could be considered a form of ice cliff instability that is characteristic for high viscosity regions where the local submerged topography is deep.

Alternatively, the advancement of the grounding line can persist if the local bedrock topography is shallow and the sub-Greenland viscosity is high. The increase in local ice thickness caused by the advancement of the grounding line does not have a significant effect on coastal depression and therefore the higher viscosity which caused the relative advancement of the grounding line causes the advancement of the grounding line to persist. Such that a high local viscosity leads to both increased ice formation via the advancement of the grounding line and increased ice retention through a local increase in surface elevation that is not offset by the subsidence of local bedrock.

Finally, consider northwestern Greenland. The retreat of the 3DE5 grounding line relative to the 1DR1 grounding line along the Petermann glacier is reduced. The high viscosity which leads to increased ice retention via GIA-melt-elevation feedback that is not observed for the weaker 1DR1 rheology also prevents the retreat of the grounding line. However, one consequence is a large difference in ice thickness near the grounding line. This results in a significant increased ice discharge across the grounding line upwards of -8 Gt/yr and is reflected in [Fig. 3.18](#). The difference in flow velocity, visualised in [Fig. 3.19](#), in NWG supports this observation. The increased ice thickness at the grounding line results in a strong increase in ice flow and thus ice discharge. However, the increased ice thickness at the grounding line serves to buttress the 3DE5 ice sheet which reduces inland flow towards the grounding line reflected in a large negative difference in flow velocity. This buttressing of the 3DE5 ice sheet is thus a consequence of the increased ice retention but cannot be ascribed to the difference in grounding line position. Other grounding line variations in NWG are a consequence of the difference in bedrock elevation at PD and will be eliminated by a third iteration.

The same processes and observations affect the simulated 3DE6 GrIS' evolution.

Thus, the inclusion of lateral variations in sub-Greenland rheology leads to the advancement of the grounding line at LGM due to the reduced GIA response to changes in applied surface loading. The advancement of the grounding line causes a regional increase in ice thickness constrained by the local topography. The strong viscosity prevents significant depression of the local bedrock by the increased ice load which causes the advancement of the GIA to persist in regions characterised by a shallow topography. In NWG the effect of GIA-elevation-melt feedback is the dominant force which dictates the rate of grounding line retreat, leads to increased discharge, and increased ice retention inland by diminishing the ice flow towards the ocean. The effect of the increased viscosity through the inclusion of lateral variations in rheology is significant for the grounding line's migration but diminishes the effect of grounding line feedback on the GrIS' evolution except for regions where the local submerged bedrock is deep.

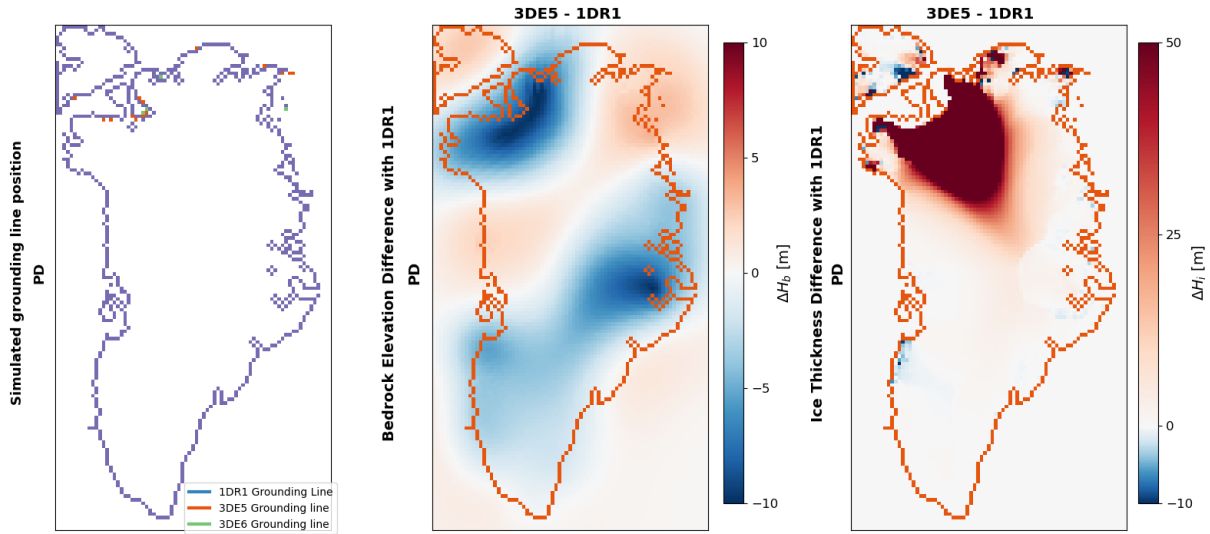


Figure 3.17: Comparison of the variation in grounding line position (left) at PD correlated with the difference in bedrock elevation (middle) and ice thickness (right) at PD for 3DE5 - 1DR1 second iteration simulation results.

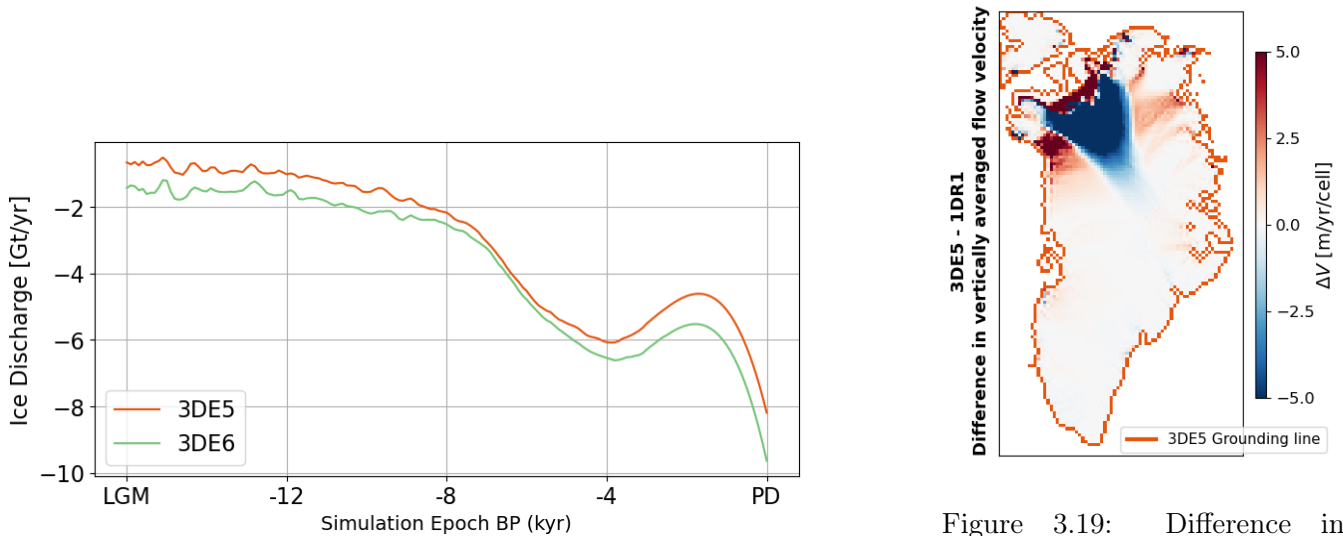


Figure 3.18: Visualisation of the temporal variation in GrIS ice discharge for 3DE5-1DR1 and 3DE6-1DR1 second iteration simulation results at PD.

Figure 3.19: Difference in vertically averaged flow velocity distributed over Greenland for 3DE5-1DR1 second iteration simulation results at PD

3.4 Uncertainty in 3D GIA

Sub-Greenland mantle water content, mantle material grain size, and mantle material composition are poorly resolved as discussed in subsection 2.3.3. The large uncertainty in mantle definition leads to a large uncertainty in the estimated lateral variations in viscosity of the sub-Greenland rheology as visualised in

Fig. 2.12. Thus, understanding the importance of the variation in parameters defining the sub-Greenland mantle is meaningful. Here, the effects of varying the assumed mantle’s water content are considered.

The results discussed in section 3.2 and section 3.3 demonstrated that there is no difference in the processes that affect 3DE5 and 3DE6. This is reflected in the difference in ice thickness at LGM visualised in Fig. 3.20 and at PD visualised in Fig. 3.21.

At LGM, the difference in ice thickness in central Greenland is a consequence of the difference in surface elevation and associated GIA-elevation-precipitation feedback. The difference in ice thickness is caused by the further advancement of the 3DE6 grounding line beyond the 3DE5 grounding line and the resultant increase in ice thickness inland. Other differences relate to the inability to accurately resolve the dynamics of individual glaciers.

at PD, the ice thickness differs in central Greenland in response to a difference in surface elevation. In NWG, the same process affects both 3DE5 and 3DE6, however the lower sub-Greenland viscosity for 3DE5 results in a decreased surface elevation at LGM which causes a substantial decrease in ice thickness relative to 3DE6 results. There are no processes that do not affect both simulations.

Both 3DE5 and 3DE6 are affected by identical processes and the difference in behaviour of 3DE5 relative to 1DR1 is identical for 3DE6 relative to 1DR1. Any variability in the GrIS’ evolution between 3DE5 and 3DE6 that is a consequence of the difference in water content is the extent of ice loss in NWG and the sporadic advancement of the grounding line. Decreasing water content will lead to increased ice retention through an increase in depth-averaged viscosity and an increase in water content will lead to decrease in water retention, forcing the simulated GrIS’ history to be closer to that of the 1DR1 model. As such, the results for 1DR1 and 3DE6 presented in this section bind the possible range of GrIS evolutionary paths well for the given model implementation. Thus, the ramifications of uncertainty in mantle water content on the GrIS’ evolution are marginal.

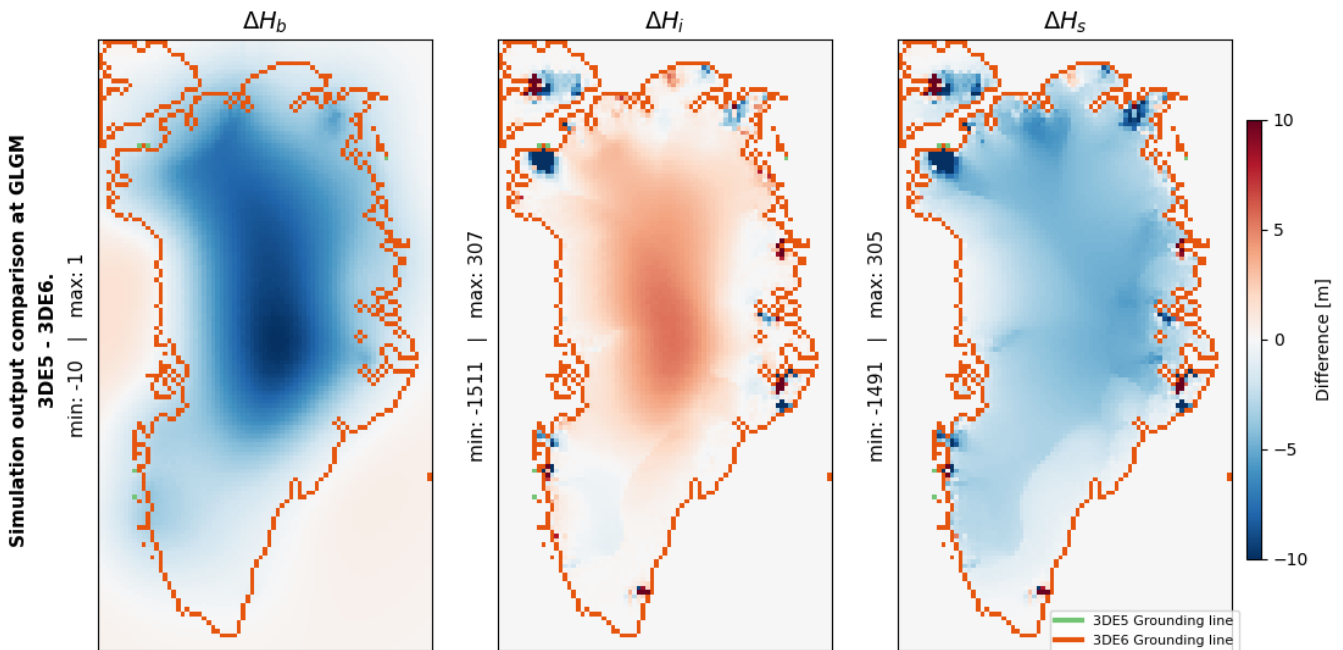


Figure 3.20: Difference in simulated bedrock elevation, ice thickness, and surface elevation at LGM for 3DE5-3DE6 second iteration simulation results

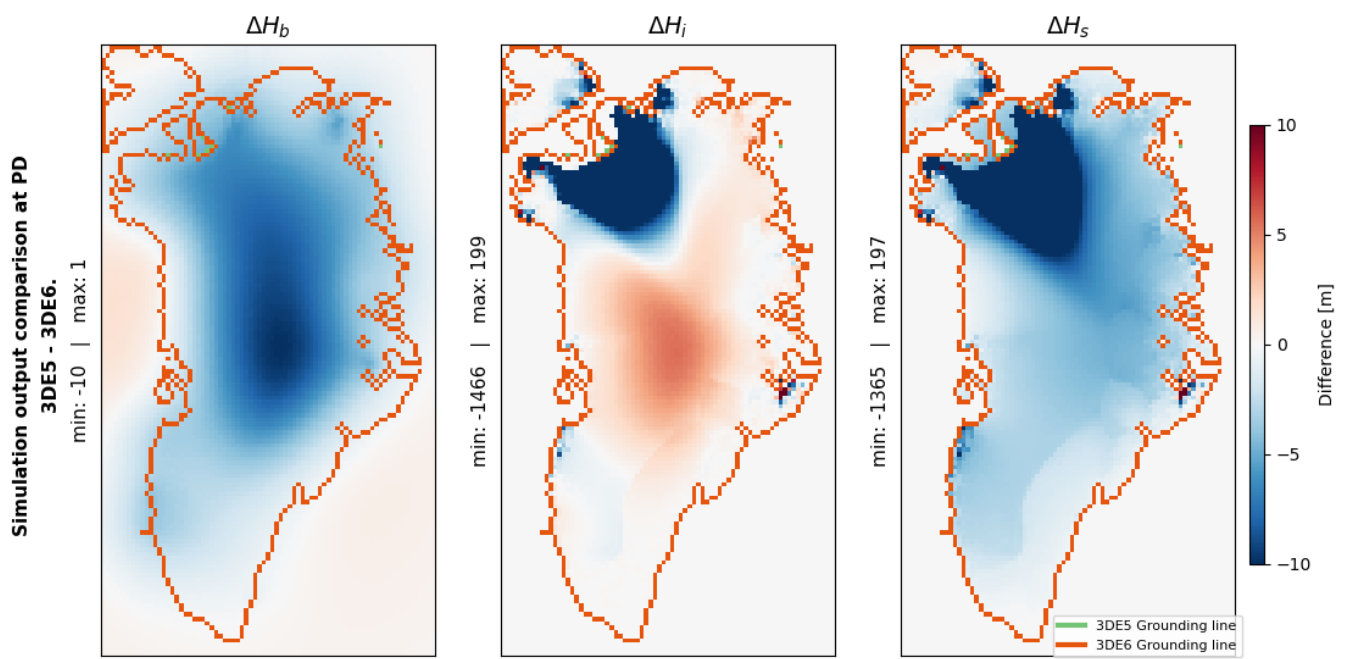


Figure 3.21: Difference in simulated bedrock elevation, ice thickness, and surface elevation at PD for 3DE5-3DE6 second iteration simulation results

Chapter 4

Conclusion

The inclusion of lateral variations in the sub-Greenland rheology has a non-negligible influence on the simulated GrIS' evolution in a coupled 3D ice sheet and 3D GIA model. Regional differences in simulated GIA when including a 3D viscosity relative to that obtained for a 1D viscosity affects regional rates of precipitation, ice ablation at the ice sheet's surface, grounding line migration, and ice flow, which leads to a divergence in the simulated ice sheet extent at present day.

Realistic sub-Greenland mantle material grain size and water content parameterisation result in a viscosity profile that is different from commonly adopted one-dimensional laterally homogeneous viscosity profiles. The definition of creep and dislocation parameters by a 3 mm grain size and a water content less than 75 ppm result in an increased upper mantle viscosity underlying central, northern, and western Greenland at depths above 220 kilometers and below the lithosphere. Conversely, including lateral variations in the sub-Greenland rheology leads to a reduction in the upper mantle viscosity underlying the southeastern Greenland.

The effect of the reduced viscosity underlying southeastern Greenland on the GrIS evolution is non-existent. The inclusion of lateral variations in sub-Greenland rheology does not affect GIA-elevation-mass balance feedback via either precipitation or ablation in both the GrIS' glaciation and deglaciation phases. It also does not lead to variation in grounding line migration on this coast when compared to simulation results obtained for a laterally homogeneous sub-Greenland rheology. Rather, the relevance of including lateral variations in sub-Greenland rheology lies with the increased viscosity underlying northwestern Greenland.

During glaciation, the increased sub-Greenland upper mantle viscosity underlying central, northern, and western Greenland leads to reduced subsidence of coastal regions and reduced uplift in central Greenland relative to results obtained with a 1D sub-Greenland rheology. The reduced uplift in central Greenland causes the ice sheet's surface to be placed in a warmer, lower elevation, atmosphere which leads to increased precipitation and an increase in ice thickness in central Greenland via a self-reinforcing GIA-elevation-accumulation feedback during the GrIS' glaciation leading up to LGM. Similarly, the decreased subsidence in coastal regions causes the ice sheet's surface to be placed in a cooler atmosphere which leads to reduced ice accumulation which in turn causes a reduction in ice thickness relative to simulated results obtained for a 1D sub-Greenland rheology. Including lateral variations in sub-Greenland rheology affects the GrIS' glaciation by affecting the melt-elevation feedback which leads to significant differences in accumulation upwards of 50 Gigatonnes relative to results obtained for a commonly adopted laterally homogeneous sub-Greenland rheology.

In a warming climate, deglaciation is also significantly affected by the inclusion of lateral variations in the sub-Greenland rheology. The inclusion of lateral variations in the sub-Greenland rheology and the corresponding increase in viscosity delay the ice sheet's decline by increasing the ice sheet's surface elevation at LGM relative to results obtained for a laterally homogeneous sub-Greenland rheology. This difference in surface elevation at LGM delays and diminishes the effect of self-reinforcing elevation-melt feedback leading to a large positive difference in the simulated SMB up to the ELA for the 3D rheology when compared with results obtained for a 1D rheology. Furthermore, the reduction in surface melt leads to a substantial

reduction in ice flow towards Greenland's periphery from central regions of the ice sheet causing a positive difference in ice thickness above the ELA that is not directly dependent on the elevation-melt feedback. The decreased surface melt and decreased flow of ice towards Greenland's periphery causes the GrIS to retain ice relative to results obtained with a laterally homogeneous sub-Greenland rheology. As such, the inclusion of lateral variations in the sub-Greenland rheology has a significant effect on both the ice sheet's waxing during the glaciation phase and by extension on the ice sheet's waning during the deglaciation phase via both melt-precipitation and melt-elevation feedback processes. The increased viscosity has an apparent stabilizing effect on the ice sheet's past deglaciation which implies that studies which use commonly adopted laterally homogeneous viscosity structures with a lower upper mantle viscosity may overestimate the GrIS' ice loss following LGM.

The increased viscosity also affects the grounding line migration. The relative uplift through decreased subsidence of coastal Greenland leads to the advancement of the grounding line relative to a the grounding line simulated for a weaker Earth rheology. Furthermore, the advancement of the grounding line is sustained by the inclusion of lateral variations in rheology in regions characterised by a shallow submerged bedrock due to the reduced effect of the increased loading caused by the relative advancement on vertical bedrock displacement. Conversely, regions characterised by a deep submerged bedrock where grounding line has advanced beyond the grounding line associated with a weaker rheology will see the inevitable retreat of said grounding line. The original advancement causes increased ice thickness inland which, when the grounding line retreats, results in ice cliff formation and increased thickness at the grounding line resulting in increased ice discharge. Thus, an increased viscosity has a stabilizing effect on the GrIS in regions characterised by grounding line advancement in shallow bedrock and a destabilizing effect on the GrIS in regions where the grounding line advances in deep bedrock. Which may have a detrimental effect on the future GrIS' evolution when RSL increases faster than GIA can compensate for because of the high local viscosity.

The ramifications of uncertainty in water content on these processes is limited. The results presented in this thesis bind the upper and lower estimate of the UMV via lateral variations in sub-Greenland rheology and via the commonly adopted 1D viscosity profile. As such, the processes described will affect a wide range of water content with the extent of the observed processes being constrained by the effective viscosity and lithosphere thickness. Thus, the uncertainty in water content extends to the magnitude of ice loss in north western Greenland and the extent of grounding line advancement but does not affect the occurrence thereof.

Chapter 5

Recommendations

The results and discussion presented in this thesis address the ramifications of including lateral variations in sub-Greenland rheology on the Greenland Ice Sheet's simulated evolution since the mid-Eemian. Results demonstrate the negligible consequence of a low viscosity region underlying Greenland's southeastern coast. Demonstrating that purported hot spot track underlying southeastern Greenland does not cause simulation results to diverge from simulation results obtained with a commonly accepted laterally homogeneous one dimensional rheology. Conversely, the relatively high viscosity underlying central, northern, and western Greenland is found to have significant repercussions for the simulated ice history. The increased sub-Greenland viscosity leads to an effective increase in the ice sheet's stability in a warming climate which is attributable to the differences in ice sheet growth and subsequent GIA in a cooling climate. However, the significance of the simulated results are subject to uncertainty in the solid-Earth's 3D approximation, uncertainty introduced by the exclusion of ice shelf formation, uncertainty in the initial topography and the Greenland ice sheet's initial state, uncertainty in the evolution of the applied surface loading applied, uncertainty in the Greenland Ice Sheet's interaction with the North American Ice Sheet, and uncertainty in the evolution of individual glaciers. Here, a number of recommendations are put forward which should lead to improvements in the realism of the simulated GrIS' evolution and/or improvements in the significance of the simulated results.

The results presented in this thesis are affected by uncertainty in the spatial variations in the defined sub-Greenland rheology, the significance of which is something that future work can explore. The three dimensional laterally heterogeneous viscosity profiles generate good simulation results but are constrained in their definition. The 3D solid-Earth approximations considered in this study are defined based on a study of best fitting upper mantle viscosity profiles for two locations near Kangerdlugssuaq Glacier. Therefore, the defined 3D solid-Earth approximation is skewed towards realistically describing southeastern Greenland. As such, inference on the GrIS' evolution based on simulated results elsewhere may be erroneous. Thus, a future iteration of this study would benefit from the definition of a 3D viscosity profile by approximating a variety of accurate 1D profiles that describe different regions and minimising the resultant error in the estimated 3D viscosity. A future iteration of this study would also benefit from studying a wider range of mantle material grain sizes and mantle material water content. The current study considers two profiles characterised by a 3 millimeter grain size and a water content of either 4.7 or 75 parts per million. However, uncertainty in sub-Greenland mantle material grain size ranges from sub-millimeter to 20 millimeter and uncertainty in water content from 0 to 1000 ppm. As such, the range of values considered does not encompass the complete range of feasible values. This is substantiated by the simulated ongoing GIA underneath GPS measuring station KUAQ which underestimates the ongoing GIA by a factor 5 and which implies strongly that a lower (regional) viscosity by increasing the water content or decreasing the grain size may yield better results and addresses the uncertainty introduced by uncertainty in the mantle's definition.

The exclusion of ice shelf formation from the current study provides an incomplete understanding of the

ramifications of grounding line migration and grounding line feedback on the GrIS' evolution. Thus, future work should pivot towards the inclusion of ice shelves which are known to have existed during the last glacial period and which affect the ice sheet's evolution by buttressing the ice sheet and reducing flow towards the ocean. Thereby introducing additional nuance in the effect of a regionally increased viscosity by the inclusion of lateral variations in sub-Greenland rheology by reducing the significance of GIA-elevation-melt (feedback) on the GrIS' evolution through diminishing the flow towards the ocean. Reducing the uncertainty introduced by the absence of ice shelves requires a revision of the mass balance by redefining the rate of ice accumulation, rate ice ablation, rate of ice discharge, and through reevaluating ice dynamics describing fast moving ice at low elevations.

The coupled model is initialised under the assumption that the present day observed Greenland topography and the ice sheet's extent reflect on the topography during the last inter-glacial. However, studies have found that the ice sheet's extent at LIG was much reduced compared to the present day observed GrIS' extent and simulation results demonstrate that the assumed initial topography is inaccurate. Consequently, studying the implications of lateral variations in sub-Greenland rheology as discussed in this thesis will benefit from a spin-up over an additional glacial-cycle whereby the accuracy of the coupled method is constrained by the ability to replicate the GrIS' extent at LIG, as defined by external sources, and the topography and rates of GIA observed at present day. Thereby improving the accuracy of the results obtained by increasing the realism of the simulated ice history for a given 3D viscosity profile. Leading to improved relevance of results discussed within the context of lateral variations in sub-Greenland rheology. Furthermore, this allows future work to consider ongoing and projected changes to the GrIS which is relevant because regional increases in sub-Greenland viscosity will cause increased ice loss through the reduced negative GIA-elevation-melt and GIA-grounding line feedback which may affect projections of ice volume loss.

Finally, three topics can be addressed for improving the significance and accuracy of the simulated GrIS results further. First, the application of a constant seeding distance of 30 km when defining the high resolution area results in an irregular mesh which causes discontinuity in the assigned dislocation and diffusion parameters. Defining a depth-dependent seeding along the surface to create an equal number of seeds at every layer interface and a layer-dependent seeding in radial direction consistent with layer depth will prevent warping of the mesh and lead to improved simulation results. Second, the inclusion of major ice sheets via proxy reflected in a eustatic sea level variation negates the effect of the nearby NAM's waxing and waning on the GrIS' evolution by ignoring self-gravitation. A future iteration of the current model will benefit from the inclusion of four fully coupled ice sheets and the implementation of which should be considered. third, introducing a higher resolution on which the ice sheet's dynamics and mass balanced are resolved should be considered. This will lead to improved understanding of instances of ice loss in coastal regions that can currently only be attributed to differences in bedrock slope near individual glaciers. To understand such behaviour would require an increase in resolution from twenty kilometers to a sub-ten kilometer scale for which model input data on the aforementioned resolution can be adapted from existing sources.

Thus, future efforts should be directed to the reduction in uncertainty associated with the 3D sub-Greenland viscosity profile, the inclusion of ice shelves, and the proper initialisation and sufficient complexity of the coupled model. Allowing for yet improved understanding of the ramifications of sub-Greenland rheology on the simulated results obtained with a coupled 3D GIA and 3D ice sheet model, paving the way for improved ice histories and the potential for improved projections.

Bibliography

- Adhikari, S., Milne, G. A., Caron, L., Khan, S. A., Kjeldsen, K. K., Nilsson, J., Larour, E., and Ivins, E. R. (2021). Decadal to centennial timescale mantle viscosity inferred from modern crustal uplift rates in greenland. *Geophysical Research Letters*, 48. <https://doi.org/10.1029/2021GL094040>.
- ADikhari, S., Ivins, E. R., Larour, E., Seroussi, H., Morlighem, M., and Nowicki, S. (2014). Future antarctic bed topography and its implications for ice sheet dynamics. *Solid Earth*, 5:569–584. <https://doi.org/10.5194/se-5-569-2014>.
- Alley, R. B., Andrews, J. T., Brigham-Grette, J., Clarke, G. K. C., Cuffey, K. M., Fitzpatrick, J. J., Funder, S., Marshall, S. J., Miller, G. H., Mitrovica, J. X., Muhs, D. R., Otto-Bliesner, B. L., Polyak, L., and White, J. W. C. (2010). History of the greenland ice sheet: Paleoclimatic insights. *Quaternary Science Reviews*, 29:1728–1756. <https://doi.org/10.1029/2006JF000664>.
- Aschwanden, A., Fahnestock, M. A., and Truffer, M. (2016). Complex greenland outlet glacier flow captured. *Nature Communications*, 7. <https://doi.org/10.1038/ncomms10524>.
- Bagherbandi, M., Amin, H., Wang, L., and Shirazian, M. (2022). Mantle viscosity derived from geoid and different land uplift data in greenland. *JGR Solid Earth*, 127. <https://doi.org/10.1029/2021JB023351>.
- Bales, R. C., McConnell, J. R., Mosley-Thompson, E., and Csatho, B. (2001). Accumulation over the greenland ice sheet from historical and recent records. *Journal of Geophysical Research*, 106:813–825. <https://doi.org/10.1029/2001JD900153>.
- Bamber, J. K., Griggs, J. A., Hurkmans, R. T. W. L., Dowdeswell, J. A., Gogineni, S. P., Howat, I., Mouginot, J., Paden, J., Palmer, S., Rignot, E., and Steinhage, D. (2013). A new bed elevation dataset for greenland. *The Cryosphere*, 7:499–510. <https://doi.org/10.5194/tc-7-499-2013>.
- Behn, M. D., Hirth, G., and Elsenbeck, J. R. (2019). Implications of grain size evolution on the seismic structure of the oceanic upper mantle. *Earth and Planetary Science Letters*, 282:178–189. <https://doi.org/10.1016/j.epsl.2009.03.014>.
- Bendixen, M., Nielsen, R. L., Plesner, J. L., and Minor, K. (2022). Opportunistic climate adaptation and public support for sand extraction in greenland. *Nature Sustainability*. <https://doi.org/10.1038/s41893-022-00922-8>.
- Bjork, A., Zhang, E., Dunk, M., Fleischer, A., Thage, K., Mouginot, J., Morlighem, M., Khan, S. MATHilde, D., and Amanda, F. Anders, B. (2021). New lang emerging beneath a retreating greenland ice sheet. *AGU Fall MEeting*. <https://ui.adsabs.harvard.edu/abs/2021AGUFM.C34C..08B/>.
- Blank, B., Barletta, V., Hu, H., Pappa, F., and Van der Wal, W. (2021). Effect of lateral and stress-dependent viscosity variations on gia induced uplift rates in the amundsen sea embayment. *Geochemistry, Geophysics, Geosystems*, 22. <https://doi.org/10.1029/2021GC009807>.
- Boers, N. and Rypdal, M. (2021). Critical slowing down suggests that the western greenland ice sheet is close to a tipping point. *PNAS*, 118. <https://doi.org/10.1073/pnas.2024192118>.

- Bradley, S. L., Reerink, T. K., Van de Wal, R. S. W., and Helsen, M. M. (2018). Simulation of the greenland ice sheet over two glacial-interglacial cycles: investigating a sub-ice-shelf melt parameterization and relative sea level forcing in an ice-sheet-ice-shelf model. *Climate of the Past*, 14(5):619–635. <https://doi.org/10.5194/cp-14-619-2018>.
- Buckland, P. C., Edwards, K. J., Panagiotakopulu, E., and Edward Schofield, J. (2008). Palaeoecological and historical evidence for manuring and irrigation at garðar (igaliku), norse eastern settlement, greenland. *The Holocene*, 19:105–116. <https://doi.org/10.1177/0959683608096660>.
- Bueler, E. and Brown, J. (2009). Shallow shelf approximation as a sliding law in a thermomechanically coupled ice sheet model. *JGR Earth Surface*, 114. <https://doi.org/10.1029/2008JF001179>.
- Bunce, C., Carr, J. R., Nienow, P. W., Ross, N., and Killick, R. (2018). Ice front change of marine-terminating outlet glaciers in northwest and southeast greenland during the 21st century. *Journal of Glaciology*, 64:523–535. <https://doi.org/10.1017/jog.2018.44>.
- Caron, L., Métivier, L., Greff-Lefftz, M., Fleitout, L., and Rouby, H. (2017). Inverting glacial isostatic adjustment signal using bayesian framework and two linearly relaxing rheologies. *Geophysical Journal International*, 208:1126–1147. <https://doi.org/10.1093/gji/ggx083>.
- Chen, J. L., Wilson, C. R., and Taply, B. D. (2011). Interannual variability of greenland ice losses from satellite gravimetry. *Solid Earth*, 116. <https://doi.org/10.1029/2010JB007789>.
- Christmann, J., Helm, V., Khan, S. A., Kleiner, T., Müller, R., Morlighem, M., Neckel, N., Rückamp, M., Steinhage, D., Zeising, O., and Humbert, A. (2021). Elastic deformation plays a non-negligible role in greenland’s outlet glacier flow. *Communications Earth & Environment*, 2. <https://doi.org/10.1038/s43247-021-00296-3>.
- Couette, P.-O., Lajeunesse, P., Ghienne, J.-F., Dorschel, B., Gebhardt, C., Hebbeln, D., and Brouard, E. (2022). Evidence for an extensive ice shelf in northern baffin bay during the last glacial maximum. *Communications Earth & Environment*, 3. <https://doi.org/10.1038/s43247-022-00559-7>.
- De Boer, B., Stocchi, P., and Van de Wal, R. S. W. (2014). A fully coupled 3-d ice-sheet–sea-level model: algorithm and applications. *Geosci. Model Dev.*, 7:2141–2156. <https://doi.org/10.5194/gmd-7-2141-2014>.
- De Boer, B., Van de Wal, R. S. W., Lourens, L. J., Bintanja, R., and Reerink, T. J. (2013). A continuous simulation of global ice volume over the past 1 million years with 3-d ice-sheet models. *Climate Dynamics*, 41(5):1365–1384. <https://doi.org/10.1007/s00382-012-1562-2>.
- Depoorter, M. A., Bamber, J. L., Griggs, J. A., Lenaerts, J. T. M., Ligtenberg, S. R. M., Van den Broeke, M. R., and Moholdt, G. (2013). Calving flux and basal melt rates of antarctic ice shelves. *nature*, 502:89–92. <https://doi.org/10.1038/nature12567>.
- Dughmore, A. J., Keller, C., and McGovern, T. H. (2007). Norse greenland settlement: Reflectiosn on climate change, trade, and the contrasting fates of human settlements in the north atlantic islands. *Arctic Anthropology*, 44:12–36. <https://doi.org/10.1353/arc.2011.0038>.
- Dziewonski, A. N., A. D. L. (1981). Preliminary reference earth model. *Physics of the Earth and Planetary Interiors*, 24:297–356. [https://doi.org/10.1016/0031-9201\(81\)90046-7](https://doi.org/10.1016/0031-9201(81)90046-7).
- Edwards, T. L., Fettweis, X., Gagliardini, O., Gillet-Chaulet, F., Golezer, H., Gregory, J. M., Hoffman, M., Huybrechts, P., Payne, A. J., Perego, M., Price, S., Quiquet, A., and Rit, C. (2014). Probabilistic parameterisation of the surface mass balance–elevation feedback in regional climate model simulations of the greenland ice sheet. *The Cryosphere*, 8:181–194. <https://doi.org/10.5194/tc-8-181-2014>.

- Fettweis, X., Franco, B., Tedesco, M., Angelen, J. H., Lenaerts, J. T. M., Van den Broeke, M. R., and Gallée, H. (2013). Estimating the greenland ice sheet surface mass balance contribution to future sea level rise using the regional atmospheric climate model mar. *The Cryosphere*, 7:369–489. <https://doi.org/10.5194/tc-7-469-2013>.
- Gao, Y., Yang, L., Mei, Y., Chu, Z., Yang, W., Xu, Q., Chen, G., Xie, Z., and Sun, L. (2020). Ice sheet changes and GIA-induced surface displacement of the larsemann hills during the last 50 kyr. *JGR Solid Earth*, 125. <https://doi.org/10.1029/2020JB020167>.
- Goelzer, H., Huybrechts, P., Loutre, M.-F., and Fichet, T. (2016). Last interglacial climate and sea level evolution from a coupled ice sheet-climate model. *Climate of the Past*, 12:2195–2213. <https://doi.org/10.5194/cp-12-2195-2016>.
- Goelzer, H., Nowicki, S., Payne, A., Larour, E., Seroussi, H., Lipscomb, W. H., Gregory, J., Abe-Ouchi, A., Shepherd, A., Simon, E., Agosta, C., Alexander, P., Aschwanden, A., Barthel, A., Calov, R., Chambers, C., Choi, Y., Cuzzone, J., Dumas, C., Edwards, T., Felikson, D., Fettweis, X., Golledge, N. R., Greve, R., Humbert, A., Huybrechts, P., Lecocq, S., Lee, V., Leguy, G., Little, C., Lowry, D. P., Morlighem, M., Nias, I., Quiquet, A., Rückamp, M., Schlegel, N. J., Slater, D. A., Smith, R. S., Straneo, F., Tarasov, L., van de Wal, R., and van den Broeke, M. (2020). The future sea-level contribution of the greenland ice sheet: a multi-model ensemble study of ismip6. *The Cryosphere*, 14:3071–3096. <https://doi.org/10.5194/tc-14-3071-2020>.
- Goelzer, H., Robinson, A., Seroussi, H., and Van de Wal, R. S. W. (2017). Recent progress in greenland ice sheet modelling. *Curr Clim Change Rep*, 3:291–302. <https://doi.org/10.1038/s41467-018-08068-y>.
- Gomez, N., Latychev, K., and Pollard, D. (2018). A coupled ice sheet–sea level model incorporating 3d earth structure: Variations in antarctica during the last deglacial retreat. *Journal of Climate*, 31:4041–2054. <https://doi.org/10.1175/JCLI-D-17-0352.1>.
- Goto-Azuma, K., Homma, T., Saruya, T., Nakazawa, F., Komuro, Y., Nagatsuka, N., Hirabayashi, M., Kondo, Y., Koike, M., Aoki, T., Greve, R., and Okuno, J. (2021). Studies on the variability of the greenland ice sheet and climate. *Polar Science*, 27. <https://doi.org/10.1016/j.polar.2020.100557>.
- Gowan, E. J., Zhang, X., Khosravi, S., Rovere, A., Stocchi, P., Hughes, A. L. C., Gyllencreutz, R., Mangerud, J., Svendsen, J.-I., and Lohmann, G. (2021). A new global ice sheet reconstruction for the past 80000 years. *Nature Communications*, 12. <https://doi.org/10.1038/s41467-021-21469-w>.
- Herman, M., Papritz, L., and Wernly (2020). A lagrangian analysis of the dynamical and thermodynamic drivers of large-scale greenland melt events during 1979-2017. *Weather Clim Dynam*, 1. <https://doi.org/10.5194/wcd-1-497-2020>.
- Huth, A., Dudde, R., and Smith, B. (2021). A generalized interpolation material point method for shallow ice shelves. 1: Shallow shelf approximation and ice thickness evolution. *Journal of Advances in Modeling Earth Systems*, 13. <https://doi.org/10.1029/2020MS002277>.
- Hutter, K. (1983). The application of the shallow-ice approximation. *Theoretical Glaciology*, 11:256–332. https://doi.org/10.1007/978-94-015-1167-4_5.
- Huybrechts, P. (2007). Ice sheet modelling. *Encyclopedia of the Antarctic, Routledge, New York and London*, pages 514–517.
- iMBIE (2020). Mass balance of the greenland ice sheet from 1992 to 2018. *Nature*, 579:233–239. <https://doi.org/10.1038/s41586-019-1855-2>.

- Ivins, E. R., Caron, L., Adhikari, S., and Larour, E. (2021). Notes on a compressible extended burgers model of rheology. *Geophysical Journal International*, 228:1975–1991. <https://doi.org/10.1093/gji/ggab452>.
- Kappelsberger, M. T., Strößenreuther, U., Scheinert, M., Horwath, M., Groh, A., Knöfel, C., Lunz, S., and Khan, S. A. (2021). Modeled and observed bedrock displacements in north-east greenland using refined estimates of present-day ice-mass changes and densified gnss measurements. *JGR Earth Surface*, 126. <https://doi.org/10.1029/2020JF005860>.
- Karato, S.-I. (2003). Mapping water content in the upper mantle. *Geophysical Monograph*, 138:135–151. <https://doi.org/10.1029/138GM08>.
- Khan, S. A., Aschwanden, A., Bjørk, A. A., Wahr, J., Kjeldsen, K. K., and Kjaer, K. H. (2015). Greenland ice sheet mass balance: a review. *Reports on Progress in Physics*, 78. <https://doi.org/10.1088/0034-4885/78/4/046801>.
- Khan, S. A., Sasgen, I., Bevis, M., Van Dam, T., Bamber, J. L., Wahr, J., Willis, M., Kjaer, K. H., Wouters, B., Helm, V., Csatho, B., Fleming, K., Bjork, A. A., Aschwanden, A., Knudsen, P., and Kuipers Munneke, P. (2016). Geodetic measurements reveal similarities between post-last glacial maximum and present-day mass loss from the greenland ice sheet. *Science Advances*, 2. <https://doi.org/10.1126/sciadv.1600931>.
- King, M. D., Howat, I. M., Candela, S. G., Noh, M. J., Jeong, S., Noël, B. P. Y., Van den Broeke, M. R., Wouters, B., and Negrete, A. (2020). Dynamic ice loss from the greenland ice sheet driven by sustained glacier retreat. *Communications earth & environment*, 1. <https://doi.org/10.1038/s43247-020-0001-2>.
- Konrad, H., Thoma, M., Sasgen, I., Klemann, V., Grosfeld, K., Barbi, D., and Martinec, Z. (2014). The deformational response of a viscoelastic solid earth model coupled to a thermomechanical ice sheet model. *Surveys in Geophysics*, 35:1441–1458. <https://doi.org/10.1007/s10712-013-9257-8>.
- Kuipers Munneke, P., Ligtenberg, S. R. M., Noel, B. P. Y., Howat, I. M., Box, J. E., Mosley-Thompson, E., McConnel, J. R., Steffen, K., Harper, J. T., Das, S. B., and Van den Broeke, M. R. (2015). elevation change of the greenland ice sheet due to surface mass balance and firn processes, 1960-2014. *The Cryosphere*, 9:2009–2025. www.the-cryosphere.net/9/2009/2015/.
- Laskar, J., Robutel, P., Joutel, F., Gastineau, M., Correia, A. C. M., and Levrard, B. (2004). A long-term numerical solution for the insolation quantities of the earth. *Astronomy and Astrophysics*, 428:261–285. <https://doi.org/10.1051/0004-6361:20041335>.
- Le Clec'h, S., Charbit, S., Quiquet, A., Fettweis, X., Dumas, C., Kageyama, M., Wyard, C., and Ritz, C. (2019). Assessment of the greenland ice sheet-atmosphere feedbacks for the next century with a regional atmospheric model coupled to an ice sheet model. *The Cryosphere*, 13:373–395. <https://doi.org/10.5194/tc-13-373-2019>.
- Le Meur, E. and Huybrechts, P. (1996). A comparison of different ways of dealing with isostasy: examples from modelling the antarctic ice sheet during the last glacial cycle. *The Cryosphere*, 14:985–1008. <https://doi.org/10.5194/tc-14-985-2020>.
- Lecavalier, B. S., Milne, G. A., Simpson, M. J. R., Wake, L., Huybrechts, P., Tarasov, L., Kjeldsen, K. K., Funder, S., Long, A. J., Woodroffe, S., Dyke, A. S., and Larsen, K. L. (2014). A model of greenland ice sheet deglaciation constrained by observations of relative sea level and ice extent. *Quaternary Science Reviews*, 102:54–84. <https://doi.org/10.1016/j.quascirev.2014.07.018>.

- Levermann, A. and Winkelmann, R. (2016). A simple equation for the melt elevation feedback of ice sheets. *The Cryosphere*, 10:1799–1807. <https://doi.org/10.5194/tc-10-1799-2016>.
- Lingle, C. S. and Clark, J. A. (1985). A numerical model of interactions between a marine ice sheet and the solid earth: Application to a west antarctic ice stream. *JGR Oceans*, 90:1100–1114. <https://doi.org/10.1029/JC090iC01p01100>.
- Malyarenko, A., Wells, A. J., Lagnhorne, P. K., Robinson, N. J., Williams, M. J. M., and Nicholls, K. W. (2020). A synthesis of thermodynamic ablation at ice-ocean interfaces from theory, observations, and models. *Ocean Modelling*, 154. <https://doi.org/10.1016/j.ocemod.2020.101692>.
- Mankoff, K. D., Colgan, W., Solgaard, A., Karlsson, N. B., Ahlstrom, A. P., Van As, D., Box, J. E., Khan, S. A., Kjeldsen, K. K., Mouginit, J., and Fausto, R. S. (2019). Greenland ice sheet solid ice discharge from 1986 through 2017. *Earth Syst. Sci. Data*, 11:769–786.
- Miller, K. G., Mountain, G. S., Wright, J. D., and Browning, J. V. (2011). A 180-million-year record of sea level and ice volume variations from continental margin and deep-sea isotopic records. *Oceanography*, 24:40–53. <https://doi.org/10.5670/oceanog.2011.26>.
- Milne, G. A., Latychev, K., Schaeffer, A., Crowley, J. W., Lecavalier, B. S., and Audette, A. (2018). The influence of lateral earth structure on glacial isostatic adjustment in greenland. *Geophysical Journal International*, 214:1252–1266. <https://doi.org/10.1093/gji/ggy189>.
- Mitrovica, J. X. and Forte, A. M. (2004). A new inference of mantle viscosity based upon joint inversion of convection and glacial isostatic adjustment data. *Earth and Planetary Science Letters*, 225:117–189. <https://doi.org/10.1016/j.epsl.2004.06.005>.
- Mordret, A. (2018). Uncovering the iceland hot spot track beneath greenland. *Journal of Geophysical Research: Solid Earth*, 123:4922–4941. <https://doi.org/10.1029/2017JB015104>.
- Morland, L. W. (1987). Unconfined ice-shelf flow. *Dynamics of the West Anatrctic Ice Sheet*, pages 99–116. https://doi.org/10.1007/978-94-009-3745-1_6.
- Morlighem, M., Williams, C. N., Rignot, E., An, L., Arndt, J. E., Bamber, J. L., Catania, G., Chauché, N., Dowdeswell, J. A., Dorschel, B., Fenty, I., Hogan, K., Howat, I., Hubbard, A., Jakobsson, M., Jordan, T. M., Kjeldsen, K. K., Millan, R., Mayer, L., Mouginit, J., Noël, B. P. Y., O’Cofaigh, C., Palmer, S., Rysgaard, S., Seroussi, H., Siegert, M. J., Slabon, P., Straneo, F., van den Broeke, M. R., Weinrebe, W., Wood, M., and Zinglensen, K. B. (2017). Bedmachine v3: Complete bed topography and ocean bathymetry mapping of greenland from multibeam echo sounding combined with mass conservation. *Geophysical Research Letters*, 44:11051–11061. <https://doi.org/10.1002/2017GL074954>.
- Mouginit, J., Rignot, E., Bjørk, A., Van den Broeke, M., Morlighem, M., Noël, B., and Scheuchl, B. abd Wood, M. (2019). Forty-six years of greenland ice sheet mass balance for 1972 to 2018. *PNAS*, 116. <https://doi.org/10.1073/pnas.1904242116>.
- Nield, G. A., Whitehouse, P. L., Van der Wal, W., Blank, B., O’Donnel, J. P., and Stuart, G. W. (2018). The impact of lateral variations in lithospheric thickness on glacial isostatic adjustment in west antarctica. *Geophysical Journal International*, 214:811–824. <https://doi.org/10.1093/gji/ggy158>.
- Ohtani, E. (2019). The role of water in earth’s mantle. *National Science Review*. <https://doi.org/10.1093/nsr/nwz071>.
- Olason, E., Boutin, G., Korosov, A., Rampal, P., Williams, T., Kimmritz, M., Dansereau, V., and Samaké, A. (2022). A new brittle rheology and numerical framework for large-scale sea-ice models. *Journal of Advances in Modeling Earth Systems*, 14. <https://doi.org/10.1029/2021MS002685>.

- Pattyn, F. and Morlighem, M. (2020). The uncertain future of the antarctic ice sheet. *Science*, 367:1331–1335. <https://doi.org/10.1126/science.aaz5487>.
- Pettersen, C., Bennartz, R., Merrelli, A. J., Shupe, M. D., Turner, D. D., and Von Walden, P. (2018). Precipitation regimes over central greenland inferred from 5 years of icecaps observations. *Atmospheric Chemistry and Physics*, 18:4715–4735. <https://doi.org/10.5194/acp-18-4715-2018>.
- Plach, A., Nisancioglu, K. H., Langebroek, P. M., Born, A., and Le clec’h, S. (2019). Eemian greenland ice sheet simulated with a higher-order model shows strong sensitivity to surface mass balance forcing. *The Cryosphere*, 13:2133–2148. <https://doi.org/10.5194/tc-13-2133-2019>.
- Plach, A., Nisancioglu, K. H., Le Clec’h, S., Born, A., Langebroek, P. M., Guo, C., Imhof, M., and Stocker, T. F. (2018). Eemian greenland smb strongly sensitive to model choice. *Climate of the Past*, 14:1436–1485. <https://doi.org/10.5194/cp-14-1463-2018>.
- Poinar, K., Joughin, I., Das, S. B., Behn, M. D., Lenaerts, J. T. M., and Van den Broeke, M. R. (2015). Limits to future expansion of surface-melt-enhanced ice flow into the interior of western greenland. *Geophysical Research Letters*, 42:1800–1807. <https://doi.org/10.1002/2015GL063192>.
- Pörtner, H.-O. et al. (2022). Climate change 2022, impacts, adaptation and vulnerability, summary for policymakers. *IPCC*. www.ipcc.ch.
- Reeh, N. (1991). Parameterization of melt rate and surface temperature on the greenland ice sheet. *Polarforschung*, 59:113–128.
- Reerink, T. J., Van Den Berg, W. J., and Van de Wal, R. S. W. (2016). Oblimap 2.0: a fast climate model–ice sheet model coupler including online embeddable mapping routines. *Geosci. Model Dev.*, 9:4111–4132. <https://doi.org/10.5194/gmd-9-4111-2016>.
- Reijmer, C. H., Van den Broeke, M. R., Fettweis, X., Ettema, J., and Stap, L. B. (2012). Refreezing on the greenland ice sheet: a comparison of parameterizations. *The cryosphere*, 6:743–762. <https://doi.org/10.5194/tc-6-743-2012>.
- Rignot, E., Jacobs, S., Mouginot, H., and Scheuchl, B. (2013a). Ice-shelf melting around antarctica. *Science*, 341:266–270. <https://doi.org/10.1126/science.1235798>.
- Rignot, E., Jacobs, S., Mouginot, J., and Scheuchl, B. (2013b). Ice-shelf melting around antarctica. *Science*, 341:266–270. <https://doi.org/10.1126/science.1235798>.
- Roe, G. H. (2002). Modeling precipitation over ice sheets: an assessment using greenland. *Journal of Glaciology*, 48:70–80. <https://doi.org/10.3189/172756502781831593>.
- Rémy, F., Shaeffer, P., and Legrésy, B. (1999). Ice flow physical processes derived from the ers-1 high-resolution map of the antarctica and greenland ice sheets. *Geophysical Journal International*, 139:546–656. <https://doi.org/10.1046/j.1365-246x.1999.00964.x>.
- Schoof, C. (2007). Ice sheet grounding line dynamics: Steady states, stability, and hysteresis. *Journal of Geophysical Research: Earth Surface*, 112. <https://doi.org/10.1029/2006JF000664>.
- Schoof, C. (2010). Coulomb friction and other sliding laws in a higher order glacier flow model. *Mathematical Models and Methods in Applied Sciences*, 20:157–189. <https://doi.org/10.1038/s43247-020-0001-2>.
- Schoof, C. and Hewitt, I. (2013). Ice-sheet dynamics. *Annu. Rev. Fluid Mech.*, 45:217–239. <https://doi.org/10.1029/2006JF000664>.

- Slater, D. A., Felikson, D., Straneo, F., Goelzer, H., Little, C. M., Morlighem, M., Fettweis, X., and Nowicki, S. (2013). Twenty-first century ocean forcing of the greenland ice sheet for modelling of sea level contribution. *Climate Dynamics*, 41(5):1365–1384. <https://doi.org/10.1007/s00382-012-1562-2>.
- Spada, G., Antonioli, A., Cianetti, S., and Giunchi, C. (2006). Glacial isostatic adjustment and relative sea-level changes: the role of lithospheric and upper mantle heterogeneities in a 3-d spherical earth. *Geophysical Journal International*, 165:692–702. <https://doi.org/10.1111/j.1365-246X.2006.02969.x>.
- Stone, E. J., Lunt, D. J., Annan, J. D., and Hargreaves, J. C. (2013). Quantification of the greenland ice sheet contribution to last interglacial sea level rise. *Clim. Past*, 9:621–639. <https://doi.org/10.5194/cp-9-621-2013>.
- Strunk, A., Larsen, N. K., Nilsson, A., Seidenkrantz, M.-S., Levy, L. B., Olsen, J., and Larudsen, T. L. (2018). Relative sea-level changes and ice sheet history in finderup land, north greenland. *Sec. Quaternary Science, Geomorphology and Paleoenvironment*. <https://doi.org/10.3389/feart.2018.00129>.
- Stuhne, G. R. and Peltier, W. R. (2015). Reconciling the ice-6g_c reconstruction of glacial chronology with ice sheet dynamics: The cases of greenland and antarctica. *JGR Earth Surface*, 120:1841–1865. <https://doi.org/10.1002/2015JF003580>.
- Sørensen, M. and Gulløv, H. C. (2012). The prehistory of inuit in northeast greenland. *Arctic Anthropology*, 49:88–104. <https://doi.org/10.1353/arc.2012.0016>.
- Uppala, S. M., Kallberg, P. W., Simmons, A. J., Andrae, U., Da Costa, V., Fiorino, M., Gibson, J. K., Haseler, J., Hernandez, A., Kelly, G. A., Li, X., Onogi, K., Saarinen, S., Sokka, N., and Allan, R. P. (2005). The era-40 re-analysis. *Quarterly Journal of the Royal Meteorological Society*, 131:2961–3921. <https://doi.org/10.1256/qj.04.176>.
- Van Calcar, C. J. (2020). Interactions between ice sheet dynamics and glacial isostatic adjustment, the development and application of a new method to simulate the antarctic ice sheet over the last glacial cycle. *TU Delft Repository*. <https://repository.tudelft.nl/islandora/object/uuid%3A8a3a4e21-a6f0-4874-a41f-e26ac95f03be>.
- Van Dam, T., Wahr, O. F. J., Khan, S. A., Bevis, M., and Van den Broeke, M. R. (2017). Using gps and absolute gravity observations to separate the effects of present-day and pleistocene ice-mass changes in south east greenland. *Earth and Planetary Sciences*, 459:127–135. <https://doi.org/10.1016/j.epsl.2016.11.014>.
- Van den Broeke, M. R., Enderlin, E. M., Howat, I. M., Kuipers Munneke, P., Noel, B. P. Y., Van de Berg, W. J., Van Meijgaard, E., and Wouters, B. (2016). On the recent contribution of the greenland ice sheet to sea level change. *The Cryosphere*, 10:1933–1946. <https://doi.org/10.5194/tc-10-1933-2016>.
- Van der Veen, C. J. and Whilliams, I. M. (1990). Flow laws for glacier ice: Comparison of numerical predictions and field measurements. *Journal of Glaciology*, 36:324–339. <https://doi.org/10.3189/002214390793701372>.
- Van der Wal, W., Barnhoorn, A., Stocchi, P., Gradmann, S., Wu, P., Drury, M., and Vermeersen, B. (2013). Glacial isostatic adjustment model with composite 3d rheology for fennoscandia. *Geophysical Journal International*, 194:61–77. <https://doi.org/10.1093/gji/ggt099>.
- Van der Wal, W., Whitehouse, P. L., and Schrama, E. J. O. (2015). Effect of gia models with 3d composite mantle viscosity on grace mass balance estimates for antarctica. *Earth and Planetary Science Letters*, 414:134–143. <https://doi.org/10.1016/j.epsl.2015.01.001>.

- Van der Wal, W., Wu, P., Wang, H., and Sideris, M. G. (2010). Sea level and uplift rate from composite rheology in glacial isostatic adjustment modelling. *Journal of Geodynamics*, 50:38–48. <https://doi.org/10.1016/j.jog.2010.01.006>.
- Van Zelst, I., Cramer, F., Pusok, A. E., Glerum, A., Dannberg, J., and Thieulot, C. (2022). 101 geodynamic modelling: how to design, interpret, and communicate numerical studies of the solid earth. *Solid Earth*, 13:583–637. <https://doi.org/10.5194/se-13-583-2022>.
- Vasskog, K., Langebroek, P. M., Andrews, J. T., E., N. J., and Nesje, A. (2015). The greenland ice sheet during the last glacial cycle: current ice loss and contribution to sea-level rise from a palaeoclimatic perspective. *Earth-Science Reviews*, 150:45–67. <https://doi.org/10.1016/j.earscirev.2015.07.006>.
- Wake, L. M., Lecavalier, B. S., and Bevis, M. (2015). Glacial isostatic adjustment (gia) in greenland: a review. *Current Climate Change Reports*, 2:101–111. <https://doi.org/10.1007/s40641-016-0040-z>.
- Weerdesteijn, M. F. M., Conrad, C. P., and Naliboff, J. B. (2022). Solid earth uplift due to contemporary ice melt above low-viscosity regions of the upper mantle. *Geophysical Research Letters*, 49. <https://doi.org/10.1029/2022GL099731>.
- Weertman, J. (1979). The unsolved general glacier sliding problem. *Journal of Glaciology*, 23:97–115. <https://doi.org/10.3189/S0022143000029762>.
- Weis, M., Greve, R., and Hutter, K. (1999). Theory of shallow ice shelves. *Continuum Mechanics and Thermodynamics*, 11:15–50. <https://doi.org/10.1007/s001610050102>.
- Whitehouse, P. L. (2018). Glacial isostatic adjustment modelling: historical perspectives, recent advances, and future directions. *Earth Surface Dynamics*, 6:401–429. <https://doi.org/10.5194/esurf-6-401-2018>.
- Whitehouse, P. L., Gomez, N., King, M. A., and Wiens, D. A. (2019). Solid earth change and the evolution of the antarctic ice sheet. *Nature Communications*, 10. <https://doi.org/10.1038/s41467-018-08068-y>.
- Winkelmann, R., Martin, M. A., Haseloff, M., Albrecht, T., Bueller, E., Khroulev, C., and Levermann, A. (2011). The application of the shallow-ice approximation. *The Cryosphere*, 5:715–726. <https://doi.org/10.5194/tc-5-715-2011>.
- Wong, G. J., Osterberg, E. C., Hawley, R. L., Courville, Z. R., Ferris, D. G., and Howley, J. A. (2015). Coast-to-interior gradient in recent northwest greenland precipitation trends (1952–2012). *Environmental Research Letters*, 10. <https://doi.org/10.1088/1748-9326/10/11/114008>.
- Zeitz, M., Haacker, J. M., Donges, J. F., Albrecht, T., and Winkelmann, R. (2022). Dynamic regimes of the greenland ice sheet emerging from interacting melt–elevation and glacial isostatic adjustment feedbacks. *Earth System Dynamics*, 13:1077–1096. <https://doi.org/10.5194/esd-13-1077-2022>.
- Zeitz, M., Reese, R., Beckmann, J., Krebs-Kanzow, U., and Winkelmann, R. (2021). Impact of the melt–albedo feedback on the future evolution of the greenland ice sheet with pism-debm-simple. *The Cryosphere*, 15:5739–5764. <https://doi.org/10.5194/tc-15-5739-2021>.
- Zhong, S. J., Paulson, A., and Wahr, J. (2003). Three-dimensional finite element modelling of earth’s viscoelastic deformation: effects of lateral variations in lithospheric thickness. *Geophysical Journal International*, 155:679–695. <https://doi.org/10.1046/j.1365-246X.2003.02084.x>.